
**Pacific Northwest
National Laboratory**

Operated by Battelle for the
U.S. Department of Energy

Investigation of Tc Migration Mechanism During Bulk Vitrification Process Using Re Surrogate

D-S. Kim	P. A. Meyer
L. M. Bagaasen	D. R. Paulsen
J. V. Crum	B. J. Riley
A. Fluegel	M. J. Schweiger
A. Gallegos	C. W. Stewart
B. Martinez	R. G. Swoboda
J. Matyáš	J. D. Yeager

December 2006

Prepared for the U.S. Department of Energy
under Contract DE-AC05-76RL01830



DISCLAIMER

This report was prepared as an account of work sponsored by an agency of the United States Government. Neither the United States Government nor any agency thereof, nor Battelle Memorial Institute, nor any of their employees, makes **any warranty, express or implied, or assumes any legal liability or responsibility for the accuracy, completeness, or usefulness of any information, apparatus, product, or process disclosed, or represents that its use would not infringe privately owned rights.** Reference herein to any specific commercial product, process, or service by trade name, trademark, manufacturer, or otherwise does not necessarily constitute or imply its endorsement, recommendation, or favoring by the United States Government or any agency thereof, or Battelle Memorial Institute. The views and opinions of authors expressed herein do not necessarily state or reflect those of the United States Government or any agency thereof.

PACIFIC NORTHWEST NATIONAL LABORATORY
operated by
BATTELLE
for the
UNITED STATES DEPARTMENT OF ENERGY
under Contract DE-ACO5-76RL01830

Printed in the United States of America

**Available to DOE and DOE contractors from the
Office of Scientific and Technical Information,
P.O. Box 62, Oak Ridge, TN 37831-0062;
ph: (865) 576-8401
fax: (865) 576 5728
email: reports@adonis.osti.gov**

**Available to the public from the National Technical Information Service,
U.S. Department of Commerce, 5285 Port Royal Rd., Springfield, VA 22161
ph: (800) 553-6847
fax: (703) 605-6900
email: orders@nits.fedworld.gov
online ordering: <http://www.ntis.gov/ordering.htm>**

Investigation of Tc Migration Mechanism During Bulk Vitrification Process Using Re Surrogate

D-S. Kim	P. A. Meyer
L. M. Bagaasen	D. R. Paulsen
J. V. Crum	B. J. Riley
A. Fluegel	M. J. Schweiger
A. Gallegos	C. W. Stewart
B. Martinez	R. G. Swoboda
J. Matyáš	J. D. Yeager

December 2006

Prepared for the U.S. Department of Energy
under Contract DE-AC05-76RL01830

Pacific Northwest National Laboratory
Richland, WA 99352

Summary

As a part of bulk vitrification (BV) performance enhancement tasks, laboratory scoping tests were performed in FY 2004–2005 to explore possible ways to reduce the amount of soluble Tc in the BV waste package. These scoping tests helped identify which mechanisms play an important role in the migration of Tc in the BV process (Hrma et al. 2005; Kim et al. 2005). Based on the results from these scoping tests, additional tests were identified that will improve the understanding of Tc migration and clearly identify the dominant mechanisms.

The additional activities identified from previous studies were evaluated and prioritized for planning for Tasks 29 and 30 conducted in FY 2006. Task 29 focused on the improved understanding of Tc migration mechanisms, and Task 30 focused on identifying the potential process changes that might reduce Tc/Re migration into the castable refractory block (CRB). This report summarizes the results from the laboratory- and crucible-scale tests in the laboratory for improved understanding of the Tc migration mechanism using Re as a surrogate performed in Task 29. Other tests performed in Task 30, which specifically aimed at testing changes to the BV process that might reduce Tc/Re migration into the CRB, will be reported in a separate report. The FY 2004–2005 work also showed that Re is an excellent surrogate for Tc. Therefore, Re was used for all the tests performed in this study because a broader set of non-radioactive Re tests could be conducted for less cost than radioactive Tc tests.

The water and molten ionic salt (MIS) capillary experiments suggested that the capillary force is a dominant mechanism for MIS penetration in the CRB, which was also supported by the preliminary modeling results.

Hot-stage microscopy observations of the feed-melting and liquid-formation processes showed that the behavior of a dry blended feed and a feed prepared from liquid simulant was significantly different. A dry blended feed seemed to form a higher fraction of liquid than a feed prepared from liquid simulant, which could cause an increase in MIS migration into CRB. This may suggest that the information obtained in the full-scale tests conducted with dry blended feed may need to be verified with drier prepared feed in future operations.

Thin-section MIS/Re profile measurements with FS-38B CRB samples provided new information on how the MIS and Re penetrate as the melt progresses.

- For the CRB above the melt line, Re penetrates into the CRB by a vapor disposition mechanism, i.e., Re deposits when the CRB is cold, becomes molten as the temperature increases, and then penetrates further into the CRB by capillary action. The extent of penetration and the concentration of Re above the melt line is small.
- For the CRB at the melt line, Re penetrates into the CRB through both the vapor deposition at the early stages of processing and then liquid MIS formation and penetration at later processing stages. The CRB at the melt line close to the glass interface exhibited the highest soluble Re concentration.
- For the CRB below the melt line, regions of the CRB that experience Re penetration through MIS migration early in the process and then are subsequently covered by the progressing melt do not incorporate the Re in an insoluble melt phase. Instead, they push the Re salt outward through evaporation and/or melting and flow of molten salt. This results in a relatively low concentration of

soluble Re on the surface layer and a higher concentration of soluble Re in the outer layer close to the CRB/sand interface

The new experimental setup developed in this study to investigate Re migration during feed processing and glass melting successfully achieved a high mass balance closure. The new setup was designed to capture all the volatiles by condensing them inside a stainless tube or dissolving them in a pair of scrub solutions. The tests with pre-melted glass showed that Re is more volatile than S and Cl with an estimated volatilization rate, $r = 20.4 \text{ wt\%/h}$ at 1200°C . The volatilization rate of Re showed a strong dependence on temperature with an activation energy of 258 J/mole .

The results of dried feed Cases 2-4 in relation to the baseline feed (Case 1) are summarized below:

- The feed with high Cl and F (Case 2) resulted in higher volatilization of Re during melting and consequently lower Re retention in glass. The high Cl and F concentrations in the feed resulted in more separated salt, which is likely responsible for higher Re volatilization.
- The addition of CaO and MgO (Case 3) resulted in comparable Re retention in glass. As expected, the CaO and MgO increased S retention in the melt, but this did not lead to the desired increase in Re retention.
- The feed with crushed soil (Case 4) resulted in a comparable Re retention in the glass. The crushed soil accelerated the formation of the glass-forming melt to a lower temperature, but that did not improve the Re retention in glass.

From the study of Re incorporation, it was found that the Re becomes incorporated into the glass-forming melt at approximately 700°C , and the incorporation of Re in the glass-forming melt reaches a maximum at $\sim 800^\circ\text{C}$ and then decreases as the temperature increases up to 1000°C . The results suggest that Re loss is not solely from volatilization from glass-forming melt but may be partly caused by partitioning to small salt inclusions that coalesce to form a separated salt phase at higher temperatures.

The present study based on thin-section MIS/Re profile measurements with FS-38B CRB samples and the investigation of Re migration during feed processing and glass melting has focused on two routes of Re (used as a surrogate for Tc) transport to the outside of the bulk glass: 1) to the offgas stream through volatilization and 2) to the CRB through MIS penetration by capillary action. The Re is a highly volatile component, and its volatilization will be enhanced by the presence of other volatile components, such as Cl and F. Due to its inherent nature of high volatility, it seems that there is no simple effective solution except for the application of a cold cap that condenses the volatiles and brings them back to the feed to maximize their retention in glass. The thicker cold cap and lower plenum temperature would help to incorporate more Re into glass.

Using clean glass feed would help to capture the Re volatilized from melting the waste-containing feed and incorporate it into glass at the end of the bulk vitrification process. However, once the clean glass becomes melted and mixed into the main body of the melt, the Re-containing melt will become exposed to the surface. The volatilization of Re also proceeds at a relatively high rate from a melt that has already incorporated the Re. The Re can escape relatively easily from the surface as the temperature increases at the end of the process. Therefore, it is important to find the optimal heating condition at the end of the process to fully melt the clean glass feed to a reasonably durable glassy phase (because the partially

melted feed may contain the volatilized Re that is soluble) but not to overheat to expose the hot glass surface for volatilization.

The main mechanism of Tc transport to the CRB is penetration of MIS. The contribution of volatilization and condensation of Re to the total Re migration into CRB seems to be very small compared to MIS penetration. The use of a cold cap, although very critical to control Re volatilization, is likely to promote MIS penetration into the CRB by providing the condition to increase the MIS formation: the cold cap helps to keep the feed at the temperatures favored for MIS formation (e.g., 350 to 550°C) for a longer time. A few promising methods to reduce the MIS migration have been identified and are being tested in crucible scale under Task 30, which will be reported in a separate report. Depending on the effectiveness of the methods developed under Task 30, the balance between the transport of Re to offgas and to the CRB can be made by controlling the formation of the cold cap during the bulk vitrification process.

References

Hrma P, J Matyas, LM Bagaasen, KBC Minister, AE Beck, MJ Schweiger, TM Brouns, DM Strachan, DD Caldwell, BP Tinsley, ML Elliott, and GW Hollenberg. 2005. *Bulk Vitrification Castable Refractory Block Protection Study*. PNNL-15193, Pacific Northwest National Laboratory, Richland, WA.

Kim D-S, CZ Soderquist, JP Icenhower, BP McGrail, RD Scheele, BK McNamara, LM Bagaasen, MJ Schweiger, JV Crum, JD Yeager, J Matyáš, LP Darnell, HT Schaef, AT Owen, AE Kozelisky, LA Snow, and MJ Steele. 2005. *Tc Reductant Chemistry and Crucible Melting Studies with Simulated Hanford Low-Activity Waste*. PNNL-15131, Pacific Northwest National Laboratory, Richland, WA.

Abbreviations and Acronyms

AES	atomic emission spectroscopy
AMEC	AMEC Earth and Environmental, Inc.
BV	bulk vitrification
CH2M HILL	CH2M HILL Hanford Group, Inc.
CRB	castable refractory block
DIW	deionized water
DOE	U.S. Department of Energy
EDS	energy dispersive spectroscopy
ES	engineering-scale
FS	full-scale
GBM	glass batching and melting
GDL	Glass Development Laboratory
HASQARD	Hanford Analytical Services Quality Assurance Requirements Document
HRTS	Horn Rapids Test Site
HT	heat treated
IC	ion chromatography
ICP	inductively coupled plasma
ILAW	immobilized low-activity waste
LAW	low-activity waste
LCR	inductance, capacitance, and resistance
LOI	loss on ignition
LRB	laboratory record book
MIS	molten ionic salt
MS	mass spectrometry
PMG	pre-melted glass
PNNL	Pacific Northwest National Laboratory
QA	quality assurance
RPD	relative percent difference
SBMS	Standards Based Management System
SEM	scanning electron microscopy
SwRI	Southwest Research Institute
WTP	Waste Treatment and Immobilization Plant

Contents

Summary	iii
Abbreviations and Acronyms	vii
1.0 Introduction.....	1.1
2.0 Quality Assurance.....	2.1
3.0 Records	3.1
4.0 Simulant Description	4.1
5.0 Capillary Action of MIS into CRB	5.1
5.1 Background.....	5.1
5.2 Experiments with Water at Room Temperature	5.1
5.3 Experiments with LAW Simulant at 450°C	5.4
5.4 Summary.....	5.8
6.0 Hot-Stage Microscopy Feed Melting Study	6.1
6.1 Test Method.....	6.1
6.2 Results	6.1
7.0 CRB Re Penetration Profile	7.1
7.1 Porosity of CRB.....	7.1
7.2 CRB Sample Descriptions	7.2
7.3 SEM-EDS Analysis of CRB for MIS Profile	7.4
7.4 Methods Development.....	7.8
7.4.1 CRB Powder Preparation.....	7.9
7.4.2 Test for Vacuum Requirements	7.9
7.4.3 Test to Check the Presence of ReO ₂	7.10
7.5 Re and MIS Profile Analyses in FS-38B CRB	7.12
7.5.1 Procedure	7.12
7.5.2 Results and Discussion	7.13
7.6 Summary.....	7.24

8.0	Modeling of Tc/Re Penetration of CRB	8.1
8.1	Saturation of the Feed by Molten Ionic Salt	8.1
8.1.1	Feed Composition and Physical Properties	8.2
8.1.2	Melt Progression Model.....	8.3
8.1.3	Reactions Affecting Melt Phase Distribution	8.5
8.1.4	Results of the Melt Calculation.....	8.6
8.2	Maximum Theoretical Concentration of MIS in the CRB.....	8.8
8.2.1	Atom Fraction Calculation.....	8.9
8.2.2	Results of Sodium Atom Fraction Analysis.....	8.10
8.3	Physical Concept of the Melting Process	8.10
8.4	Mathematical Model for Molten Salt Migration into the CRB.....	8.14
8.4.1	Equations	8.15
8.4.2	Scaling	8.17
8.5	Summary.....	8.18
9.0	Re Migration Tests.....	9.1
9.1	Feeds and Pre-Melted Glass Preparation.....	9.1
9.2	Experimental Methods.....	9.3
9.3	Results and Discussion	9.6
9.3.1	Tests with Pre-Melted Glass	9.16
9.3.2	Tests with Dried Feed	9.21
9.4	Summary.....	9.30
10.0	Incorporation of Re into Glassy Phase.....	10.1
10.1	Experimental.....	10.1
10.2	Results and Discussion	10.1
10.3	Summary.....	10.5
11.0	Conclusions.....	11.1
12.0	References.....	12.1
13.0	Technical Procedure	13.1

Figures

Figure 5.1. CRB Sample in Water after 1808 s (0.5 h).....	5.2
Figure 5.2. CRB Sample in Water after 13,304 s (3.7 h).....	5.2
Figure 5.3. Capillary Rise of Water in the CRB at Room Temperature	5.3
Figure 5.4. Experimental Setup for Measuring LAW Salt Melt Capillary Rise in CRB	5.5
Figure 5.5. Typical Capillary Rise Result of LAW Simulant Melt at 450°C in CRB.....	5.6
Figure 5.6. Typical Capillary Rise Result of LAW Simulant Melt at 450°C in CRB, Fractured Surface (exaggerated color contrast for better visibility).....	5.7
Figure 5.7. Capillary Rise of LAW Simulant Melt in CRB at 450°C.....	5.8
Figure 6.1. Hot-Stage Microscopy Images of Dry LAW (6-Tank Composite) Simulant.....	6.2
Figure 6.2. Hot-Stage Microscopy Images of 38B (Left) and Baseline (Right) Feeds.....	6.3
Figure 7.1. Porosity of As-Received and Heat-Treated CRB Samples.....	7.2
Figure 7.2. Picture of East Wall from Test FS-38B Showing the Locations for CRB Sampling	7.3
Figure 7.3. CRB Samples from Test FS-38B.....	7.3
Figure 7.4. CRB Samples Prepared for SEM-EDS.....	7.4
Figure 7.5. SEM Images of CRB Surface Showing Pores and Inhomogeneous Microstructure	7.5
Figure 7.6. SEM Image of CRB Showing Small Pores	7.5
Figure 7.7. Na, S, and Cl Concentrations in CRB Sample from ~38.1 cm Above the Melt Line.....	7.7
Figure 7.8. Na, S, and Cl Concentrations in CRB Sample from at the Melt Line	7.7
Figure 7.9. Na, S, and Cl Concentrations in CRB Sample from ~15.2 cm Below the Melt Line.....	7.8
Figure 7.10. CRB Pieces Taken from ~15.2 cm Below the Melt Line (lined up from glass/CRB interface on left to outer wall).....	7.12
Figure 7.11. Concentration of Soluble Re, Na, and S in the CRB ~38.1 cm Above the Melt Line.....	7.19
Figure 7.12. Concentration of Insoluble Re, Na, and S in the CRB ~38.1 cm Above the Melt Line	7.20
Figure 7.13. Concentration of Soluble Re, Na, and S in the CRB at the Melt Line	7.20
Figure 7.14. Concentration of Insoluble Re, Na, and S in the CRB at the Melt Line.....	7.21
Figure 7.15. Concentration of Soluble Re, Na, and S in the CRB ~15.2 cm Below the Melt Line.....	7.21

Figure 7.16. Concentration of Insoluble Re, Na, and S in the CRB ~15.2 cm Below the Melt Line	7.22
Figure 7.17. Concentration of Re in the CRB Samples from Different Locations	7.22
Figure 7.18. Concentration of Na in the CRB Samples from Different Locations	7.23
Figure 7.19. Concentration of S in the CRB Samples from Different Locations	7.23
Figure 8.1. Solid Matrix Unsaturated (left) and Effectively Saturated (right) with Liquid	8.1
Figure 8.2. Melting Model: Melting Solid (left) Reduces Feed Volume (right) (solids were labeled A through I so that migrating solids can be easily tracked).....	8.2
Figure 8.3. Phase Volume Fractions Versus Temperature.....	8.7
Figure 8.4. Phase Densities Versus Temperature.....	8.7
Figure 8.5. Atomic Concentrations in CRB after ES-31B Test [Figure 5.16 from Hrma et al. (2005)]... 8.8	8.8
Figure 8.6. Melt Process Concept—Vertical Progression	8.11
Figure 8.7. Temperature Contours from Simulation of Test 38A.....	8.12
Figure 8.8. Melt Process Concept—Lateral Progression	8.13
Figure 8.9. Possible Scenarios for the Melt Model.....	8.14
Figure 8.10. Illustrating the MIS Layer and Transport into CRB.....	8.15
Figure 9.1. Schematic of Experimental Setup for Cold Finger Crucible Tests Used in the Previous Study (Kim et al. 2005).....	9.3
Figure 9.2. Schematic of New Experimental Setup Proposed for Re Migration Tests.....	9.4
Figure 9.3. Wt% of Total Analyzed in Condensate Solutions from the Tests with Pre-melted Glass....	9.18
Figure 9.4. Wt% of Total Retained in Glass from the Tests with Pre-melted Glass.....	9.18
Figure 9.5. Wt% of Total Re Retained in Glass and Analyzed in Condensate Solutions from the Tests with Pre-melted Glass.....	9.19
Figure 9.6. Wt% of Total S Retained in Glass and Analyzed in Condensate Solutions from the Tests with Pre-melted Glass.....	9.19
Figure 9.7. Average Volatilization Rate of Re, S, and Cl from Pre-melted Glass.....	9.20
Figure 9.8. Natural Log of Average Volatilization Rate of Re, S, and Cl from Pre-melted Glass	9.20
Figure 9.9. Measured Versus Calculated Accumulated Re wt% Volatilized.....	9.21
Figure 9.10. Wt% of Total Analyzed in Crucible Rinse from Case 1 (Baseline Feed)	9.23

Figure 9.11. Wt% of Total Analyzed in Condensate Solutions from Case 1 (Baseline Feed).....	9.24
Figure 9.12. Wt% of Total Analyzed in Crucible Rinse from Case 2 (High Cl/F Feed)	9.24
Figure 9.13. Wt% of Total Analyzed in Condensate Solutions from Case 2 (High Cl/F Feed)	9.25
Figure 9.14. Wt% of Total Analyzed in Crucible Rinse from Case 3 (High CaO/MgO Feed)	9.25
Figure 9.15. Wt% of Total Analyzed in Condensate Solutions from Case 3 (High CaO/MgO Feed) ...	9.26
Figure 9.16. Wt% of Total Analyzed in Crucible Rinse from Case 4 (Crushed Soil Feed)	9.26
Figure 9.17. Wt% of Total Analyzed in Condensate Solutions from Case 4 (Crushed Soil Feed).....	9.27
Figure 9.18. Wt% of Total Re Analyzed in All Crucible Rinses and Condensate Solutions.....	9.27
Figure 9.19. Wt% of Total S Analyzed in All Crucible Rinses and Condensate Solutions.....	9.28
Figure 9.20. Wt% of Total Cl Analyzed in All Crucible Rinses and Condensate Solutions	9.28
Figure 9.21. Wt% of Total Re and S Retained in Glass Tested at 1200°C.....	9.29
Figure 9.22. Wt% of Total Re Retained in Glass and Analyzed in Crucible Rinse and Condensate Tested at 1200°C	9.29
Figure 9.23. Wt% of Total S Retained in Glass and Analyzed in Crucible Rinse and Condensate Tested at 1200°C	9.30
Figure 10.1. Wt% of Total Batched Re, Na, and S Analyzed in Crucible Rinse.....	10.3
Figure 10.2. Wt% of Total Batched Re, Na, and S Analyzed in Solid	10.4
Figure 10.3. Sum of Wt% of Total Batched Re, Na, and S Recovered in Crucible Rinse and Solid	10.4

Tables

Table 4.1. Composition of 1 Liter of 5 M Sodium “6 Tank Composite” Simulant (Rassat et al. 2003) ..	4.1
Table 4.2. Compositions of Simulant, HRTS Soil, and Resulting Glass in Mass Fraction of Oxides and Halogens	4.2
Table 5.1. Capillary Rise of Water in CRB at Room Temperature	5.3
Table 5.2. Dry LAW Simulant Composition Used in Capillary Test	5.4
Table 5.3. Surface Tension of Sodium Nitrate Melt (Gale and Totemeier 2004).....	5.4
Table 5.4. Viscosity of Sodium Nitrate Melt (Gale and Totemeier 2004).....	5.5
Table 5.5. Capillary Rise of LAW Simulant in CRB at 450 °C.....	5.7
Table 7.1. Density and Porosity of As-Received and Heat-Treated CRB Samples.....	7.2
Table 7.2. Soluble and Insoluble Re Concentrations from CRB (in µg/kg)	7.11
Table 7.3. Summary of Duplicate Analytical Results.....	7.15
Table 7.4. Concentrations of Re, Na, and S in Leach Solutions (soluble) and in Remaining CRB Particles (insoluble) (in µg or mg of element per kg of CRB)	7.16
Table 7.5. Soluble Re Concentration in CRB Blanks Determined by Centrifugal Extraction Method (Cooley et al. 2006)	7.17
Table 7.6. Comparison of Soluble Re Concentrations by Two Different Methods for the FS-38B CRB Samples Taken from Similar Locations (in µg Re/kg CRB)	7.17
Table 8.1. Overall Bulk Feed Recipe.....	8.3
Table 8.2. Mixed Feed Composition By Melting Point.....	8.3
Table 8.3. Composition of Castable Refractory Solids in Terms of Metal Oxides.....	8.9
Table 8.4. Values Used for Evaluating MIS Penetration Model.....	8.17
Table 9.1. Feed Recipe and Oxide Loading.....	9.2
Table 9.2. Target Glass Compositions (in mass fraction except for Re metal in mg/kg)	9.2
Table 9.3. Summary of Chemical Analyses To Be Performed for Various Samples	9.6
Table 9.4. Summary of Re Mass Balance Closure from Preliminary Tests.....	9.6
Table 9.5. Analyzed Composition of 6-Tank Composite Simulant Compared to Target.....	9.7

Table 9.6 Analyzed Composition of Dried Feeds Compared to Target Compositions (in mass fraction for oxides/halogens and mg/kg for Re metal)	9.8
Table 9.7. Relative Percent Difference ¹⁾ between Target and Analyzed Compositions in Dried Feeds...	9.9
Table 9.8. Re, Na, and S Concentration in Pre-melted Glass Samples (in mg/kg)	9.9
Table 9.9. Analyzed Composition of Pre-melted Glass Compared with Target Composition (in mass fraction).....	9.10
Table 9.10 Analyzed Concentrations in Crucible Rinse and Condensate Solutions (in mg/L)	9.11
Table 9.11. Wt% of Total Analyzed in Crucible Rinse or Condensate Solution	9.13
Table 9.12. Analyzed Concentration and Wt% of Total Retained in Glass for Re, Na, and S	9.14
Table 9.13. Summary of Duplicate Analytical Results	9.15
Table 9.14. Comparison of Results from Duplicate Tests	9.15
Table 9.15. Calculated Re Volatilization Rate.....	9.17
Table 10.1. Analyzed Concentration of Re, Na, and S in Crucible Rinse and Solids.....	10.1
Table 10.2. Mass of Re, Na, and S in Crucible Rinse and Solids and Total Batched.....	10.2
Table 10.3. Wt% of Total Analyzed in Crucible Rinse and in Solids and Total Recovered	10.2

1.0 Introduction

The Hanford Site has the largest volume of high-level radioactive tank waste in the United States stored in 177 underground tanks containing 53 million gallons of waste and 200 million Curies of radioactivity. The life-cycle cost for cleanup has been estimated at nearly \$50 billion over 50 years. The Waste Treatment and Immobilization Plant (WTP) is under construction and will immobilize both high-level waste for disposal at a national repository and low activity waste (LAW) for onsite disposal at Hanford. However, vitrification of the high volume of LAW is the rate-limiting step in the WTP and results in the 50-year project duration. The U.S. Department of Energy (DOE) accelerated cleanup mission for the Hanford Site is a strategic initiative to accelerate tank waste treatment by increasing the capacity of the WTP and using supplemental technologies for waste treatment and immobilization for as much as 70% of the LAW. Bulk vitrification (BV) was selected for further evaluation as a potential supplemental treatment technology for treating LAW at Hanford (Raymond et al. 2004). The use of this supplemental waste form would help DOE meet the long-term groundwater protection criteria for disposing of waste in a shallow land burial facility.

The FY 2003 risk assessment (Mann et al. 2003) of BV waste packages used 0.3 wt% of the technetium (Tc)^(a) inventory as a leachable salt and found it sufficient to create a significant peak in the groundwater concentration in a 100-meter down-gradient well in approximately 1500 years after facility closure. Although this peak met regulatory limits, the CH2M HILL Hanford Group, Inc. (CH2M HILL) has requested that the soluble fraction of Tc in the BV waste package be significantly reduced; the ideal goal (not a requirement) is to reduce the amount of soluble salt in the BV waste package to the point that peak concentrations in the 100-meter down-gradient well do not exceed the highest levels seen for WTP glass. Early attempts to include a castable refractory block (CRB) in place of the refractory sand layer and to use a bottom-up melting technique have eliminated the two main areas where soluble Tc was depositing in the previous process design. However, the refractory block is still quite porous, and early analyses have shown that larger-than-desired quantities of rhenium (Re, a chemical surrogate for Tc) are depositing in the pores of the CRB.

As a part of the BV performance enhancement efforts to explore possible ways to reduce the amount of soluble Tc in the BV waste package, laboratory scoping tests, Tasks 14 and 15, were conducted in FY 2004–2005. Tasks 14 and 15 helped identify which mechanisms play an important role in the migration of Tc in the BV process. Task 14 focused on the volatilization of Tc from the melting feed and molten glass (Kim et al. 2005), and Task 15 focused on the migration of Tc into the CRB (Hrma et al. 2005). Based on the results from these scoping tests, additional tests were identified that will improve the understanding of Tc migration and clearly identify the dominant mechanisms.

The additional activities identified from Tasks 14 and 15 were evaluated and prioritized for planning for Tasks 29 and 30 conducted in FY 2006. Task 29 focused on the improved understanding of Tc migration mechanisms, and Task 30 focused on identifying the potential process changes that might reduce Tc/Re migration into the CRB. This report summarizes the results from the laboratory- and crucible-scale tests in the laboratory under Task 29 to improve our understanding of the mechanism for Tc migration. Other

(a) Technetium used in this study was all ⁹⁹Tc. The symbol “Tc” is used for “⁹⁹Tc” throughout this report.

tests performed in Task 30, which specifically aimed at testing changes to the BV process that might reduce Tc/Re migration into the CRB, will be reported in a separate report.

The FY 2004–2005 work also showed that Re is an excellent surrogate for Tc. The engineering-scale tests ES-32A and 32B used both Re and Tc and found an overall good correlation between Re and Tc except for CRB migration: the CRB extraction measurements resulted in a significantly lower Tc concentration than Re (Pierce et al. 2005), indicating that Re is a conservative CRB migration surrogate in engineering-scale tests. The crucible tests performed in a previous study on the Re/Tc volatilization (Kim et al. 2005) also used both Re and Tc and obtained a very good agreement between Re and Tc. Therefore, Re was used for all the tests performed in this study because a broader set of non-radioactive Re tests could be conducted for less cost than radioactive Tc tests.

2.0 Quality Assurance

All the tests in this report were proof-of-principle^(a) in nature and were performed in accordance with Pacific Northwest National Laboratory's (PNNL's) Standards-Based Management System (SBMS) as specified in the Supplemental Technologies Support Project Tank Waste Support Quality Assurance Plan, Rev. 7 (QAP 46029, January 2006). The SBMS Quality Assurance Program meets DOE Order 414.1C and 10 CFR 830, Subpart A. Staff training is documented and test plans, procedures, and instructions are approved and in project records.

(a) Proof-of-principle testing indicates that the tests performed in this study are not intended to supply data for major project decisions without further verification through testing that complies with the Hanford Analytical Services Quality Assurance Requirements Document (HASQARD).

3.0 Records

Records for this report are the data sheets from the test instructions, applicable procedures, and any laboratory record book (LRB) pages used to record data and test information. These include instrument calibrations, test setup and standards, data logging, calculations, and review comments and signatures. Copies of all test records are provided to the project records custodian for storage in accordance with the quality assurance (QA) plan.

4.0 Simulant Description

The simulant used in this study was the same as used in a previous study (Kim et al. 2005), 5 M sodium “6 tank composite” simulated Hanford LAW developed by Rassat et al. (2003). Table 4.1 shows the reagent masses used to prepare 1 L of liquid simulant. The simulant was spiked with 0.0090 g/L Re_2O_7 to provide a target concentration of 8.1 ppm Re (metal basis) in glass based on the baseline glass formulation (Kim et al. 2003) at 20 wt% Na_2O with 12 wt% total additive and using Horn Rapids Test Site (HRTS) soil. The measured density of the simulant was 1.23 g/cm^3 , which is very close to the calculated value of 1.24 g/cm^3 (Rassat et al. 2003). Table 4.1 also shows the wt% of each chemical for a mixture of dry chemicals, which was used in some subtasks instead of liquid simulant.

Table 4.2 shows the composition of the simulant in terms of oxides and halogens that will remain in glass (assuming 100% retention). Table 4.2 also shows the compositions of HRTS soil and the resulting glass from the baseline formation. The soil composition given in Table 4.2 (designated as HRTS05) has been updated since the last study (Kim et al. 2005), resulting in a slightly different target glass composition.

Table 4.1. Composition of 1 Liter of 5 M Sodium “6 Tank Composite” Simulant (Rassat et al. 2003)

Reagent	Mass (g)	Dry Wt%
H_2O	860	
$\text{Na}_2\text{C}_2\text{O}_4$	1.58	0.416
CH_3COONa	10.79	2.84
NaNO_3	196.11	51.63
KNO_3	1.25	0.329
NaOH	29.58	7.79
$\text{Al}(\text{NO}_3)_3 \cdot 9\text{H}_2\text{O}$	23.90	6.292
Na_2CO_3	50.35	13.25
Na_2SO_4	12.78	3.364
Na_2CrO_4	1.68	0.442
$\text{Na}_3\text{PO}_4 \cdot 12\text{H}_2\text{O}$	18.70	4.923
NaCl	2.56	0.674
NaF	1.33	0.350
NaNO_2	29.26	7.702

Table 4.2. Compositions of Simulant, HRTS Soil, and Resulting Glass in Mass Fraction of Oxides and Halogens

Component	Simulant	HRTS05 soil	Glass
Al ₂ O ₃	0.0188	0.1239	0.0878
B ₂ O ₃	-	-	0.0500
BaO	-	0.0008	0.0005
CaO	-	0.0436	0.0295
Cl	0.0090	-	0.0018
Cr ₂ O ₃	0.0046	0.0001	0.0010
F	0.0035	-	0.0007
Fe ₂ O ₃	-	0.0682	0.0462
K ₂ O	0.0034	0.0318	0.0223
MgO	-	0.0213	0.0144
MnO	-	0.0011	0.0007
Na ₂ O	0.8987	0.0268	0.2000
P ₂ O ₅	0.0203	0.0023	0.0057
SiO ₂	-	0.6687	0.4531
SO ₃	0.0418	-	0.0085
SrO	-	0.0004	0.0003
TiO ₂	-	0.0109	0.0074
ZrO ₂	-	-	0.0700
SUM	1.0000	1.0000	1.0000

5.0 Capillary Action of MIS into CRB

This subtask determines the degree to which capillary action influences Re/molten ionic salt (MIS) penetration into the CRB. One of the proposed mechanisms suggested by Hrma et al. (2005) is that MIS penetrates into the CRB by capillary force through small open pores present in the CRB. To evaluate the proposed mechanism, a test setup was designed to demonstrate capillary action drawing MIS into the CRB.

5.1 Background

In capillaries with a small radius, the capillary action follows the law (Washburn 1921; Whitehead and Greenfield 1932)

$$h = Kt^{1/2} \quad (5.1)$$

where h is the capillary rise height, t is the time, and K is a constant that depends on the viscosity and surface tension of the liquid as well as the wetting angle between the liquid and the solid in which the capillary action takes place. The gravity force is neglected in Equation (5.1) because it is very small compared to the capillary force in fine capillaries. Washburn (1921) showed that the influence of the contact angle between liquid and solid on K also can be neglected (as long as the liquid wets the solid) if the capillary radius is small. Hence, K can be determined using Equation (5.2)

$$K = \left(\frac{r\sigma}{2\eta} \right)^{1/2} \quad (5.2)$$

where σ is the surface tension of the liquid, η is its viscosity, and r is the capillary radius.

5.2 Experiments with Water at Room Temperature

The cylindrical CRB bars of ~4 cm diameter and ~20 cm height used in this study were supplied by the same supplier of the CRB for engineering-scale and full-scale tests. Initial tests were conducted with water because it has viscosities and surface tensions similar to molten salt and would allow long tests at room temperature to be conducted.

The capillary rise of water in the castable refractory was monitored as a function of time. The measurement started from the water surface level. Figure 5.1 and Figure 5.2 show the observations of capillary rise of water in the CRB after 1,808 (0.5) and 13,304 (3.7) seconds (hrs) of reaction time, respectively. Table 5.1 shows the results, and Figure 5.3 depicts the results graphically.

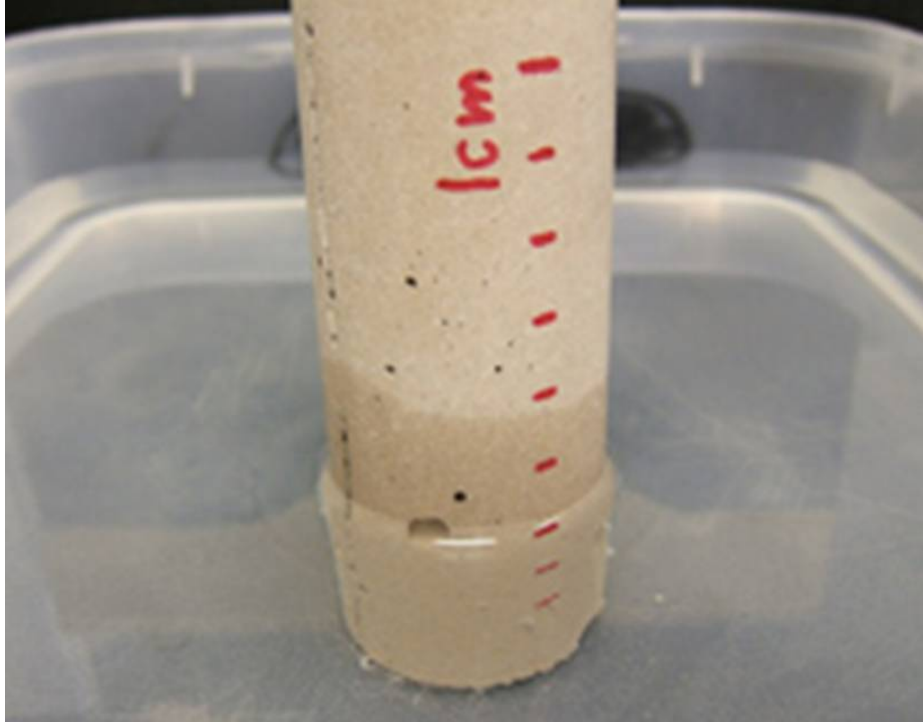


Figure 5.1. CRB Sample in Water after 1808 s (0.5 h)

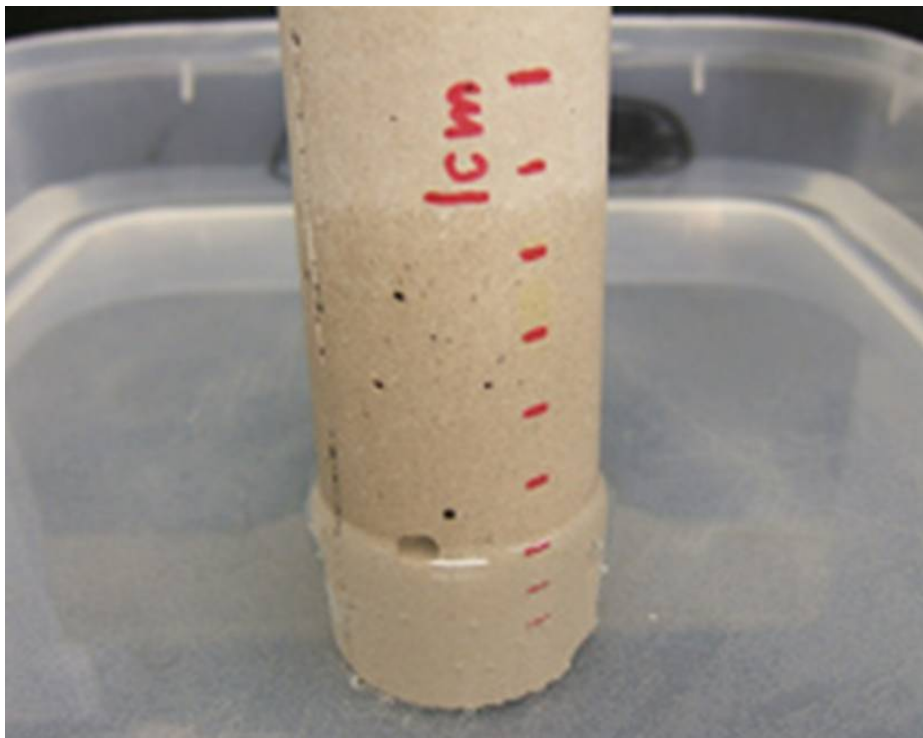


Figure 5.2. CRB Sample in Water after 13,304 s (3.7 h)

Table 5.1. Capillary Rise of Water in CRB at Room Temperature

Time, s	<i>h</i> , mm
0	0
29	1.6
79	2.4
119	3.2
259	4.8
354	6.4
592	8.4
1808	15.6
2398	18.4
3700	24.2
5512	30.8
6824	33.7
13304	45.3
55716	66.9

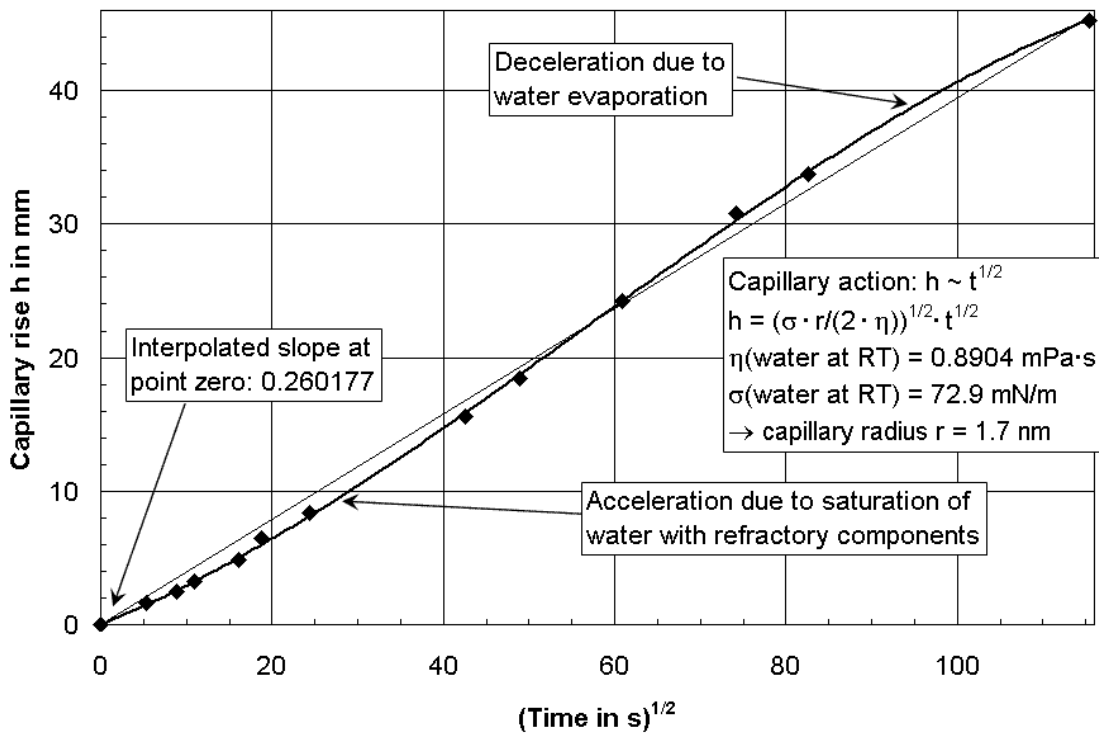


Figure 5.3. Capillary Rise of Water in the CRB at Room Temperature

From the experiment with water, an effective capillary radius of 1.7 nm can be calculated, using the interpolated slope at time zero of 0.2602, a viscosity of 0.8904 mPa·s, and a surface tension of 72.9 mN/m of water at room temperature. The effective radius is equivalent to the radius of a single capillary tube and is likely represented by the size of small channels (necks) that connect the open pores.

Figure 5.3 also demonstrates that the capillary rise of water in the castable refractory did not take place under ideal conditions. The water properties changed because the refractory components dissolved, and water evaporated during the experiment. Therefore, the interpolated slope at the time zero was used in the calculations.

5.3 Experiments with LAW Simulant at 450°C

The dry LAW simulant was mixed in a ball mill as listed in Table 5.2, which is the same as in Table 4.1 except that the sodium chromate was added in threefold excess as a coloring agent. The main component of the dried LAW simulant is sodium nitrate.

Table 5.2. Dry LAW Simulant Composition Used in Capillary Test

Component	wt%
NaOH	7.72
Al(NO ₃) ₃ *9H ₂ O	6.24
Na ₂ CrO ₄	1.32
Na ₂ C ₂ O ₄	0.41
CH ₃ COONa	2.82
NaNO ₃	51.17
KNO ₃	0.33
Na ₂ CO ₃	13.14
Na ₂ SO ₄	3.33
Na ₃ PO ₄ *12H ₂ O	4.88
NaCl	0.67
NaF	0.35
NaNO ₂	7.64

Table 5.3 and Table 5.4 list the surface tension and viscosity of sodium nitrate, the main component in dry LAW. These values were used as approximate values to help estimate the capillary action of the LAW salt melt in the refractory according to Equations (5.1) and (5.2).

Table 5.3. Surface Tension of Sodium Nitrate Melt (Gale and Totemeier 2004)

Temperature, °C	σ , N/m
310	0.11621
400	0.11270
450	0.11075
500	0.10880
600	0.10490

Table 5.4. Viscosity of Sodium Nitrate Melt (Gale and Totemeier 2004)

Temperature, °C	η , mPa·s
300	3.156
400	1.901
450	1.521
500	1.305

Figure 5.4 shows that the LAW simulant mix melted at 450°C in a platinum crucible. At 450°C, most of the LAW simulant melts with vigorous gas evolution; unmelted material such as Al₂O₃, which forms from Al-nitrate, settles to the bottom of the crucible. The refractory sample with Inconel wire wrapped around the bottom end was lowered into the crucible until contact with the melt was established; that is, the resistivity dropped to zero. Then the refractory was lowered another ~5 mm into the melt, causing the melt level to rise proportionally. Samples were held at temperature for a specified period of time and then removed and allowed to cool. After cooling, the samples were fractured to measure the height of the capillary rise. Multiple samples were used to obtain heights at different times.

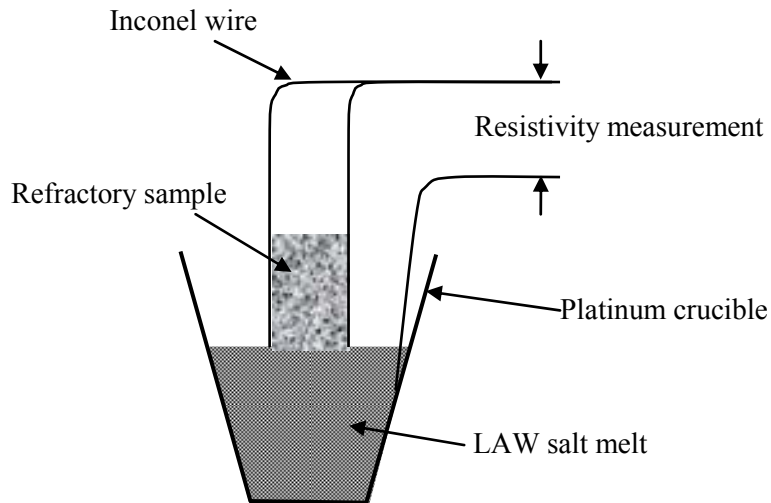


Figure 5.4. Experimental Setup for Measuring LAW Salt Melt Capillary Rise in CRB

Figure 5.5 shows a typical experimental result. The capillary action fronts are clearly visible. Figure 5.6 displays a CRB cross-section with exaggerated colors for better contrast. The chromate coloring agent appears to interact with the refractory in such a way that it penetrates to a limited depth, in contrast to the remainder of the LAW simulant melt. It appeared that the chromate capillary action stopped completely, but more tests would be needed to confirm this preliminary observation.

Table 5.5 and Figure 5.7 display the capillary action results in the castable refractory using LAW simulant salt melt at 450°C. The force of gravity and the liquid pressure from the salt above the CRB bottom were neglected, allowing the capillary rise height to be estimated as the distance from the bottom of the castable refractory to the capillary action front.

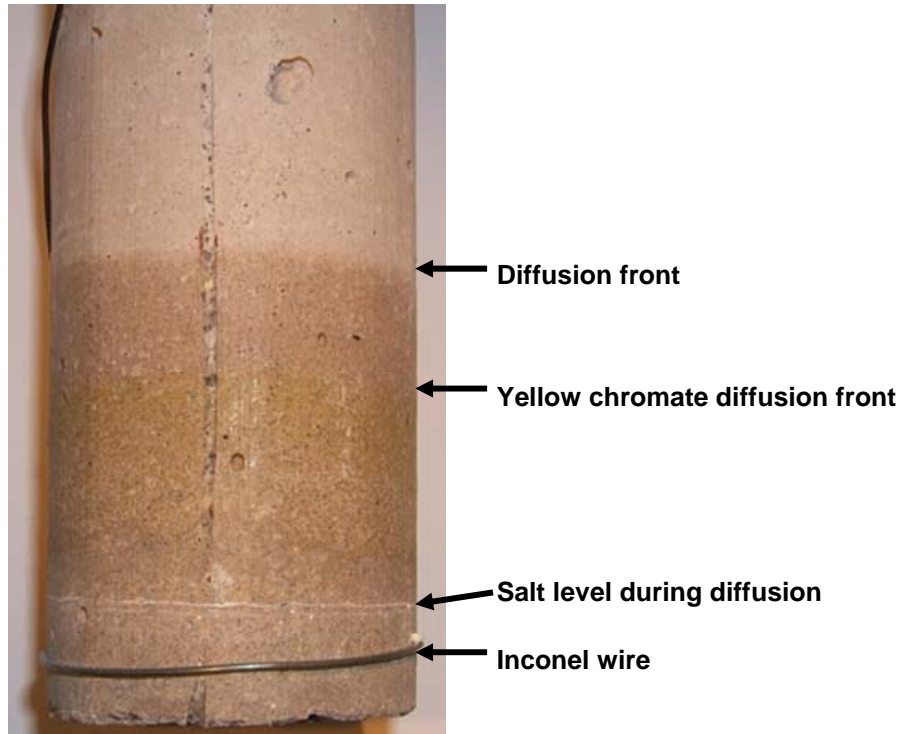


Figure 5.5. Typical Capillary Rise Result of LAW Simulant Melt at 450°C in CRB

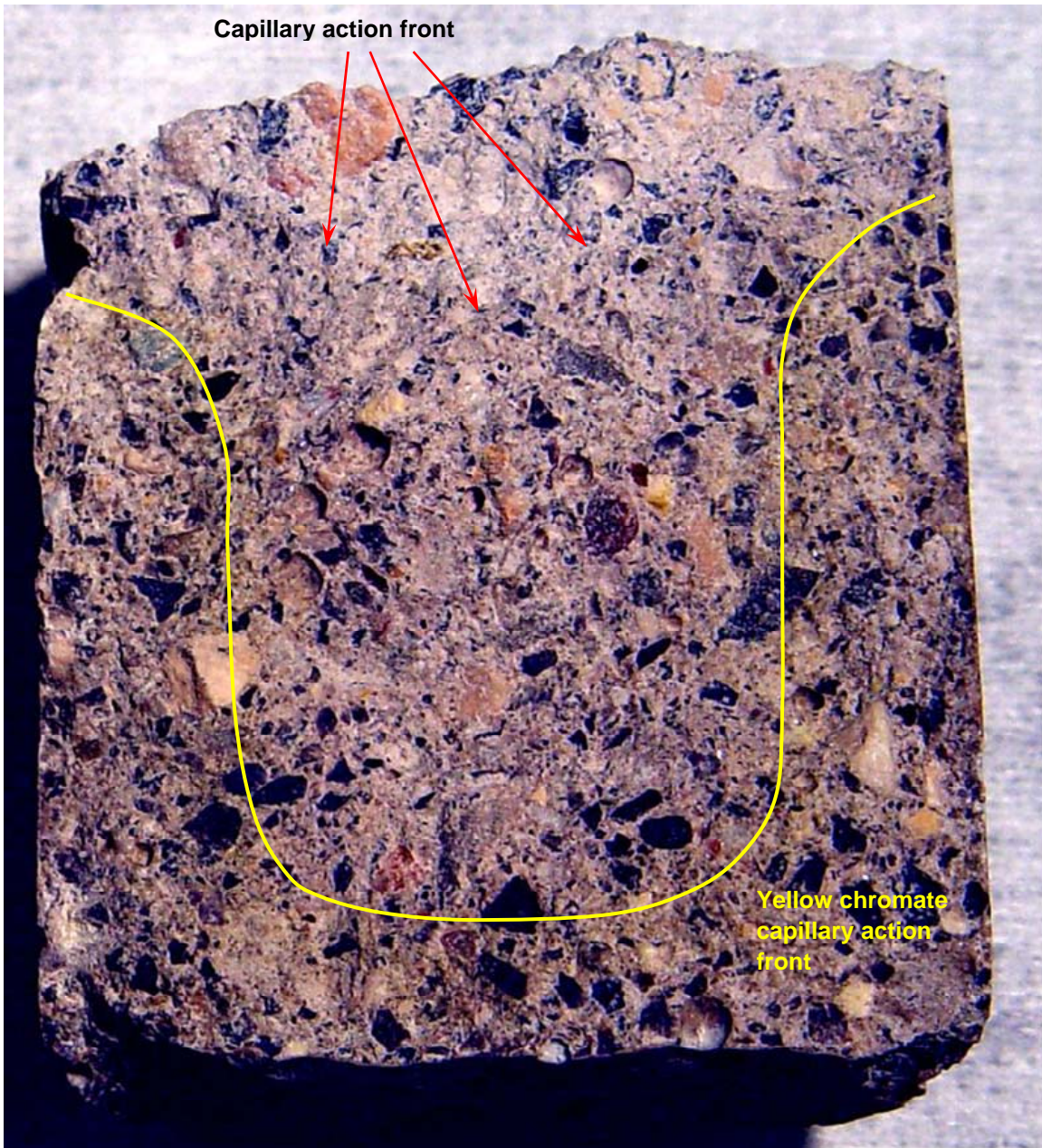


Figure 5.6. Typical Capillary Rise Result of LAW Simulant Melt at 450°C in CRB, Fractured Surface (exaggerated color contrast for better visibility)

Table 5.5. Capillary Rise of LAW Simulant in CRB at 450 °C

Time, s	h , mm
0	0
1800	5
5400	15
10800	21

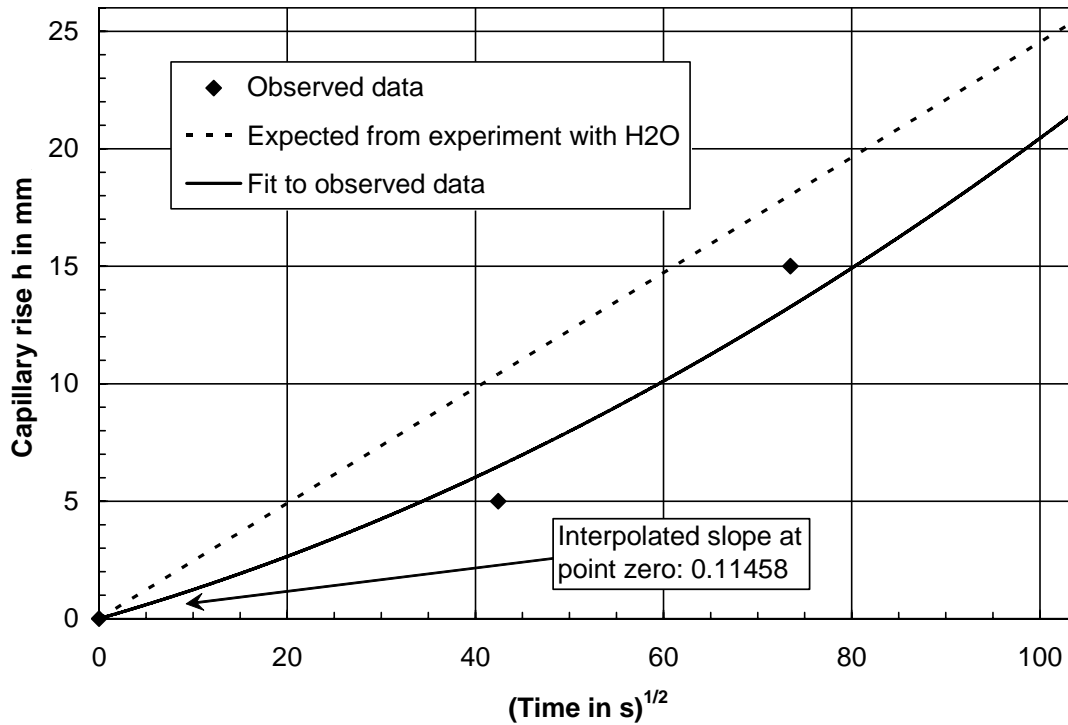


Figure 5.7. Capillary Rise of LAW Simulant Melt in CRB at 450°C

Using the viscosity and surface tension data of NaNO_3 in Table 5.3 and Table 5.4, the “effective” capillary radius in the refractory would be 0.4 nm compared to 1.7 nm determined from the experiment with water. The capillary rise curve based on the “effective” capillary radius obtained from the water penetration test is also shown in Figure 5.7 for comparison. Figure 5.7 shows that there is a reasonable agreement between the water and LAW simulant tests. The difference in the expected and observed data is likely from the assumption that the viscosity and surface tension of the LAW simulant melt at 450°C is the same as the pure NaNO_3 . If the capillary radius of 1.7 nm determined from the experiment with water is assumed to be accurate, the ratio of surface tension in N/m to viscosity in Pa·s of the LAW melt at 450°C would be 15.9, as opposed to 72.8 for pure NaNO_3 . In other words, if the viscosity of the MIS is slightly higher or the surface tension slightly lower than pure NaNO_3 , the expected and observed data would match better. Also, more scatter in the data is expected in the experiments with the LAW melt compared to the water experiments because a new refractory rod was used for each time period, and the capillary radius in different refractory rods may be somewhat variable.

5.4 Summary

The experiments in this report confirmed that the penetration of LAW simulant salt melt into a CRB through capillary force is the dominant force for Tc transport. The effective capillary radius in the castable refractory was estimated as 1.7 nm from the experiment with water. At 450°C, the ratio of surface tension in N/m to viscosity in Pa·s of the LAW melt was predicted as 15.9.

6.0 Hot-Stage Microscopy Feed Melting Study

This section documents the result of a small-scale, hot-stage melting study on the simulated BV feeds. The purpose of this subtask was to investigate the feasibility of applying hot-stage melting studies to the fast verification of BV melting mechanisms and to the screening of alternate additive materials that mitigate MIS penetration into CRB.

6.1 Test Method

Approximately 100 mg of feed was loaded into a small cylindrical platinum (Pt) crucible 6 to 7 mm in diameter and 4 mm in height, heated in a hot-stage furnace, and viewed microscopically. The crucible was covered with a 1.6-mm-thick fused quartz window through which the feed melting was observed. The feed was heated stepwise from room temperature at 10 to 25°C increments to keep a rough average heating rate of 5°C/min. The heating was stopped when all the feed melted and became a clear liquid. Because the hot-stage furnace was not equipped with an automatic temperature controller, the heating had to be adjusted manually, resulting in unavoidable variations in the heating rate between different samples.

The dry simulant mix (as shown in Table 4.1) and two feed variations were tested: 1) 38B feed: a mixture of all dry chemicals as used in a recent FS-38B test, and 2) baseline feed: a full-scale design feed prepared from liquid simulant that was mixed with all additives to have the same composition as the 38B feed.

6.2 Results

Figure 6.1 displays the change of morphology of a dry 6-tank composite simulant with temperature. At 330°C, local melting was apparent; at 450°C, the simulant was mainly liquid with some undissolved particles and bubbles; at 550°C, it was almost clear liquid; between 700 and 760°C, the liquid started to generate foam, likely from decomposing chemicals (likely NaNO_3); at 850°C, bubbles started disappearing; and by 940°C, the bubbles were gone, and solids were shown to have precipitated at the lower-right corner of the crucible.

Figure 6.2 displays hot-stage microscopy images of two feeds as a function of temperature: 1) left: 38B feed and 2) right: baseline feed. At 700°C, some chemical particles at the top and bottom of the pan melted for the 38B feed while most of the soil particles remained in the same place. The baseline feed at 675°C showed little evidence of liquid formation. At 875°C for the 38B feed and at 850°C for the baseline feed, there was a clear indication of liquid-phase formation. At 900 and 1100°C for 38B feed and at 950 and 1075°C for the baseline feed, the progress of liquid formation was obvious for both feeds, but a higher fraction of liquid seemed to have formed for the 38B feed than the baseline feed. The 38B feed also seemed to have a greater degree of segregation of the different particles than the baseline feed.

These observations show that the behavior of a dry blended feed and a feed prepared from liquid simulant is significantly different. Although there was important information obtained in the full-scale tests conducted with dry blended feed, it is important to verify results with drier prepared feed in future operations.

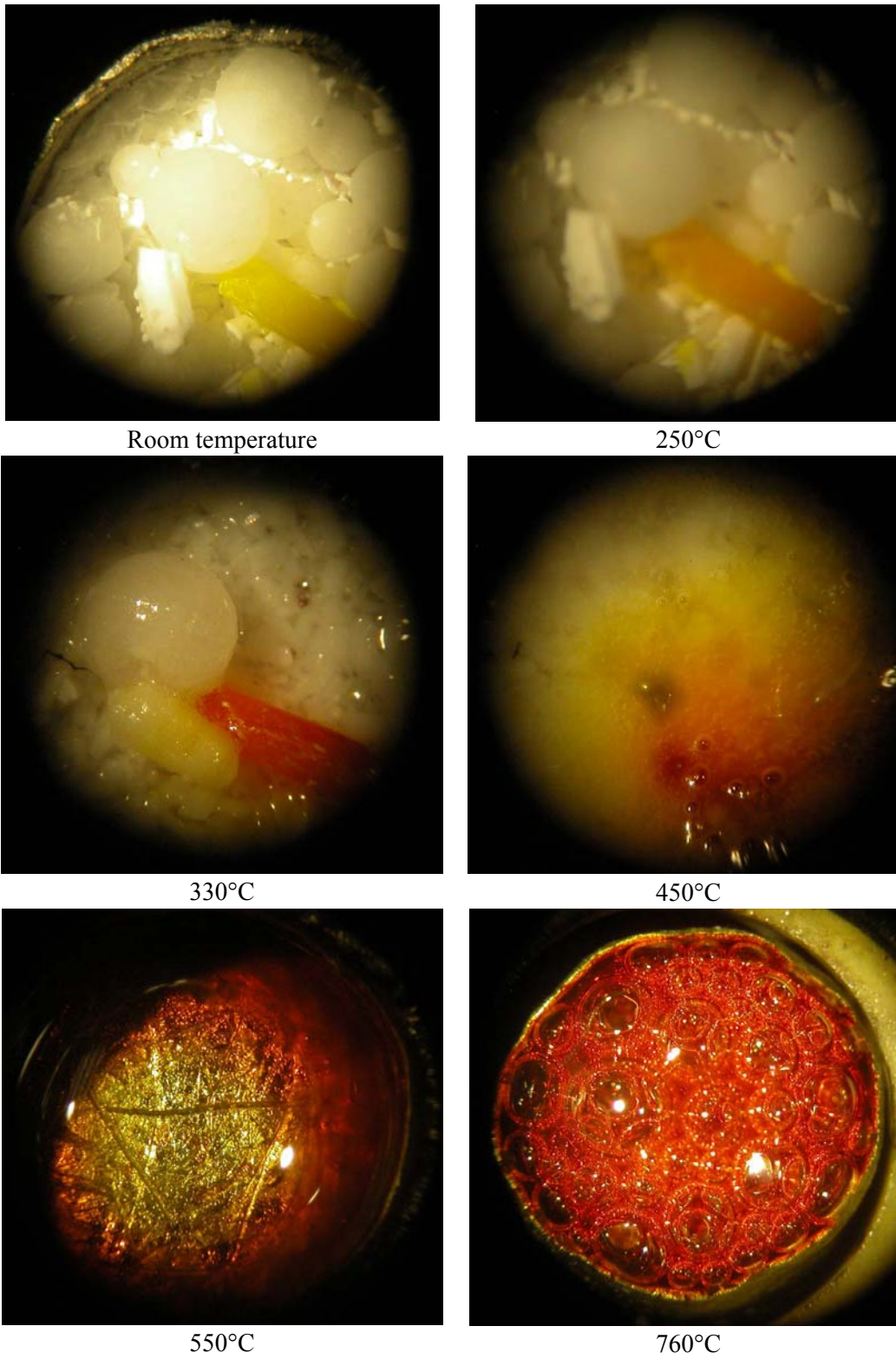
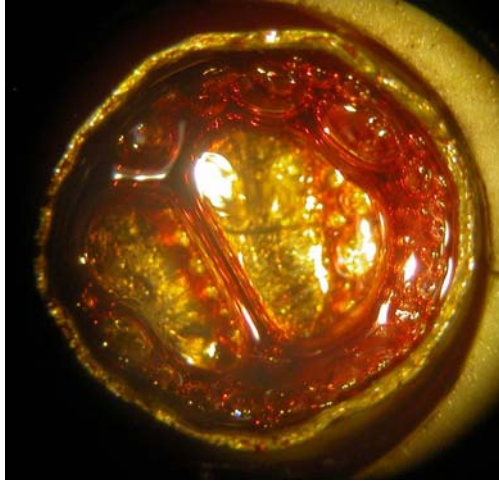


Figure 6.1. Hot-Stage Microscopy Images of Dry LAW (6-Tank Composite) Simulant



850°C



940°C

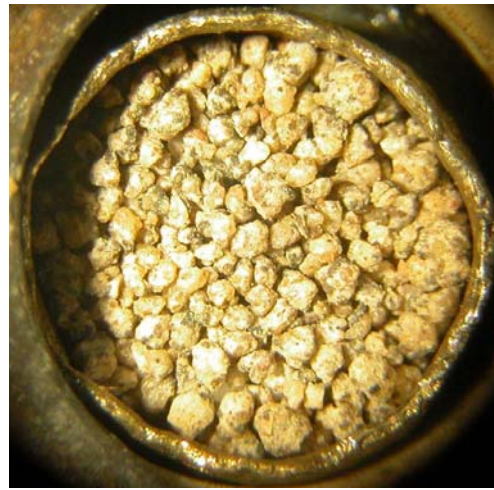
Figure 6.1 (Contd)

38B Feed



Room temperature

Baseline Feed

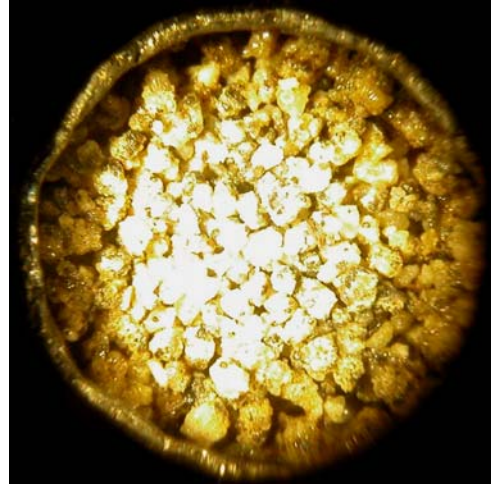


Room temperature

Figure 6.2. Hot-Stage Microscopy Images of 38B (Left) and Baseline (Right) Feeds



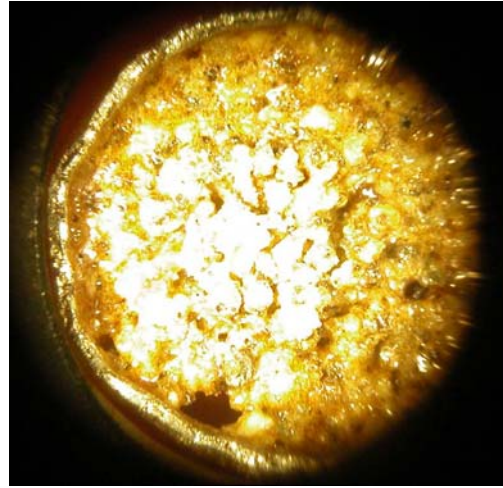
700°C



675°C



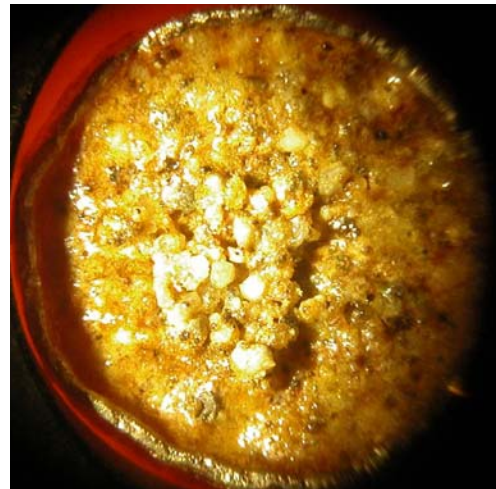
875



850

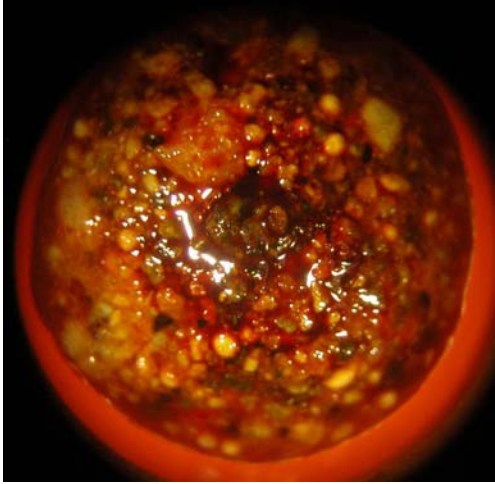


900°C



950°C

Figure 6.2 (Contd)



1100°C



1075°C

Figure 6.2 (Contd)

7.0 CRB Re Penetration Profile

This section documents the results of MIS penetration profile analyses of CRB samples from the FS-38B test. The purpose of this subtask was to provide important information of the mechanism for Re and Tc penetration/deposition and investigate mechanistic differences between the top and bottom portions of the CRB.

7.1 Porosity of CRB

The porosity of the CRB was measured to estimate the maximum amount of MIS that would be present in a fully saturated CRB. The open and total porosity were measured for both as-received and heat-treated CRB cylinder samples.

Six samples of approximately equal size were cut from the ~4-cm-diameter cylinder using a large cutoff saw. Each sample was ~2.4 cm tall. After drying overnight in a 90°C oven, three of the samples were heat treated at 1200°C for 1 h. The heat-treated samples were labeled H1, H2, and H3, while the non-heat-treated samples were labeled A1, A2, and A3 for “as-received.” The bulk density was measured from the mass and volume of each CRB sample. The sample volume was determined from multiple height and diameter readings for each sample.

For measuring open porosity, each weighed sample was immersed into deionized water (DIW) in a container that was evacuated using the building vacuum system. After holding the sample under a vacuum for 2 h, each sample was re-weighed. The total mass gain was attributed to water absorption into the open pores, which was then converted to a volume of open pores by assuming a water density of 1 g/cm³. The volume-fraction open porosity is the volume of open pores divided by the total sample volume.

For measuring the density of CRB material, ~1 g was removed from each sample and ground in a tungsten carbide mill for 4 min. The density of fine CRB particles was measured using a calibrated gas pycnometer. The total porosity was then obtained from $(\text{total porosity}) = 1 - (\text{bulk density})/(\text{particle density})$. The closed porosity is obtained by subtracting the open porosity from the total porosity.

Table 7.1 summarizes the result of measuring density and porosity on the as-received and heat-treated CRB samples. Figure 7.1 shows that heat treatment increased the closed porosity slightly but without noticeable change in the open porosity. The total porosity of 22% measured in this study was higher than the 17% reported by the CRB manufacturer.

Table 7.1. Density and Porosity of As-Received and Heat-Treated CRB Samples

CRB	Sample	Bulk density (g/cm ³)	Material density (g/cm ³)	Open porosity (%)	Closed porosity (%)	Total porosity (%)
As-received	A1	2.480	3.154	15.8	5.6	21.4
	A2	2.450	3.135	16.1	5.7	21.9
	A3	2.440	3.119	15.4	6.4	21.8
	Average	2.456	3.136	15.8	5.9	21.7
	STD	0.021	0.018	0.38	0.44	0.25
Heat-treated	H1	2.437	3.155	15.2	7.5	22.7
	H2	2.448	3.175	14.9	8.0	22.9
	H3	2.444	3.132	15.0	6.9	21.9
	Average	2.443	3.154	15.1	7.5	22.5
	STD	0.006	0.022	0.16	0.52	0.51

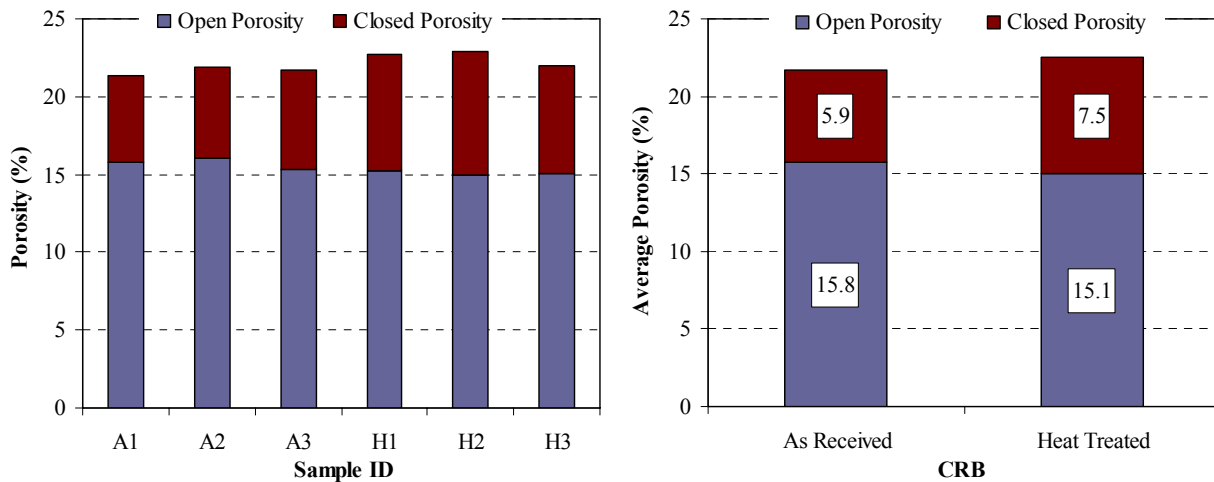


Figure 7.1. Porosity of As-Received and Heat-Treated CRB Samples

7.2 CRB Sample Descriptions

Figure 7.2 displays the east wall of Test FS-38B showing the locations for CRB samples taken for this study. Figure 7.3 shows the sample blocks after they were removed from the CRB panel: #1 was from ~38.1 cm above the melt line, #2 just above the melt line, #3 at the melt line, and #4 ~15.2 cm below the melt line. CRB samples #1, #3, and #4 were used to study the Re penetration profile. Tests included a semi-quantitative scanning electron microscopy-energy dispersive spectroscopy (SEM-EDS) analysis, a preliminary method development study, and a quantitative thin section study. These sample locations represent different areas of the CRB and were also in the same locations as the CRB samples taken for the Re Extraction Study (Cooley et al. 2006) so that direct comparisons can be made. The #4 sample block was used for the preliminary method development study.



Figure 7.2. Picture of East Wall from Test FS-38B Showing the Locations for CRB Sampling

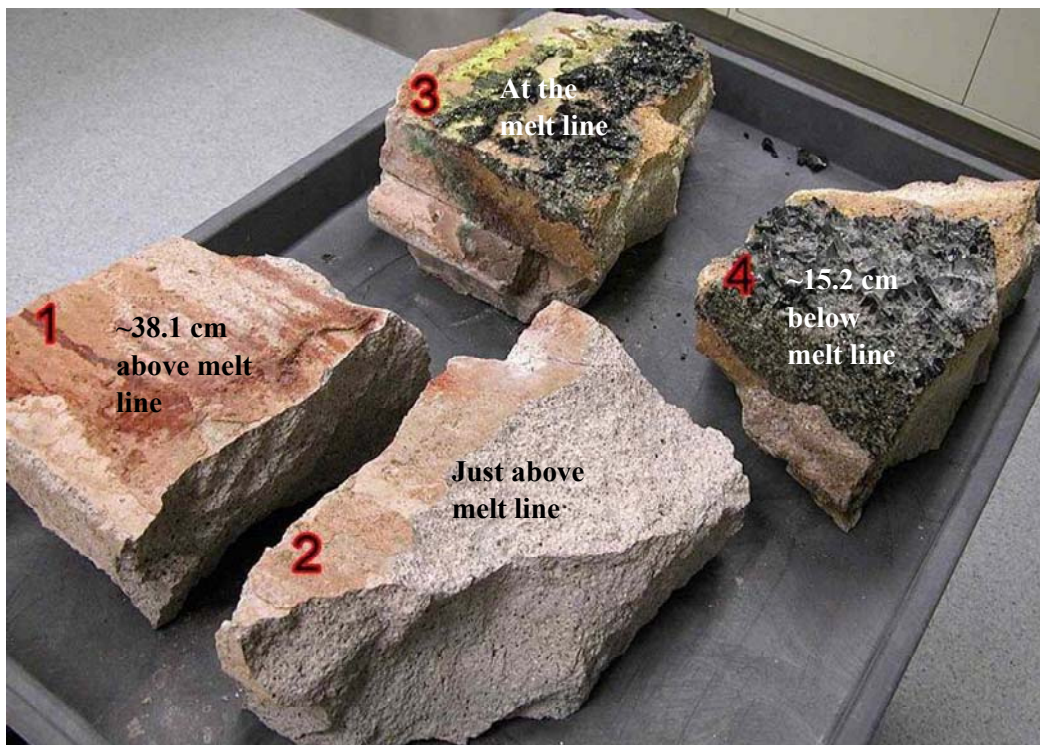


Figure 7.3. CRB Samples from Test FS-38B

7.3 SEM-EDS Analysis of CRB for MIS Profile

The CRB samples from three locations were used to determine the preliminary MIS profile using sodium (Na) as an indication of MIS penetration. The samples for the SEM-EDS study were taken right next to the samples that were taken to analyze the thin-section profiles. To facilitate loading into the SEM, the CRB blocks were split into three pieces of ~5 to 8 cm wide and ~5 cm depth using a jackhammer. Figure 7.4 shows the CRB samples used for SEM-EDS. The samples labeled as I are from the glass/refractory interface (inside wall), and samples labeled as III are from the sand/refractory interface (outside wall). For the CRB from ~38.1 cm above the melt line (CRB block 1), piece I was 5.1 cm, piece II was 4.3 cm, and piece III was 4.2 cm long with ~0.6 cm of piece II and ~0.8 cm of piece III lost during the sample preparation. For the CRB at the melt line (CRB block 3), piece I was 6.7 cm, piece II was 3.6 cm, and piece III was 4.7 cm long with minimal sample loss. For the CRB from ~15.2 cm below the melt line (CRB block 43), piece I was 5 cm, piece II was 3 cm, and piece III was 4 cm long. Red-crossed areas for the CRB from ~15.2 cm below the melt line in Figure 7.4 were lost during sample preparation.

Each CRB piece was coated with carbon under high vacuum ($\sim 10^{-7}$ torr) and analyzed using SEM-EDS. The distribution of Na, sulfur (S), and chlorine (Cl) was measured at depth intervals of 1 to 3 mm using a measurement area of $\sim 0.5 \times 0.5$ mm at each interval.

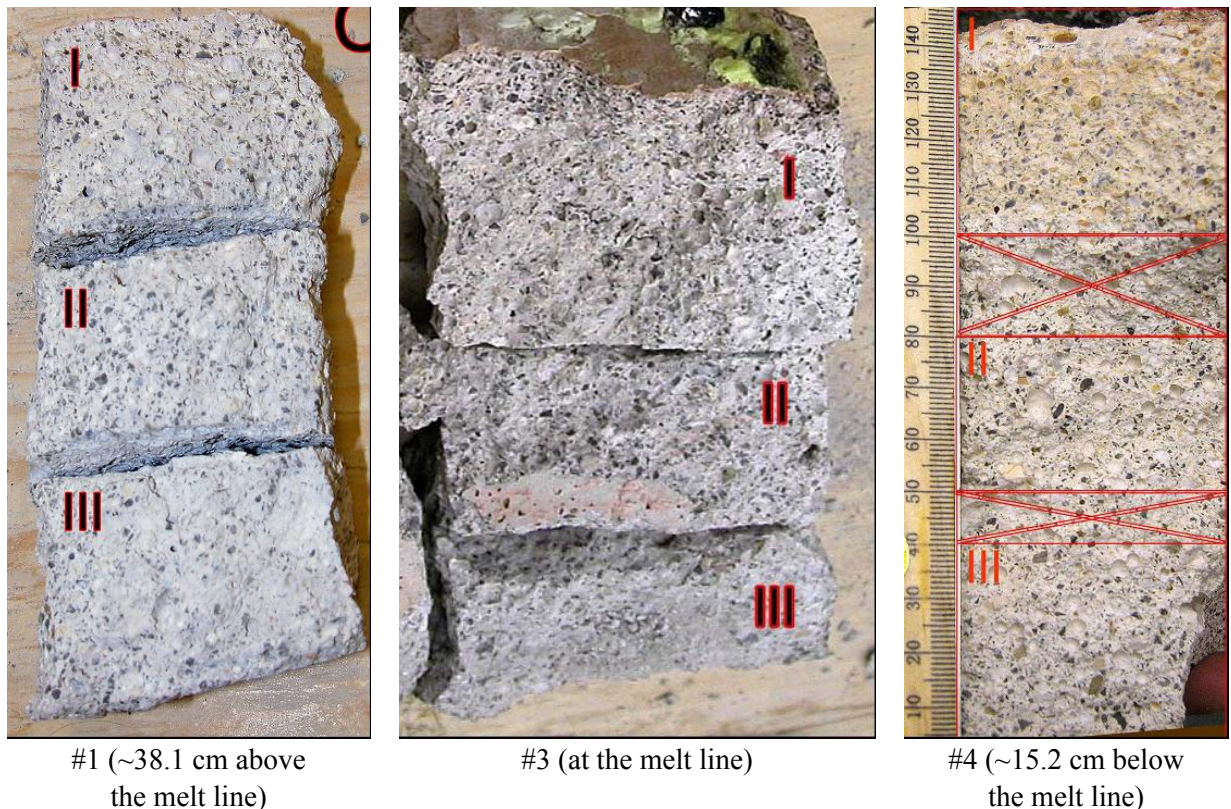


Figure 7.4. CRB Samples Prepared for SEM-EDS

The EDS analysis detected a low and somewhat variable concentration of Na in the CRB blank sample not exposed to MIS. For five randomly chosen areas, three contained sodium below the detection limit, one contained about 0.21 atomic %, and the other 0.37 atomic % of Na.

The CRB is composed of large grains and fine particles embedded in binding material. There are regions with high concentrations of binding material with high porosity and regions with high concentrations of large particles having minimal porosity. Figure 7.5 shows the inhomogeneous microstructure of the CRB and the highly porous regions available for MIS penetration. Figure 7.6 is a high-magnification picture of the CRB showing small pores between small particles.

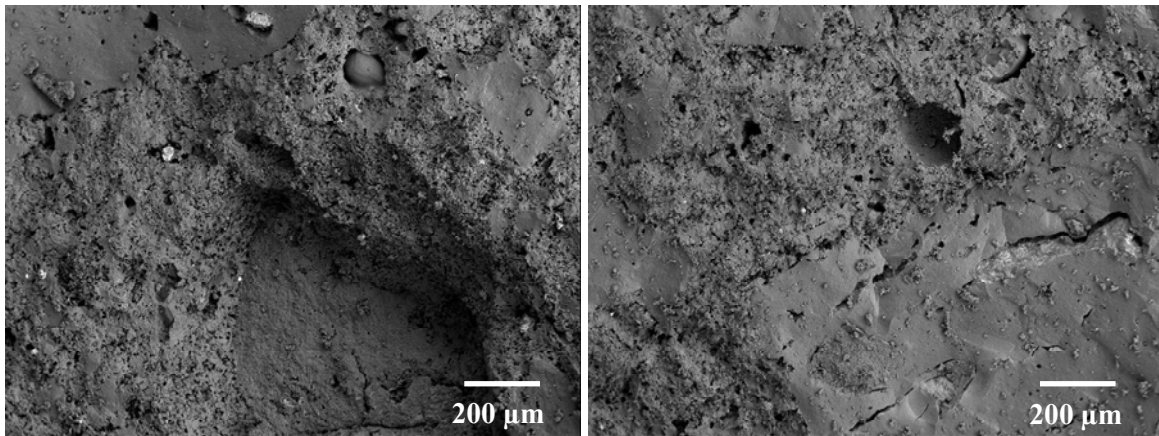


Figure 7.5. SEM Images of CRB Surface Showing Pores and Inhomogeneous Microstructure

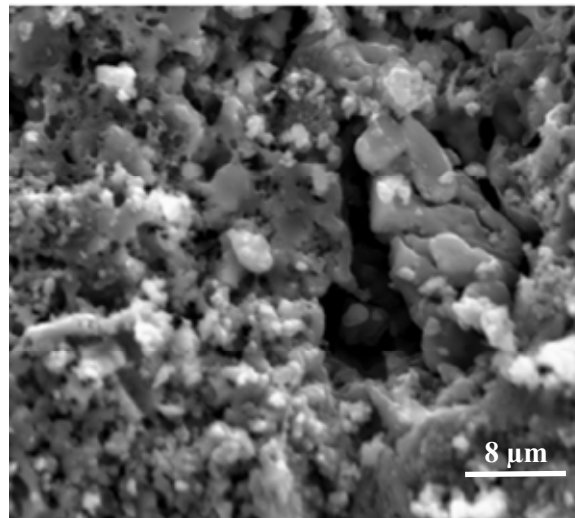


Figure 7.6. SEM Image of CRB Showing Small Pores

Figure 7.7 through Figure 7.9 display the concentration profile of Na, S, and Cl (in atomic %) determined by SEM-EDS as a function of distance from the glass/CRB interface (inside CRB wall) for the CRB samples from ~38.1 cm above the melt line (Figure 7.7), at the melt line (Figure 7.8), and ~15.2 cm below the melt line (Figure 7.9). The EDS was not calibrated with the standard samples, and thus the results are semi-quantitative, and only relative comparisons are valid. Based on Na concentration, the MIS penetrated ~1 cm or less into the CRB ~38.1 cm above the melt line, ~2.5 cm into the CRB at the melt line, and ~10 cm into the CRB ~15.2 cm below the melt line, assuming that the ~0.3 atomic % Na is background, and the minor jump at the CRB/sand interface is not a result of MIS penetration.

For the CRB ~15.2 cm below the melt line, the Na concentration dropped to background at ~5 cm and had another peak between 7 and 10 cm depth (the sample was lost between 5 and 7 cm), whereas for the CRB samples from ~38.1 cm above the melt line and at the melt line, the Na concentration sharply decreased from the glass/CRB interface to the background level. It is interesting to note that there are only a couple of points with high S (~8.5 cm and close to the CRB/sand interface) in the CRB from ~38.1 cm above the melt line. The S concentration in the CRB at the melt line dropped to background much earlier than Na (1 cm compared to 2.5 cm) and increased again between 5 and 7 cm. If the MIS penetration depth at the melt line were based on S, it would be ~7 cm. For the area between 5 and 7 cm, there is an indication of a slight increase of Na, but it is unclear if this is a result of MIS penetration or just variation in the Na background. For the CRB sample from ~15.2 cm below the melt line, the S concentration starts to increase above the background level only after 7 cm where the Na peak reappears and extends to a depth of 12 cm. If S concentration is used for MIS penetration, it would be 12 cm compared to 10 cm.

For Cl, the CRB from ~38.1 cm above the melt line had only two points of high Cl above the background (~11 cm and close to the CRB/sand interface). The Cl concentration in the CRB at the melt line had high and low fluctuation throughout the sample, whereas the CRB sample from ~15.2 cm below the melt line had high fluctuation only in the 8 to 9 cm depth, which is within the area with high S and Na.

Assuming that Cl is a result of volatilization, not MIS penetration, the MIS penetration depth was estimated as 1 cm or less, ~7 cm, and 12 cm based on Na and S concentrations, for the sample above, at, and below the melt line, respectively. Based on this information, the depth of Re profile measurement for each sample was determined. The above melt line sample was analyzed to depths of 4 cm, the at melt line sample to 8 cm, and the below melt line sample to 15 cm.

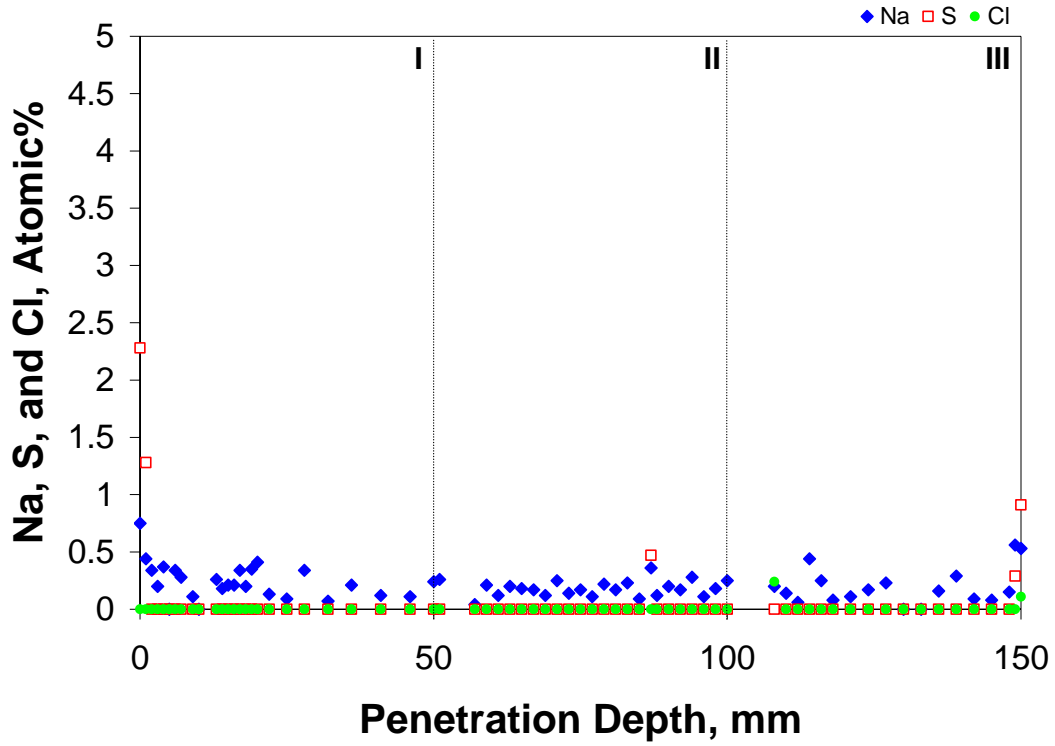


Figure 7.7. Na, S, and Cl Concentrations in CRB Sample from ~38.1 cm Above the Melt Line

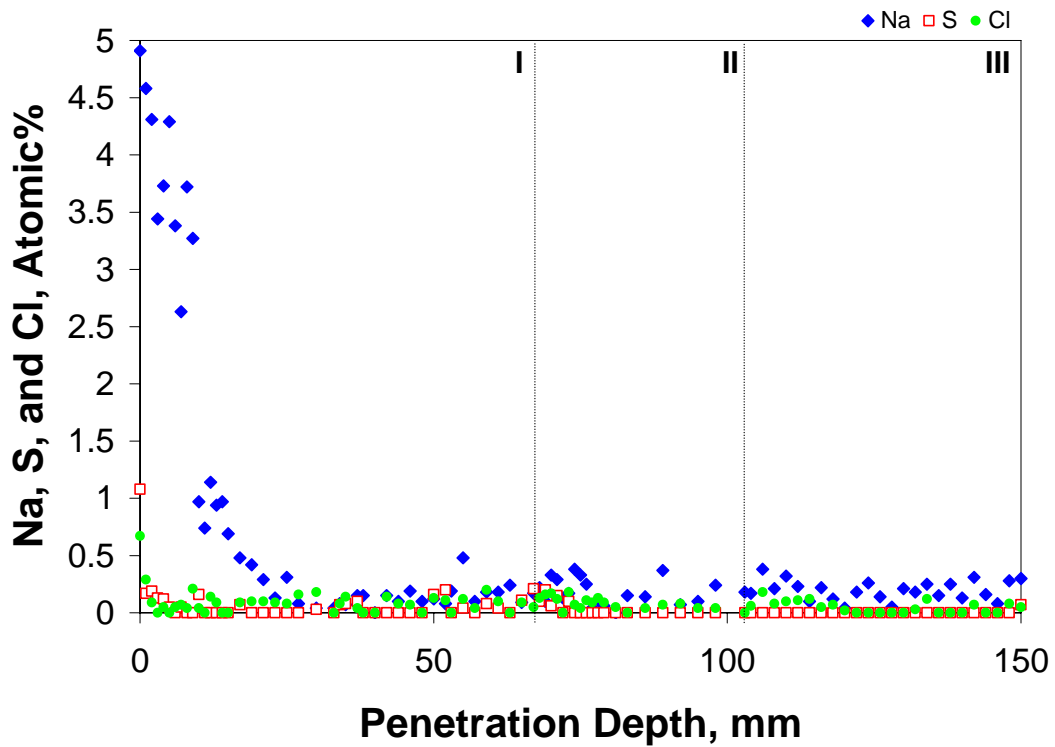


Figure 7.8. Na, S, and Cl Concentrations in CRB Sample from at the Melt Line

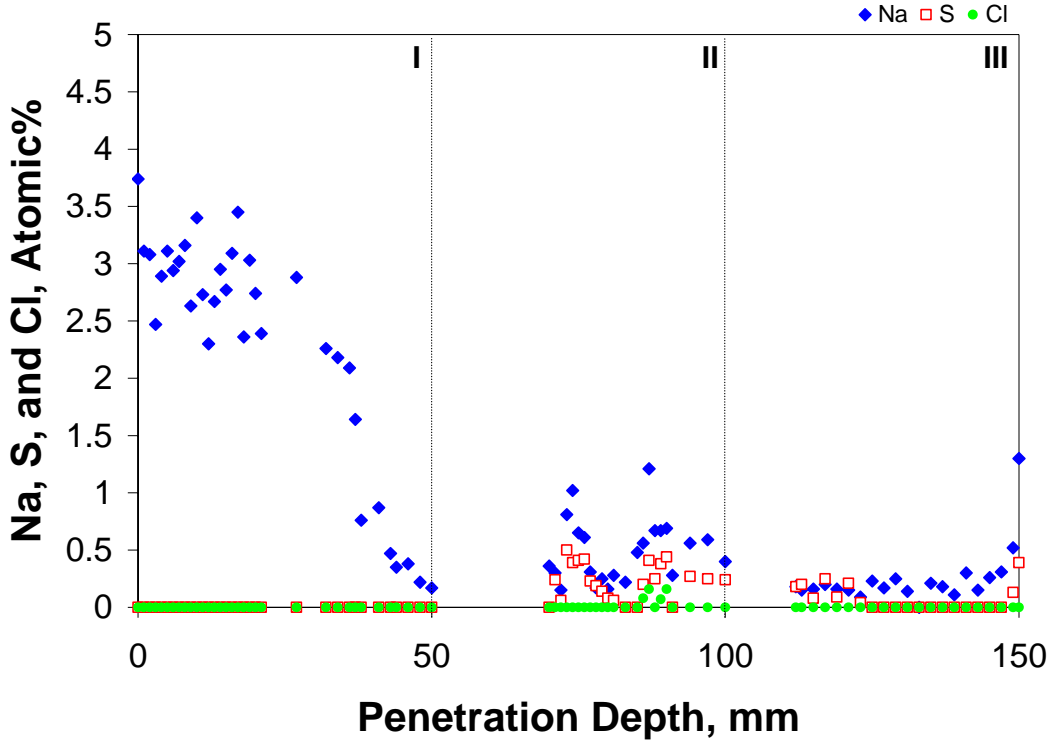


Figure 7.9. Na, S, and Cl Concentrations in CRB Sample from ~15.2 cm Below the Melt Line

7.4 Methods Development

In a previous study (Hrma et al. 2005), the CRB taken from ES-31B was ground into powder layer by layer in 1-mm intervals starting at the glass refractory interface and moving into the refractory block. The resulting refractory powder was washed and analyzed for soluble Re, and the remaining solids were dried and analyzed for Re. The penetration of salt components (Na, S, Cl) was analyzed by SEM/EDS. These preliminary methods supplied good scoping results, but did not result in a clear understanding of Re penetration depths. The concentration profiles for both soluble and insoluble forms of Re were relatively flat over the measured 10-mm depth, and the depth where Re concentrations dropped off was not determined. The MIS penetration profile determined by SEM/EDS (e.g., Na, S, Cl penetration) showed that MIS penetrated up to 15 mm, indicating that greater penetration depths needed to be examined for Re.

The following modified method was used to obtain a better understanding of the Re penetration profiles in the CRB:

1. The FS-38B CRB block for thin section analysis was first examined by SEM/EDS to get a rough measurement of the penetration depth of MIS components as discussed in Section 7.3.
2. The CRB was cut into planar sections of roughly constant thickness that were oriented perpendicular to the movement of the MIS. The sections were dry cut with a diamond saw without using water lubricant. The thin slice of CRB was broken into smaller pieces and then ground into powder with a tungsten carbide mill.

3. The resulting ground CRB powder was washed with a dilute (0.001 M) nitric acid (HNO₃) solution.^(a) The resulting solutions were analyzed for Re, Na, and S.
4. The CRB powder was dried and then prepared with the fusion method to completely dissolve all the materials into solution, and the fusion solutions were analyzed for Re, Na, and S.

The final experimental procedure is described in the following sections.

7.4.1 CRB Powder Preparation

A sample out of the CRB block that was ~15.2 cm below the melt line was used for preliminary tests. The CRB section was extracted using a high-speed diamond-bladed concrete saw and a power hammer. An ~5-cm piece was cut into four rough cubes of 1-cm depth. The sample was cut with a low-speed diamond saw without water or other type of lubricant to prevent any MIS component from dissolving that may have been in the CRB. Each 1-cm cube was then crushed separately in a tungsten carbide mill for 3 s to reduce the cube into granular/powder form. The crushing time of 3 s was determined from preliminary crushing tests varying crushing times. The resulting particle size of roughly 500 μm or smaller was deemed to be small enough to provide a short distance for DIW penetration into the CRB pores and solute diffusion into solution, but large enough to avoid producing fine particles that might release the otherwise insoluble Na/Re/S. The granular/powder samples made from all four cubes were then mixed by shaking and rolling for several minutes in a vial to obtain a homogeneous mix of grains. The mix was divided into five equivalent portions that were used for the preliminary method-development tests as described below. The same cutting/crushing sample preparation steps were used for the thin-section profile tests.

7.4.2 Test for Vacuum Requirements

There was a potential concern that the extraction solution would not penetrate deep enough into the very small pores in the CRB powder to extract all of the soluble Re present. Therefore, the first set of method-development extraction tests was performed with and without vacuum to determine whether vacuum extraction was necessary. Extraction solutions were evaluated using electrical resistance as an indication of relative extraction efficiency.

Teflon extraction vessels were cleansed by washing in hot, soapy water and then in boiling DIW for 1 h with a DIW rinse after each washing step. This cleaning process was used for all extraction tests performed in this study. Two clean Teflon vessels with 15 mL of DIW and 2.8 g ground CRB were prepared for the extraction tests. One vessel was placed at room temperature for 24 h, while the other vessel was placed in a vacuum chamber for 1 h before a 23-h room-temperature extraction. The extraction solutions were decanted into smaller clean vials, and their electrical resistances were measured using an inductance, capacitance, and resistance (LCR) meter and Pt probe at a probe depth of 12.5 cm. The measured electrical resistance was 9.0 kΩ for the solution with a 1-h vacuum exposure and 9.2 kΩ

(a) Dilute nitric acid was used to promote the dissolution of all the soluble phases because some phases may have a slow dissolution rate in DIW. The same solution was used in the extraction of soluble Re from CRB that was performed in support of the 2005 Integrated Disposal Facility Performance Assessment (Pierce et al. 2005).

for the solution without the vacuum exposure, indicating that there is no significant difference.^(a) It appears that water can penetrate into pores to extract the soluble MIS components without the assistance of vacuum. Based on this result, it was determined that vacuum application was not necessary for acceptable extraction, so all subsequent tests were performed without vacuum.

7.4.3 Test to Check the Presence of ReO₂

As discussed in Section 7.4, the Re profile test planned to use dilute nitric acid. It was assumed that MIS penetrates the CRB pores and forms a glassy phase that contains an insoluble Re based on the results of a previous study (Hrma et al. 2005). It was suggested that the insoluble fraction of Re (assumed to be bound within a glassy layer inside the pore surface) may include ReO₂ that was not incorporated in a glass phase. ReO₂ is not readily soluble in dilute nitric acid solution but may be oxidized to higher valence states over time and released into the environment in a short time relative to the time frame of a performance assessment. Therefore, other method development tests were conducted to determine if the ReO₂ phase was present. An ammonium hydroxide (NH₄OH)-hydrogen peroxide (H₂O₂) solution should dissolve ReO₂ at room temperature if present in a crystalline form on pore surfaces. The ReO₂ encapsulated in a glassy layer will not be released by this method. It was also decided to compare the DIW wash and dilute nitric acid wash. Below is a summary of comparison tests:

- Test 1: (1) first DIW wash, (2) second DIW wash, and (3) fusion of dried CRB powder
- Test 2: (1) first dilute nitric acid solution wash, (2) second dilute nitric acid solution wash, and (3) fusion of dried CRB powder
- Test 3: (1) dilute nitric acid solution wash, (2) ammonium hydroxide solution wash, and (3) fusion of dried CRB powder.

For Tests 1 and 2, 15 mL of DIW (Test 1) or dilute nitric acid (Test 2) was added to a Teflon vessel with one 2.8-g portion of the ground CRB. The samples were kept at room temperature for 24 h, and then the liquid leachate was decanted and filtered for chemical analysis. The treated CRB powder samples were then rinsed with ~50 mL DIW for 1 h to remove residuals of the first leach solution. The rinsed solution was archived for potential analysis later if necessary. This CRB powder was then combined with 15 mL of DIW (Test 1) or dilute nitric acid (Test 2) and held for 24 h, and then the liquid leachate was decanted and filtered for chemical analysis. The resulting CRB powder samples were again rinsed with ~50 mL DIW for 1 h to remove residual leach solution. The CRB powder samples were then placed in a drying oven at 105°C overnight to evaporate any remaining water. The dried powder samples were ground to fine powder in a tungsten carbide mill and sent to the Southwest Research Institute (SwRI) for Re analysis by KOH fusion/inductively coupled plasma-mass spectrometry (ICP-MS).

For Test 3, the first leach with dilute nitric acid was performed exactly the same as Test 2 up to the DIW rinse. The second extraction used the following procedure: a 50:50 solution of ammonium hydroxide (~30 mL) and DIW (~30 mL) was mixed with the CRB in a beaker along with 8 mL of 30% hydrogen peroxide (referred to as the NH₄OH leach). The mixture was then stirred for an hour to allow the solution to dissolve the ReO₂ if present in the CRB. After stirring, the fluid contents were vacuum-filtered and

(a) Based on the KCl solution resistance data as a function of concentration, it is calculated that the 9 kΩ corresponds to roughly 5.2 mg/L for K (this was the same range as Na concentration in the leach solution). The increase of K concentration by 50% to 7.8 mg/L would result in the decrease of electrical resistance to 6.6 kΩ.

rinsed into another beaker. The solution was then evaporated at moderate temperatures on a hot plate to 1.5 to 2 mL of condensed solution. The condensed solution was poured into a vial and diluted with DIW to exactly 10 mL, which was sent for Re analysis. Similar to Tests 1 and 2, the CRB powder samples were dried in a drying oven at 105°C overnight, ground to fine powder in a tungsten carbide mill, and sent to SwRI for Re analysis by KOH fusion/inductively coupled plasma-mass spectrometry (ICP-MS).

Table 7.2 summarizes the Re analysis results from the comparison tests. The soluble Re from the first leach was lower when DIW was used (Test 1) compared to dilute nitric acid (Tests 2 and 3). The agreement between the two dilute nitric acid leaches is good, indicating that the CRB powder was well homogenized. These results indicate that dilute nitric acid leach provides a little more aggressive leach condition than DIW. The soluble Re from the second leach was the same for all three tests. The DIW leach was comparable to two other tests, likely because the first leach left more soluble Re. There was no difference between a second leach with dilute nitric acid or a second leach with NH₄OH, indicating that there was not a significant amount of ReO₂ present in the CRB pores.

For Tests 2 and 3, the second leach resulted in 33% of the Re from the first leach on average, which suggests that, if the same rate is assumed for further leaches, about 99% of all potential soluble Re will leach out after four repeated leach and wash steps. The same calculation indicates that the present two-step leach would result in 67% of total Re in the first leach and 89% of the total after the second leach. After reviewing the results, it was decided to use a one-step leach process with a larger volume of dilute nitric acid (45 mL versus 15 mL), longer leach times (48 h versus 24 h), and added stirring. The one-step leach is preferred to save time and reduce analytical costs.

Table 7.2 shows that the soluble Re is less than 10% of the insoluble Re for all tests. This could indicate that the Re formed “insoluble” glassy phases in the CRB, or Re could be an impurity in the CRB materials. The average of insoluble Re was 391 µg/kg with a relative percent standard deviation of 17.3%.

Table 7.2. Soluble and Insoluble Re Concentrations from CRB (in µg/kg)

Test	Soluble Re, µg/kg			Insoluble Re, µg/kg
	1 st leach	2 nd leach	Total	
Test 1 (DIW - DIW)	15.5	7.6	23.1	468
Test 2 (Dilute HNO ₃ - Dilute HNO ₃)	22.4	7.4	29.8	366
Test 3 (Dilute HNO ₃ - NH ₄ OH)	23.4	7.5	30.9	340
Blank CRB*	-	-	-	<239

* Taken from engineering-scale test^(e) CRB (upper part of the outside wall) used in zirconia test settling that did not have Re. Leach tests were not performed.

(e) D Kim, MJ Schweiger, JV Crum, BP Tinsley, PR Hirma, and ML Elliott. 2005. Letter report (Unpublished), Estimation of ZrO₂ Dissolved in Engineering-Scale-ZrO₂ Test Products, Pacific Northwest National Laboratory, Richland, WA.

7.5 Re and MIS Profile Analyses in FS-38B CRB

7.5.1 Procedure

The CRB sample sections were cut into increments ~1 cm deep starting at the glass/CRB interface (or inner surface in the case of Section 1) up to the depth determined based on SEM-EDS results discussed in Section 7.3.

- ~4 cm for the CRB taken from ~38.1 cm above the melt line (Sample #1 in Figure 7.3)
- ~8 cm for the CRB taken at the melt line (Section #3)
- ~15 cm (entire depth), for the CRB taken from ~15.2 cm below the melt line (Section #4).

Each CRB sample piece was an ~1-cm cube, with allowances for material losses during the cutting process. The cutting process was done by low-speed diamond-chip-bladed saws without using any form of lubricant as discussed earlier.

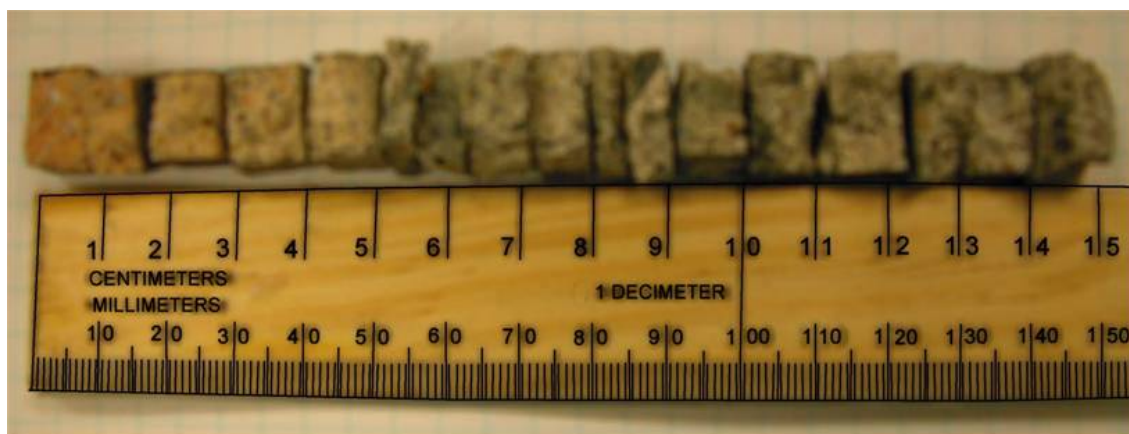


**Figure 7.10. CRB Pieces Taken from ~15.2 cm Below the Melt Line
(lined up from glass/CRB interface on left to outer wall)**

Figure 7.10 displays the 15 CRB cut pieces taken from ~15.2 cm below the melt line. As illustrated in Figure 7.10, the CRB pieces are not exactly cube shaped or the same size because of the difficulty in cutting hard materials without using water. Each sample was crushed in the tungsten carbide mill for 3 s. The grinding time was not adjusted for sample size. Overall, the mass of ground CRB ranged from 2.72 g to 5.08 g. The tungsten carbide mill was thoroughly cleaned after each grinding to prevent possible cross contamination.

For the extraction test, 45 mL of 0.001 M HNO₃ and the ground CRB samples were added to a clean Teflon vessel. The test assembly was mixed for 48 h at room temperature by rotating the Teflon vessel at 45 rpm in a ball mill roller. After the 48-h test, the extraction solution was decanted and filtered using a clean 10-mL syringe and a 0.45- μ m filter. A solution sample of ~20 mL was sent out for Re analysis by ICP-MS and Na, and S analysis by ICP-atomic emission spectroscopy (AES). The ground CRB sample was rinsed with DIW to remove the residual extraction solution.

For the two samples taken from ~15.2 cm below the melt line (the sample from 2 to 3 cm and the sample from 11 to 12 cm), another extraction with 45 mL of 0.001 M HNO₃ was performed after completing the first extraction and DIW rinse to check how much additional soluble Re remained after the first extraction. After the second 0.001 M HNO₃ extraction was complete, the ground CRB sample was prepared and rinsed as described in the previous paragraph.

The ground CRB samples were dried overnight in a 90°C drying oven, finely ground for 2 min in the tungsten carbide mill, and sent to SwRI for analyses. The tungsten carbide mill was thoroughly cleaned after each grinding to prevent possible cross contamination.

7.5.2 Results and Discussion

Table 7.3 displays the analytical results of Re, Na, and S concentrations for those samples with duplicate analyses. Table 7.3 shows that the reproducibility of analyses is good with a relative percent difference (RPD) of 10% or smaller except for the Re concentration in one blank sample, which may be explained by a low Re concentration close to the equipment detection limit.

Table 7.4 summarizes the concentrations of Re, Na, and S in the leach solutions (soluble) and in the ground CRB samples after leaching (insoluble). The concentrations of soluble components are given in units of µg (for Re) or mg (for Na and S) of each element per kg of CRB so that direct comparison with the concentrations in the ground CRB can be made. The average is given for duplicate analyses.

As seen in Table 7.4, the blank CRB contained a significant concentration of soluble Re in addition to soluble Na and S. Similar high concentrations of soluble Re in CRB blanks were also observed from the CRB centrifugal extraction study (Cooley et al. 2006) as summarized in Table 7.5.^(f) The “Heat Treated Manufactured Blank” samples were prepared from the same manufacturer’s lot number as used in this study, but different pieces of cylinder were used. The two “Heat Treated Manufactured Blank” samples had essentially the same soluble Re concentration. However, the FS-38A blank samples had highly variable Re concentrations that ranged from 0.58 to 18.9 µg/kg with an average of 6.7 µg/kg. This confirms that the material itself had non-negligible background levels of soluble Re with high variations. The heat-treated CRB blank tested in this study had a comparable level of soluble Re to those from FS-38A. The untreated blank in this study had higher soluble Re than any blanks tested by Cooley et al. (2006).

The CRB centrifugal extraction method uses a larger sample size, ~500 g^(g) compared to ~4 g for the thin-section method, but it still had substantial variations, which may signify that the distribution of Re within the CRB is extremely inhomogeneous.

The heat-treated CRB in this study had lower concentrations of all three elements than the untreated CRB. This could possibly be the result of the soluble species that were present on the inside surface of the open pores escaping during heat treatment. However, based on the variations found in the CRB samples in the

(f) Engineering-scale (ES) results are not included because the high Re results were suspected to result from potential contamination from previous Re spiked tests.

(g) Based on a typically sized CRB of 2 × 2 × 3 in. (5.1 × 5.1 × 7.6 cm) with a bulk density of 2.5 g/cm³.

study of the centrifugal extraction method, the difference between heat-treated and untreated samples could be within the range of variation of the samples.

The blank CRB contained 0.67 mg/kg total Re (soluble plus insoluble) on average compared to 3.1 and 6.3 mg/kg Re measured in FS-38B and 38C glasses (average from six samples taken from different locations; 8.1 mg/kg Re target for FS-38B and 38C glasses), which signifies that CRB contains roughly 10% of the Re in full-scale test glasses. The background level of Re in soda-lime glass frit and Hanford soil measured within the study of FS-38C was 0.45 and 0.76 mg/kg, respectively, which is comparable to the present CRB blank results. This may suggest that the 0.67 mg/kg Re level is the typical background concentration found in these materials.

The concentration of insoluble Na and S in the blank CRBs given in Table 7.4 (153 mg/kg Na and 21 mg/kg S on average) corresponds to oxide concentrations of 0.13 wt% Na₂O and 0.03 wt% SO₃.

The average values from the two blank samples measured in this set of tests were used as a basis for background soluble and insoluble Re, Na, and S concentrations for the interpretation of test results. The Na concentration in the heat-treated blank CRB was less than the reporting limit of 69.4 mg/kg. Half of this reporting limit was used as the assumed value for this sample in calculating the average.

As mentioned earlier, the CRB samples used in this study were collected from the same CRB pieces that were used in the centrifugal extraction study (Cooley et al. 2006) so that direct comparisons can be made. Table 7.6 compares the concentration of soluble Re obtained by two different methods for the FS-38B samples collected from similar locations (from the same piece in Figure 7.3). Sample #2 was not measured in this study, but the data by Cooley et al. (2006) are included in Table 7.6 for reference. The results from each cube were averaged to obtain the inner and outer ~7.5-cm results. The data from the thin-section method for the above the melt line sample (measured up to 4 cm depth only) were calculated assuming that the rest of samples not analyzed had the same soluble Re concentration as the averaged blank. For outer half results for Samples #1 and #3, the blank results are included as a reference. Table 7.6 shows that there is a reasonable agreement in the general trend of the Re distribution for the CRB samples taken at and below the melt line, although there are large differences in value-to-value comparisons.

Table 7.3. Summary of Duplicate Analytical Results

In leach solutions (soluble)							
Sample ID	Sample Description	Analyzed concentration			RPD, %		
		Re (µg/L)	Na (mg/L)	S (mg/L)	Re	Na	S
CRBASHT	Blank	0.681	<5.00	0.619	30.3%	-	3.6%
Duplicate		0.924	<5.00	0.597			
S1CRB01	~38.1 cm above ML, 0 - 1 cm	38.4	9.18	-	0.0%	1.1%	-
Duplicate		38.4	9.08	-			
S4CRB12	~15.2 cm below ML, 1 - 2 cm	-	-	0.583	-	-	1.2%
Duplicate		-	-	0.576			
S4CRB1314	~15.2 cm below ML, 13 - 14 cm	-	-	48.6	-	-	0.6%
Duplicate		-	-	48.9			
In remaining CRB particles (insoluble)							
Sample ID	Sample Description	Analyzed concentration			RPD, %		
		Re (µg/Kg)	Na (mg/Kg)	S (mg/Kg)	Re	Na	S
S1CRB23G	~38.1 cm above ML, 2 - 3 cm	<481	1260	106	-	3.9%	1.9%
Duplicate		<483	1310	104			
S4CRB1415G	~15.2 cm below ML, 14 - 15 cm	480	1490	97	10.1%	0.0%	3.0%
Duplicate		531	1490	100			
ML: melt line							
RPD: relative percent difference (the absolute value of difference was divided by the average of two)							

Table 7.4. Concentrations of Re, Na, and S in Leach Solutions (soluble) and in Remaining CRB Particles (insoluble) (in μg or mg of element per kg of CRB)

Distance ^(a) (cm)	Soluble			Insoluble		
	Re ($\mu\text{g}/\text{kg}$)	Na (mg/kg)	S (mg/kg)	Re ($\mu\text{g}/\text{kg}$)	Na (mg/kg)	S (mg/kg)
FS-38B CRB ~38.1 cm above the melt line						
0.5	340	912	409	707	4110	156
1.5	27.5	240	105	571	2240	112
2.5	21.6	86.5	172	<481	1285	105
3.5	15.5	59.5	185	565	956	111
FS-38B CRB at the melt line						
0.5	5243	1104	376	4530	9240	271
1.5	52.9	160	76.4	719	1900	92.6
2.5	28.3	<56.5	87.6	523	1040	88.2
3.5	14.2	<58.5	131	721	879	94.2
4.5	14.6	73.3	298	<465	880	107
5.5	18.6	<63.4	254	531	912	149
6.5	11.7	<77.0	462	639	883	103
7.5	12.9	<82.9	262	<464	837	98.2
FS-38B CRB ~15.2 cm below the melt line						
0.5	43.7	117	17.8	<483	21500	222
1.5	20.0	59.8	7.29	647	18000	87.9
2.5	21.2	62.7	10.5	589	15500	74.8
3.5	25.3	47.6	9.90	<480	13600	77.1
4.5	52.7	32.2	783	<481	9970	139
5.5	4.17	6.59	8.09	<490	1220	<49.7
6.5	6.83	6.40	16.2	<466	974	<49.4
7.5	5.16	6.96	29.0	<458	962	<49.0
8.5	6.09	6.47	86.3	525	927	57.6
9.5	7.11	7.35	194	<493	989	69.3
10.5	10.6	6.28	333	<465	1100	109
11.5	24.4	7.97	605	482	805	85.3
12.5	58.5	8.46	760	688	1020	83.4
13.5	133.1	9.63	783	589	919	98.1
14.5	130.2	21.6	180	506	1490	98.5
Blank CRB^(b)						
No HT	34.3	271	33.3	569	735	179
HT ^(c)	11.1	<69.4	8.44	726	1260	85.8
(a) Average distance from the glass/CRB interface for each $\sim 1 \text{ cm}^3$ cubes of CRB. (b) The same CRB as used in capillary tests described in Section 5.0 (separately manufactured). (c) Heat treated (HT) at 1100°C for 8 h.						

Table 7.5. Soluble Re Concentration in CRB Blanks Determined by Centrifugal Extraction Method (Cooley et al. 2006)

Description	Sample ID	Re ($\mu\text{g}/\text{kg}$)
Untreated Refractory	Refractory Blank	0.17
Heat-Treated Manufactured Blanks	MF-BLK-01	1.04
	MF-BLK-02	0.98
FS-38A Full-Scale Blanks	FS_38A_01 Inner Segment	18.79
	FS_38A_01 Outer Segment	5.72
	FS_38A_01 Sample Average	12.11
	FS_38A_02 Inner Segment	0.58
	FS_38A_02 Outer Segment	1.78
	FS_38A_02 Sample Average	1.08

Table 7.6. Comparison of Soluble Re Concentrations by Two Different Methods for the FS-38B CRB Samples Taken from Similar Locations (in μg Re/kg CRB)

CRB Location ^(a)	Extraction Method (Cooley et al. 2006)			Thin Section Method (this study)	
	Sample ID	Inner Sample	Outer Sample	Inner ~7.5 cm	Outer ~7.5 cm
Above melt line (Sample #1)	FS-38B-01	5	21	65.0	~23 ^(b)
	FS-38B-02	5	38		
Above melt line (Sample #2)	FS-38B-03	24	54	NA	NA
	FS-38B-04	14	29		
At melt line (Sample #3)	FS-38B-05	1197	14	674	~23 ^(b)
	FS-38B-06	989	73		
Below melt line (Sample #4)	FS-38B-07	49	516	22.4	46.9
	FS-38B-08	33	105		

(a) Sample # is as given in Figure 7.3.
(b) Not analyzed by thin section method. Assumed to be similar to the blank CRB based on SEM-EDS examination.
NA: not analyzed.

Figure 7.11 and Figure 7.12 display the concentration of soluble (Figure 7.11) and insoluble (Figure 7.12) Re, Na, and S as a function of distance from the inside wall in the CRB samples from ~38.1 cm above the melt line. The soluble components penetrated up to ~2 cm for Na and up to ~1 cm for Re, whereas S was higher than the blank level in all four samples tested up to ~4 cm. However, the change of all three soluble components had the same trend in that they were high in the first 1-cm layer and drop to the level of the blank or become relatively constant (this could be background level for the CRBs in this study). This observation suggests that Re penetrates through volatilization only to the thin surface layer, which seems to be the case for Na and S too. The concentrations of insoluble components were very close to the blank level for both Re and S for all four samples. However, the concentration of insoluble Na is higher than the blank level up to ~2 cm. It is possible that this high level of Na was due to volatilization from the clean glass feed that does not contain Re or S at the final stage of feed processing. This explanation suggests that Na that volatilized from the clean glass feed reacted with CRB materials to form insoluble

phases (e.g., glass) at the pore surface but did not dissolve the soluble Re and S that were present (presumably in the salt form) at 340 µg/kg for Re and 409 mg/kg for S.

Figure 7.13 and Figure 7.14 show the concentration of soluble (Figure 7.13) and insoluble (Figure 7.14) Re, Na, and S as a function of distance from the glass interface in the CRB samples from at the melt line. The soluble components were detected above the CRB blank levels only at the surface layer to ~1 cm for all three components. They were more than 10 times higher in concentration than the ~38.1 cm above the melt line material for Re and had a similar concentration as the ~38.1 cm above the melt line material for Na and S. However the concentration of S initially decreased to nearly the blank level but tended to increase as the distance increased. The insoluble Re and Na were higher than the blank up to 1 or 2 cm, and the insoluble S was close to the blank level for all samples. Overall, the trend is similar to the ~38.1 cm above the melt line sample but with a much-higher concentration of soluble and insoluble Re. The soluble Re was comparable to the insoluble Re level. This high level of Re may suggest that the Re was soaked into CRB via liquid MIS (initially by vapor deposition), indicating that this final melt line was covered by the melting feed for part of the processing time. In addition, the separated salt layer (mainly sodium sulfate) that formed on the surface of the FS-38B melt was likely the reason for the high concentration of Re in the CRB at the glass surface. The operational challenges experienced in FS-38B resulted in the extensive formation of the salt layer concentrated with Re (Cooley et al. 2006).

Figure 7.15 and Figure 7.16 display the concentration of soluble (Figure 7.15) and insoluble (Figure 7.15) Re, Na, and S as a function of distance from the glass interface in the CRB samples from ~15.2 cm below the melt line. The soluble Na was below the blank level for all 15 samples. The soluble Re and S showed similar trends in that both had a spike in concentration at the sample at 4 to 5 cm and a second increase to concentrations above the blank level at 8 to 9 cm for S and at 12 to 13 cm for Re. Re was also higher than the blank level in the 0- to 1-cm sample. The insoluble components, Re and S, were close to the blank level or lower for all 15 samples, whereas the concentration of Na was high at the glass interface and gradually decreased to the blank level at the 5- to 6-cm sample. The highest concentration of insoluble Na at the 0- to 1-cm sample (21,500 mg/kg) corresponds to 2.9 wt% Na₂O in the CRB.

If the 15% open porosity is completely filled with glass, the concentration in the CRB is 2.9 wt% Na₂O, which is a good agreement with the highest Na concentration at the interface. This suggests that the observed trend of high concentration of Na at the glass interface and a gradual concentration decrease as the distance from the surface increases is the result of glass-forming melt penetrating into the CRB pores. CRB components dissolving in the glass will make the glass viscosity higher, slowing further penetration into the CRB.

If the Re peak at the 4- to 5-cm distance sample is excluded as an exception, it is speculated that, for the CRB below the melt line, the glass flows into open pores and pushes the soluble Re that was present close to the inside wall towards the outside wall; that is, the glass does not dissolve S or Re as it penetrates.

If the CRB that contains 648 µg/kg insoluble Re (measured in blank CRB) and has 15% open porosity is completely filled with glass that contains 3100 µg/kg Re (measured in 38B glass), the resulting glass-filled CRB would have a Re concentration of 992 µg/kg. However, the measured insoluble Re concentration in the entire sample of CRB from ~15.2 cm below the melt line was <700 µg/kg, suggesting that it is unlikely that the glass within the CRB has a higher Re than the bulk of the 38B glass. This result refutes earlier assumptions that MIS penetrates into open pores of the CRB and forms a glass layer that

contains high a concentration of insoluble Re. The high concentration of insoluble Re is a more likely result due to a high insoluble Re blank level.

The observed high concentration of soluble Re towards the outside of the CRB suggests that some portion of Re may have passed through the CRB and deposited in the sand layer. However, the sand in 38B was not analyzed.

Figure 7.17 through Figure 7.19 display the concentrations of Re (Figure 7.17), Na (Figure 7.18), and S (Figure 7.19) as a function of distance from the glass interface in the CRB samples from different locations. Both soluble and insoluble forms are plotted in a logarithmic scale.

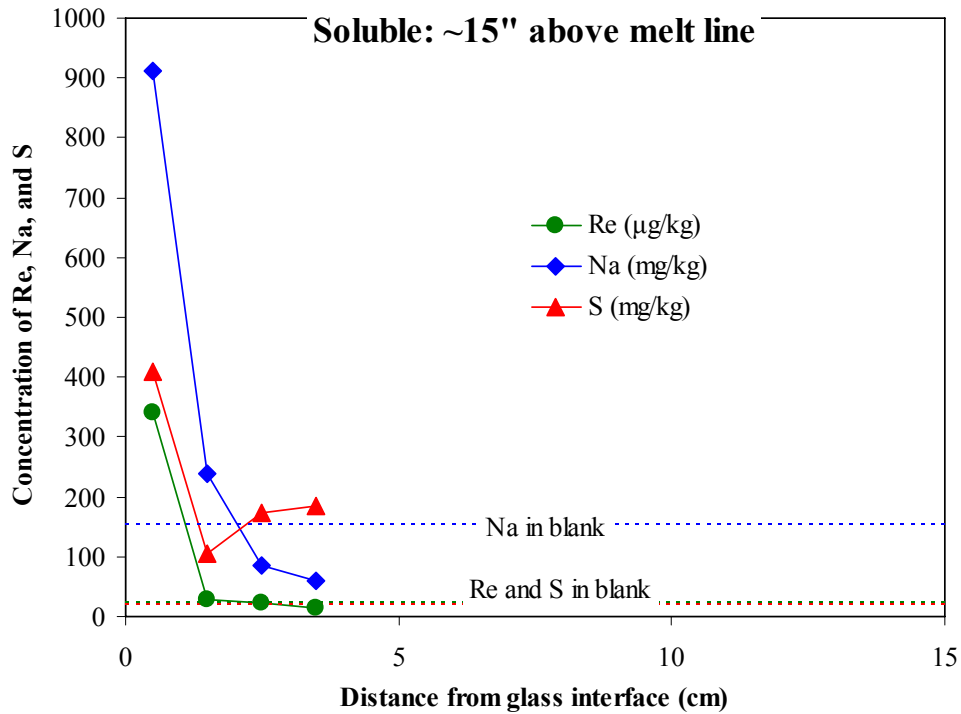


Figure 7.11. Concentration of Soluble Re, Na, and S in the CRB ~38.1 cm Above the Melt Line

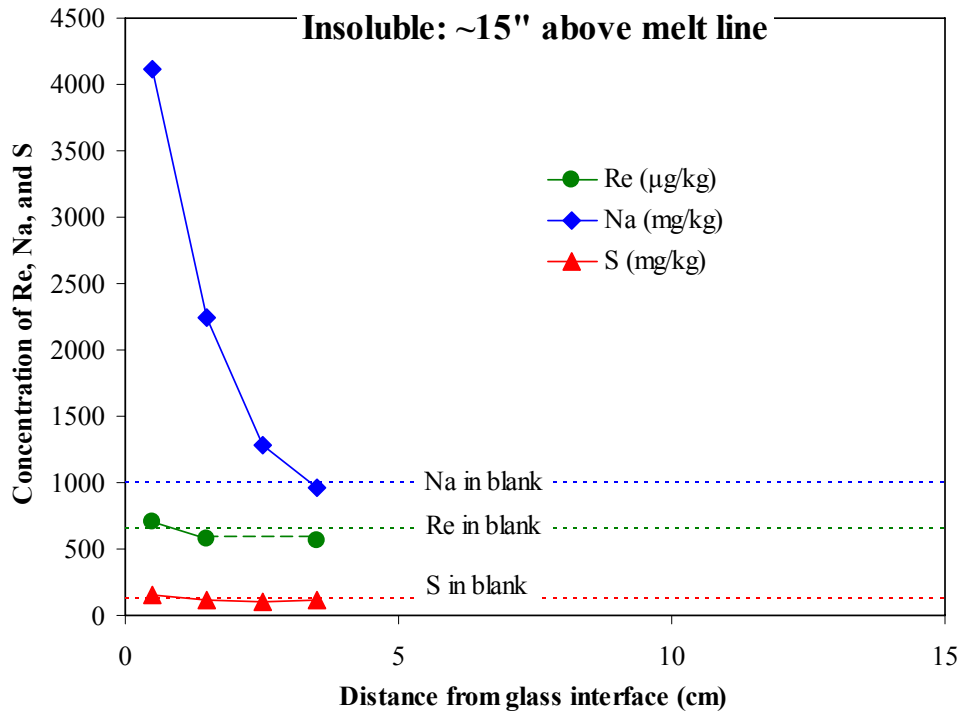


Figure 7.12. Concentration of Insoluble Re, Na, and S in the CRB ~38.1 cm Above the Melt Line

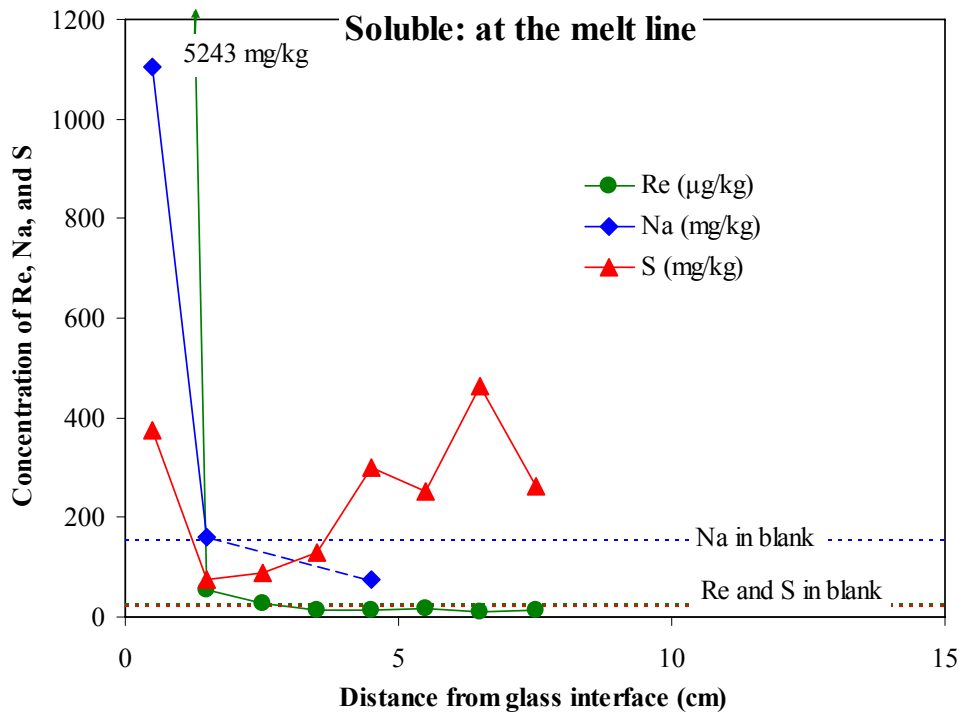


Figure 7.13. Concentration of Soluble Re, Na, and S in the CRB at the Melt Line

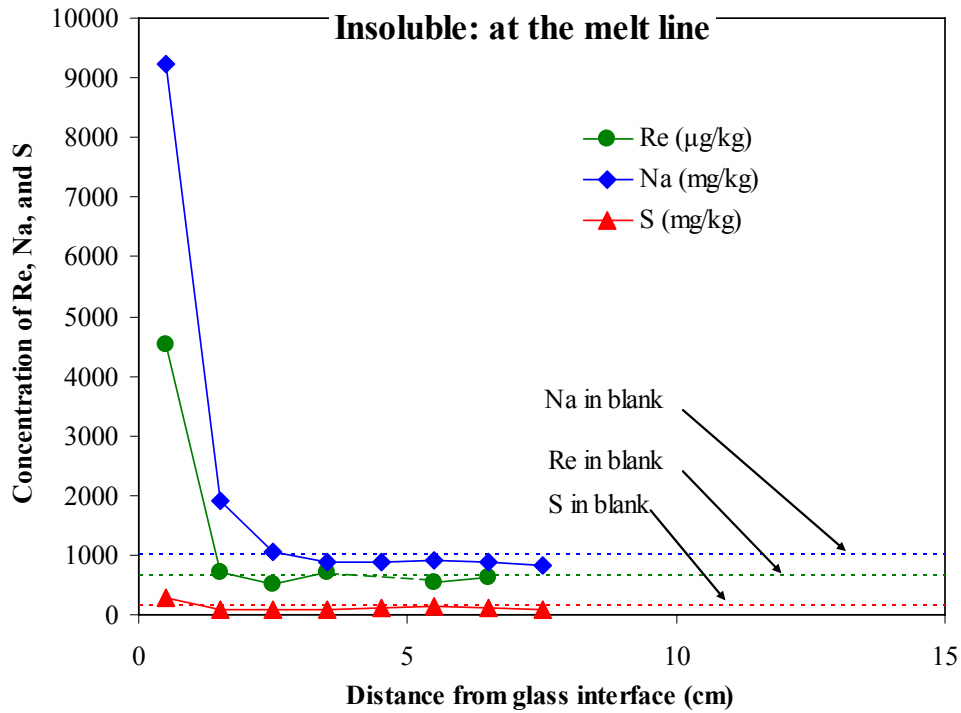


Figure 7.14. Concentration of Insoluble Re, Na, and S in the CRB at the Melt Line

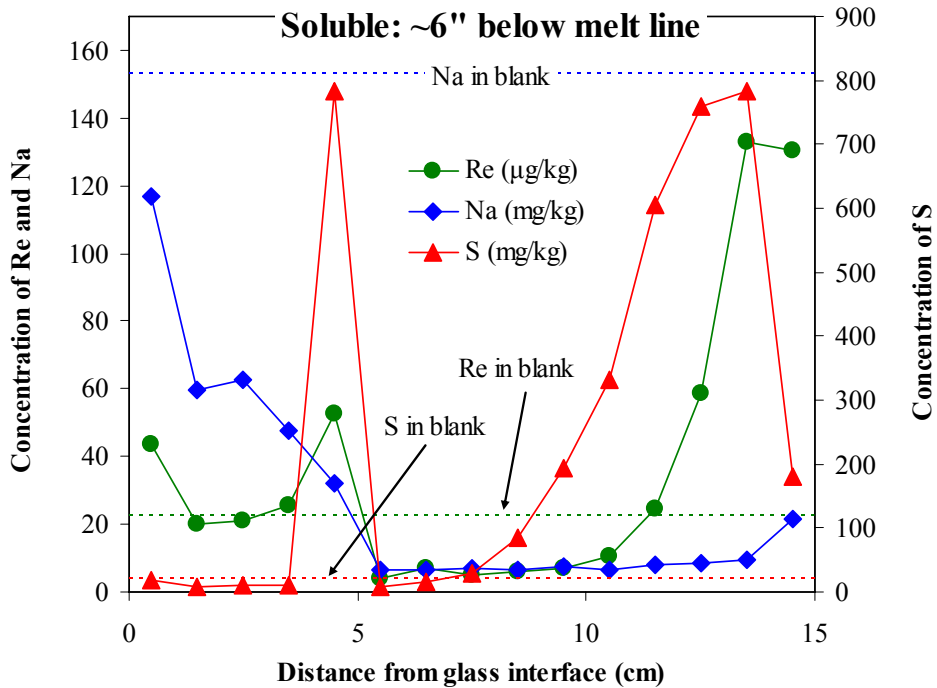


Figure 7.15. Concentration of Soluble Re, Na, and S in the CRB ~15.2 cm Below the Melt Line

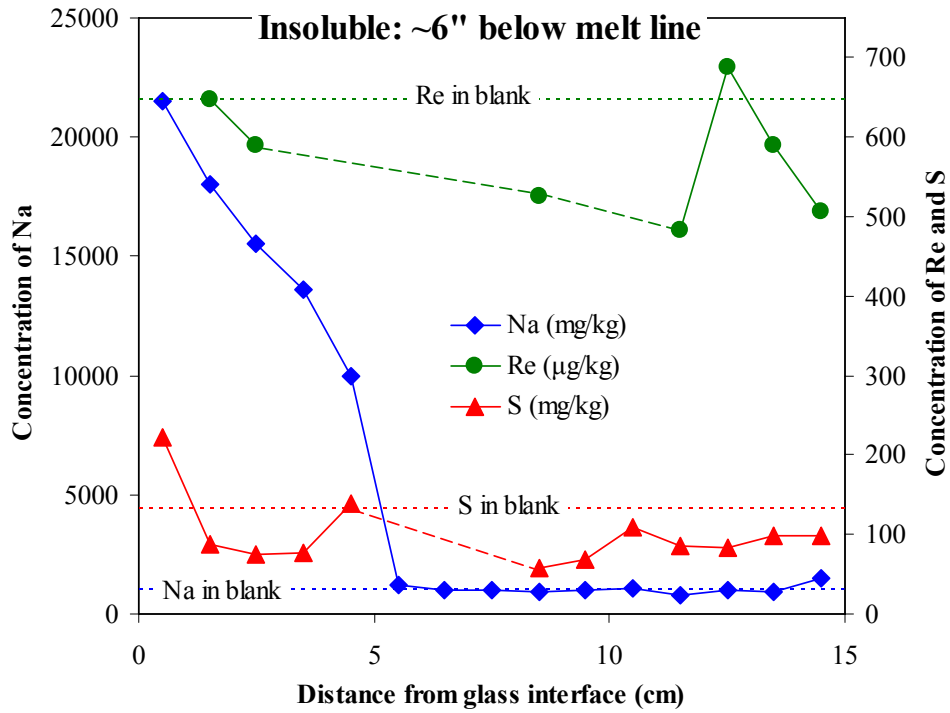


Figure 7.16. Concentration of Insoluble Re, Na, and S in the CRB ~15.2 cm Below the Melt Line

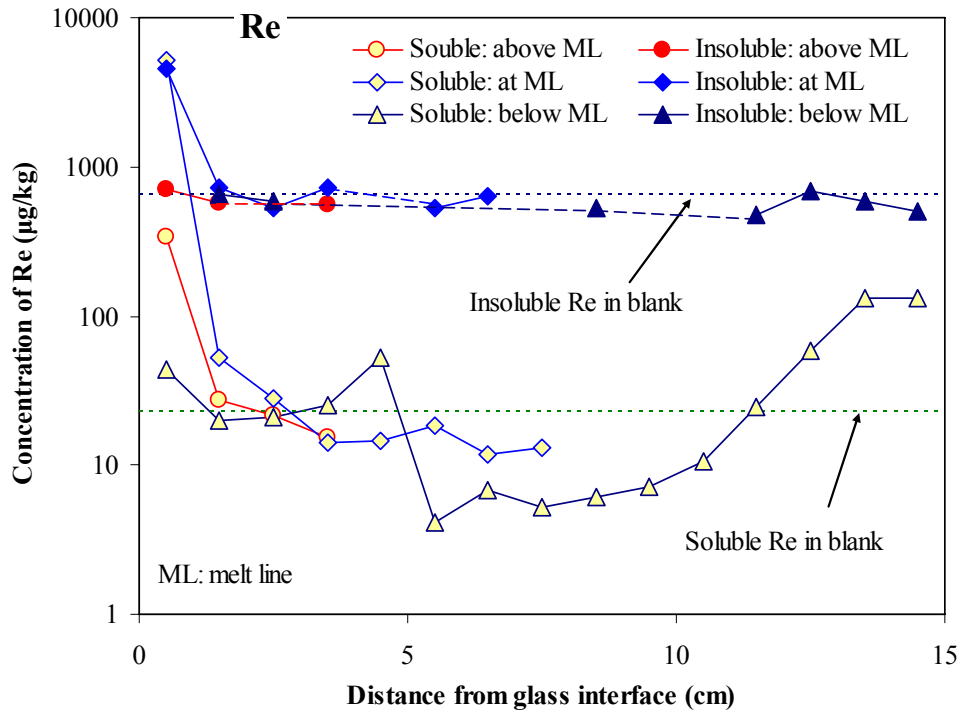


Figure 7.17. Concentration of Re in the CRB Samples from Different Locations

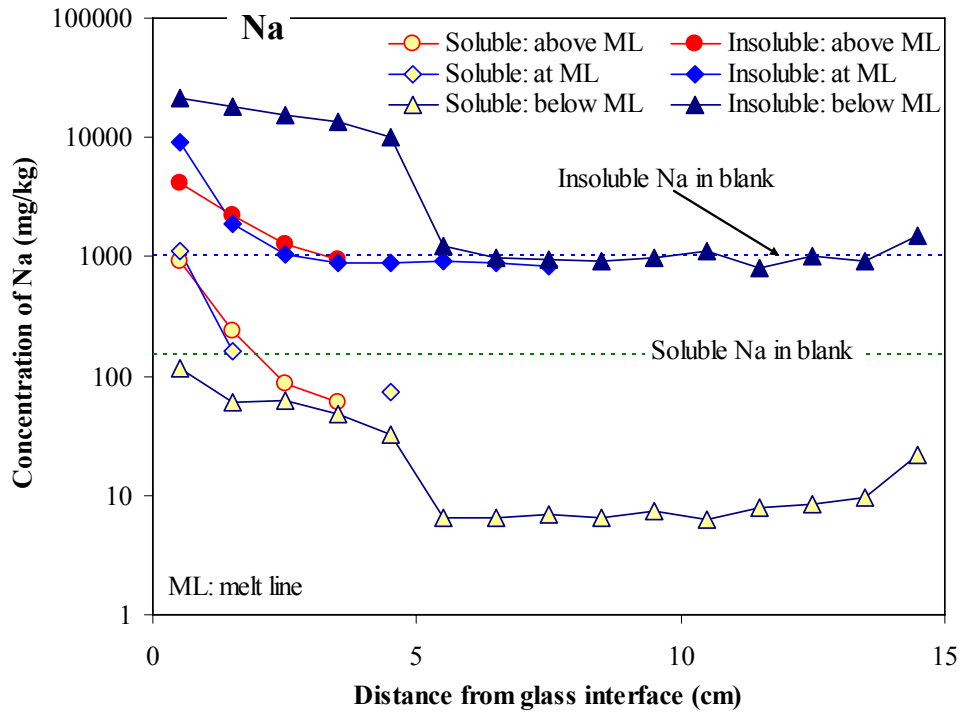


Figure 7.18. Concentration of Na in the CRB Samples from Different Locations

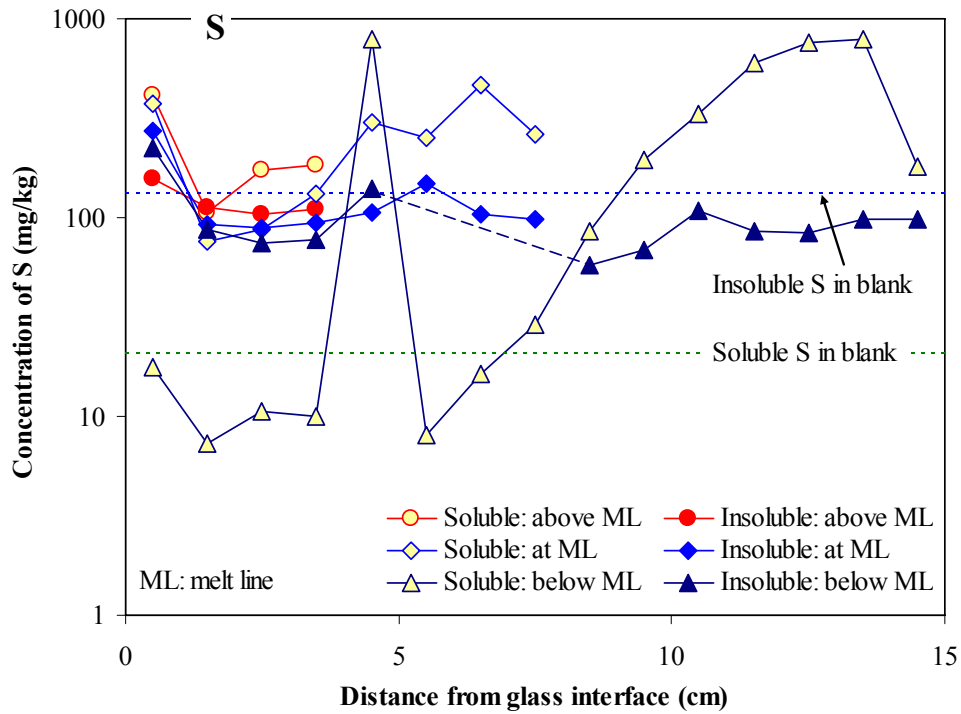


Figure 7.19. Concentration of S in the CRB Samples from Different Locations

7.6 Summary

In summary, for the CRB samples from above the melt line and at the melt line, soluble Re is present only up to ~2 cm from the glass interface. For the CRB above the melt line, Re appears to penetrate into the CRB through a vapor disposition mechanism; that is, Re deposits when the CRB is cold, becomes molten as the temperature increases, and then penetrates further into the CRB by capillary action. The extent of penetration and the concentration of Re above the melt line is small. For the CRB at the melt line, Re penetrates into the CRB through both vapor deposition at the early stages of processing and then liquid MIS formation and penetration at later processing stages. The CRB at the melt line close to the glass interface had the highest soluble Re concentration. For the CRB below the melt line, a relatively low concentration of soluble Re is present on the surface layer while a higher concentration of soluble Re is observed in the outer layer close to the CRB/sand interface. Insoluble Re at a higher concentration than the blank level was observed only in the first 0- to 1-cm layer of the CRB at the melt line. The below melt line results indicate that regions of the CRB that experience Re penetration through MIS migration early in the process that are subsequently covered by the progressing melt do not incorporate the Re in an insoluble melt phase but instead push the Re salt outward through evaporation and/or melting and flow of molten salt.

8.0 Modeling of Tc/Re Penetration of CRB

This section documents a series of calculations and model-building efforts aimed at understanding the mechanisms by which Tc or Re might concentrate in the CRB during melting and the scaling principles that control the process. The primary effort has been directed toward the formation and flow of molten ionic salt.

8.1 Saturation of the Feed by Molten Ionic Salt

MIS cannot flow into the CRB in any volume unless it effectively saturates the particulate medium in which it forms.^(h) MIS is expected to form in the dry feed as the highly miscible salts melt and flow together. Until the MIS fills or saturates the pore space between the unmelted solid particles such that the liquid can develop a hydrostatic pressure, very little of it can flow into the CRB lining the melter. Effective liquid saturation, where not all the pores are liquid filled, but the liquid can develop hydrostatic pressure, should occur above a liquid volume fraction of ~ 0.3 .⁽ⁱ⁾ Figure 8.1 illustrates effectively unsaturated and saturated conditions.

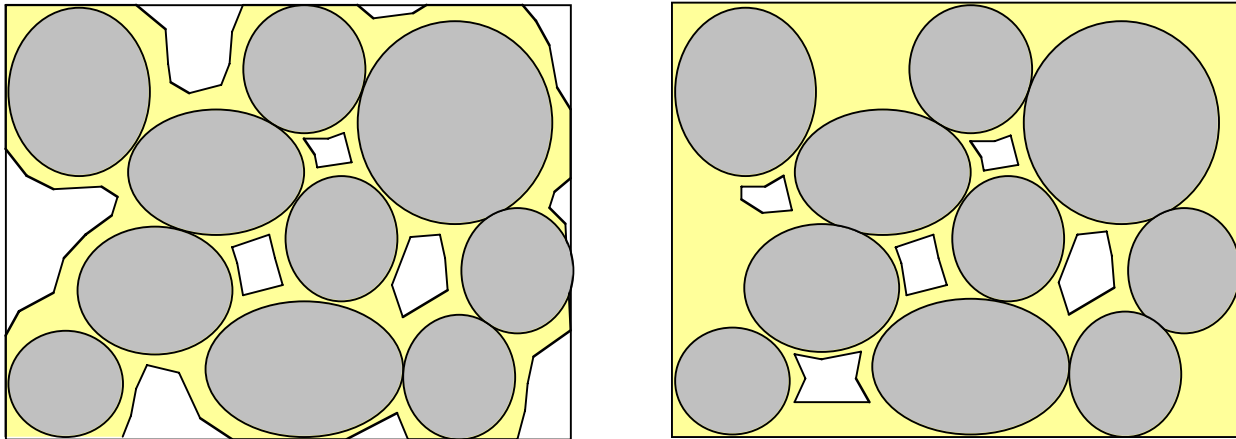


Figure 8.1. Solid Matrix Unsaturated (left) and Effectively Saturated (right) with Liquid

To determine whether MIS saturates the feed, a model of the melting process with a simple algorithm that tracked the mass and volume of solid and liquid and the void volume was constructed. Each solid species was assumed to become liquid at its melting-point, for the most part ignoring chemical reactions and eutectic liquid formation at lower temperatures (exceptions will be described later). This is conservative in that including these effects would increase the amount of liquid available, possibly indicating saturation at lower temperatures.

(h) Effective saturation is achieved when the liquid phase is sufficiently connected to establish a hydrostatic pressure gradient that can drive flow.

(i) A close-packed array of uniform spheres has a porosity of 0.26 and a square array of 0.476. A randomly packed array of spheres averages a porosity of 0.36. Non-uniform spheres pack more closely because small ones fill the space between the larger, but beds of non-spherical ground crystalline solids would have higher porosities.

The algorithm assumed that the total mass of solid per unit initial mass of feed decreased by the mass fraction of the melting component, and the total mass of liquid per unit initial mass of feed increased by the same amount. The total volume of solid per unit initial mass of feed decreased by the melting component's mass fraction divided by its solid density and the total volume of liquid per unit initial mass of feed increased by the same amount, conservatively ignoring any volume change on melting. Assuming that each solid particle supported other particles, the melting of a particle causes the bed to contract, removing a void volume equal to the volume of the solid melted. This process has been observed experimentally^(j) and is illustrated in Figure 8.2.

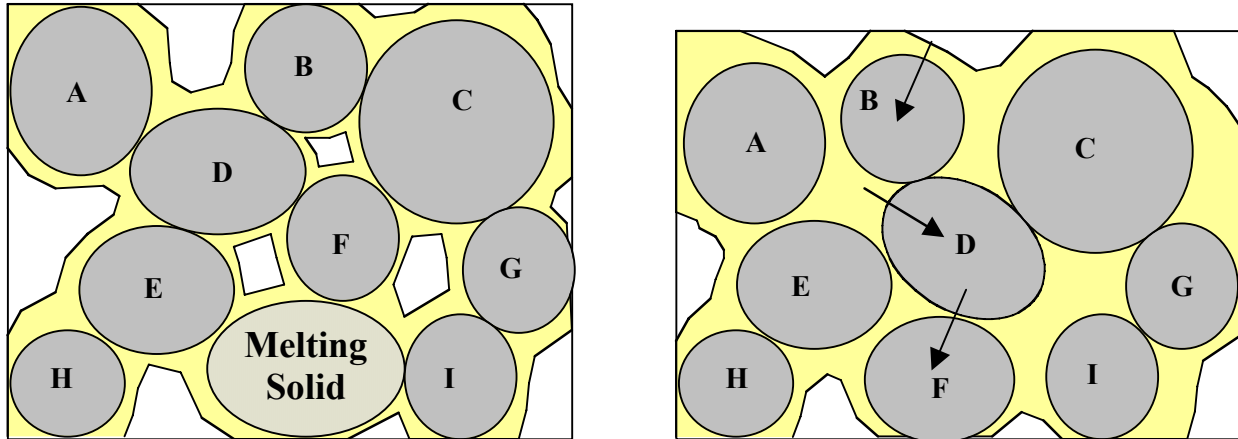


Figure 8.2. Melting Model: Melting Solid (left) Reduces Feed Volume (right) (solids were labeled A through I so that migrating solids can be easily tracked)

8.1.1 Feed Composition and Physical Properties

The feed in this study is a mixture of dry LAW simulant, Hanford soil, and other glass additives as given in Table 8.1. The composition of the LAW simulant was given in Table 4.1. The overall composition of the low-melting temperature (<1000°C) components of initial feed is given in Table 8.2, arranged by melting point. The mass fraction of a component in the mixture (Table 8.2) is the product of the mass fraction of the component in the LAW simulant (Table 4.1) and the mass fraction of the submixture in the bulk feed (Table 8.1). The soil is assumed to be inert in the MIS temperature range.^(k) The volume per unit mass of initial feed of a component in Table 8.2 is the mass fraction divided by the solid density.

(j) Personal communication with Pavel Hrma, PNNL.

(k) Ibid.

Table 8.1. Overall Bulk Feed Recipe

Component	Name	Mass Fraction
B ₂ O ₃	Boron oxide	0.043
Dry LAW simulant	LAW simulant (dry)	0.347
Re ₂ O ₇	Rhenium oxide	0.00009
Soil	Soil	0.546
ZrO ₂	Zirconium oxide	0.062

Table 8.2. Mixed Feed Composition By Melting Point

No.	Component	Name	Source	Molecular Weight	Melting point (°C) ^(a)	Density (g/mL) ^(a)	Mass Fraction
1	Al(NO ₃) ₃ ·9H ₂ O	Aluminum nitrate nonahydrate	feed + LAW sim	375	73	1.72	0.0409
2	Na ₃ PO ₄ ·12H ₂ O	Sodium phosphate dodecahydrate	LAW sim	380	75	1.62	0.0148
3	Na ₂ C ₂ O ₄	Sodium oxalate	LAW sim	134	250	2.34	0.0012
4	NaNO ₂	Sodium nitrite	LAW sim	69	271	2.17	0.0231
5	Re ₂ O ₇	Rhenium oxide	feed	484	297	6.10	0.0001
6	NaNO ₃	Sodium nitrate	LAW sim	85	307	2.26	0.1549
7	NaOH	Sodium hydroxide	feed + LAW sim	40	323	2.13	0.0504
8	KNO ₃	Potassium nitrate	LAW sim	101	337	2.11	0.0010
9	NaC ₂ H ₃ O ₂	Sodium acetate	LAW sim	82	382	1.59	0.0085
10	B ₂ O ₃	Boron oxide	feed	70	450	2.55	0.0430
11	Na ₂ CrO ₄	Sodium chromate	LAW sim	162	792	2.72	0.0013
12	NaCl	Sodium chloride	LAW sim	58	801	2.17	0.0020
13	Na ₂ CO ₃	Sodium carbonate	LAW sim	106	858	2.54	0.0398
14	Na ₂ SO ₄	Sodium sulfate	LAW sim	142	884	2.70	0.0101
15	NaF	Sodium fluoride	LAW sim	42	996	2.78	0.0011

(a) CRC Handbook of Chemistry and Physics, 71st Ed., 1990 to 1991.

8.1.2 Melt Progression Model

The total initial volume of solids per unit initial mass of feed, $v_{s,f}$, is the sum of the volumes for each component given by:

$$v_{s,f} = \sum_{i=1}^N v_{s,i} = \sum_{i=1}^N \frac{\omega_{s,i}}{\rho_{s,i}} \quad (8.1)$$

Using the values given in Table 8.2, the mixed-feed solid-specific volume calculated using Equation (8.1) is 0.3881 mL/g.

The initial liquid mass and volume fractions are zero. The initial void volume fraction is determined from the bulk density and mass-averaged solids density by:

$$\alpha_f = 1 - \frac{\rho_f}{\rho_{s,f}} = 1 - \rho_f v_{s,f} \quad (8.2)$$

Measurements of the bulk density of the mixed feed samples for FS-38, which is represented by the recipes above, averaged 1.64 g/mL.⁽¹⁾ The average solid density of the feed is simply the inverse of the feed-specific volume given by Equation (8.1) or 2.576 g/mL. Using Equation (8.2) with these densities gives an initial feed void fraction of 0.363, making the initial solid volume fraction 0.637.

The melt progresses through each component, subtracting its mass from the total solid mass and adding it to the cumulative liquid mass at its melting point. Similarly, the component volume is subtracted from the total solid volume per unit initial feed mass, added to the cumulative liquid volume per unit feed mass and subtracted from the total void volume per unit initial feed mass. The masses, volumes, volume fractions, and phase densities are computed by the following equations:

At melting of feed component i at temperature, T_i after component $i-1$ has melted at T_{i-1} :

$$\text{solid mass fraction: } \omega_{s,f}(T_i) = \omega_{s,f}(T_{i-1}) - \omega_{s,f,i} \quad (8.3a)$$

$$\text{liquid mass fraction: } \omega_{l,f}(T_i) = \omega_{l,f}(T_{i-1}) + \omega_{s,f,i} \quad (8.3b)$$

$$\text{total mass fraction: } \omega_f(T_i) = \omega_{s,f}(T_i) + \omega_{l,f}(T_i) \quad (8.3c)$$

$$\text{solid volume: } v_{s,f}(T_i) = v_{s,f}(T_{i-1}) - v_{s,f,i} \quad (8.3d)$$

$$\text{liquid volume: } v_{l,f}(T_i) = v_{l,f}(T_{i-1}) + v_{s,f,i} \quad (8.3e)$$

$$\text{void volume: } v_{g,f}(T_i) = v_{g,f}(T_{i-1}) - v_{s,f,i} \quad (8.3f)$$

$$\text{total volume: } v_f(T_i) = v_{s,f}(T_i) + v_{l,f}(T_i) + v_{g,f}(T_i) \quad (8.3g)$$

$$\text{solid density: } \rho_{s,f}(T_i) = \frac{\omega_{s,f}(T_i)}{v_{s,f}(T_i)} \quad (8.3h)$$

$$\text{liquid density: } \rho_{l,f}(T_i) = \frac{\omega_{l,f}(T_i)}{v_{l,f}(T_i)} \quad (8.3i)$$

$$\text{solid volume fraction: } \alpha_{s,f}(T_i) = \frac{v_{s,f}(T_i)}{v_f(T_i)} \quad (8.3j)$$

$$\text{liquid volume fraction: } \alpha_{l,f}(T_i) = \frac{v_{l,f}(T_i)}{v_f(T_i)} \quad (8.3k)$$

(1) Memo from Renee Russell, PNNL, February 22, 2006, reporting measurements obtained under Test Instruction AMEC-TI-06-02.

$$\text{void volume fraction: } \alpha_{g,f}(T_i) = \frac{v_{g,f}(T_i)}{v_f(T_i)} \quad (m) \quad (8.31)$$

8.1.3 Reactions Affecting Melt Phase Distribution

Equations (8.3a) through (8.31) apply to each component at its melting temperature if there are no reactions that change the mass and volume of liquids and solids. However, several reactions have significant effects on masses and volumes and are accounted for in the calculation. As in the melting process, volumes of individual species formed and consumed are assumed to be conserved in the process. This assumption conservatively leads to a larger liquid volume than would actually occur.

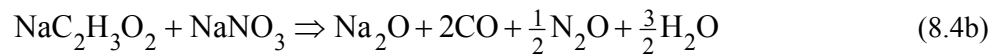
Loss of water of hydration from aluminum nitrate and sodium phosphate: This reaction is assumed to occur between the melting temperatures of these components (73 and 75°C, respectively) and 200°C. Aluminum nitrate loses 9 mole of water for each mole of hydrated aluminum nitrate, and sodium phosphate loses 12 moles per mole. The water released is assumed to leave as a vapor, reducing the liquid mass by the water mass lost and reducing the liquid volume by the value of water mass loss divided by the solid component density (density of mass lost assumed to be that of the original compound).

Sodium oxalate decomposition: Sodium oxalate decomposes or reacts with sodium nitrate/nitrite between 150 to 200°C (Hrma et al. 2005). We assume a direct decomposition of sodium oxalate into sodium oxide and gas via the greatly simplified reaction:



Because there is relatively little oxalate in the feed (see Table 8.2), the exact reaction is not important. The sodium oxalate is assumed to have already melted, and the sodium oxide formed is assumed to exist as a liquid while the gas escapes without affecting the interstitial void fraction.

Reaction of sodium acetate with nitrate and nitrite: In the range of ~300 to 450°C, the sodium acetate from the waste reacts with sodium nitrite, nitrate, and carbonate. It may also decompose into sodium carbonate. Many reactions and chains of reactions are possible, but the following nitrate reaction is assumed to dominate for the purpose of describing the phase distribution:

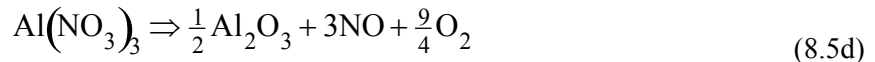
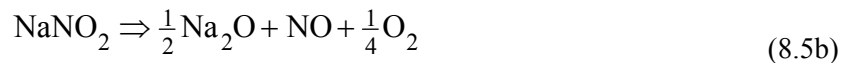
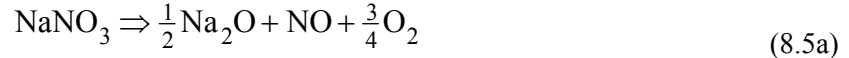


Though the reaction begins below its melting point, we assume that the sodium acetate is already liquid and the sodium oxide produced remains as a liquid. As above, the density of a liquid component, whether reactant or product, is assumed equal to the solid-phase density, and the evolving gas escapes without disturbing the remaining interstitial void volume.

(m) Because the total volume is the sum of the individual phase volumes, the three fractions automatically sum to 1.0.

Eutectic liquid includes salts with higher melting points: As temperatures approach 600°C, where nitrate/nitrite decomposition begins, we assume that some sodium salts with higher melting points are incorporated in a eutectic liquid. These salts are sodium chromate, chloride, carbonate, sulfate, and fluoride. Because the exact temperatures at which these salts join the liquid are not known, all are included at once by repeated application of Equations (8.3a) through (8.3l) for rows 11 to 15 of Table 8.2 at 600°C.⁽ⁿ⁾ The total mass and volume changes computed in this way (negative for solids and positive for liquid) are 0.054 g/g of initial feed with a volume of 0.021 mL/g of initial feed, respectively.

Decomposition of nitrates and nitrites: Beginning about 600°C and completing at about 750°C, nitrate, nitrite, and carbonate salts decompose into oxides and gases. The non-gas products of these reactions are assumed to remain in the liquid. The large volume of gas escaping from the matrix is also assumed to create a large disturbance that releases all remaining interstitial gas so that the void volume within the solid matrix goes to zero (though bubbles may exist in the liquid). Sodium salts are by far the largest contributor, but aluminum nitrate is also included (the small concentration of potassium nitrate is ignored). The reactions are as follows:



8.1.4 Results of the Melt Calculation

Figure 8.3 plots the volume fractions of solids, liquids, and void as a function of temperature. The liquid volume fraction abruptly rises to 0.26 at 323°C when sodium nitrate (15 wt% of the feed) and sodium hydroxide (5 wt%) have melted. The volume fraction reaches 0.34 when boron oxide melts at 450°C. Eutectic liquid forms from compounds with higher melting points, which increases the liquid fraction to 0.41 at 600°C. At this point, nitrate decomposition begins to convert liquid to gas, and interstitial void escapes as the matrix is agitated by gas generation. There is probably enough molten salt available to effectively saturate the solid matrix at temperatures above 450°C and possibly as low as 350°C, which matches experimental observations.^(o) Figure 8.4 shows the phase and bulk densities as a function of temperature. All densities continue to increase as more dense solids melt, and decomposition removes gases. The density of solids left after nitrate decomposition is almost 3.0 g/mL. The corresponding liquid density at 750°C is 2.3 g/mL.

(n) Per personal communication with Pavel Hrma, this temperature may be too high. Laboratory tests indicate that LAW is all melted at 450°C. We do not know what compounds precipitate when liquid LAW is dried during preparation and what kinds of eutectics are formed when it is heated.

(o) Ibid.

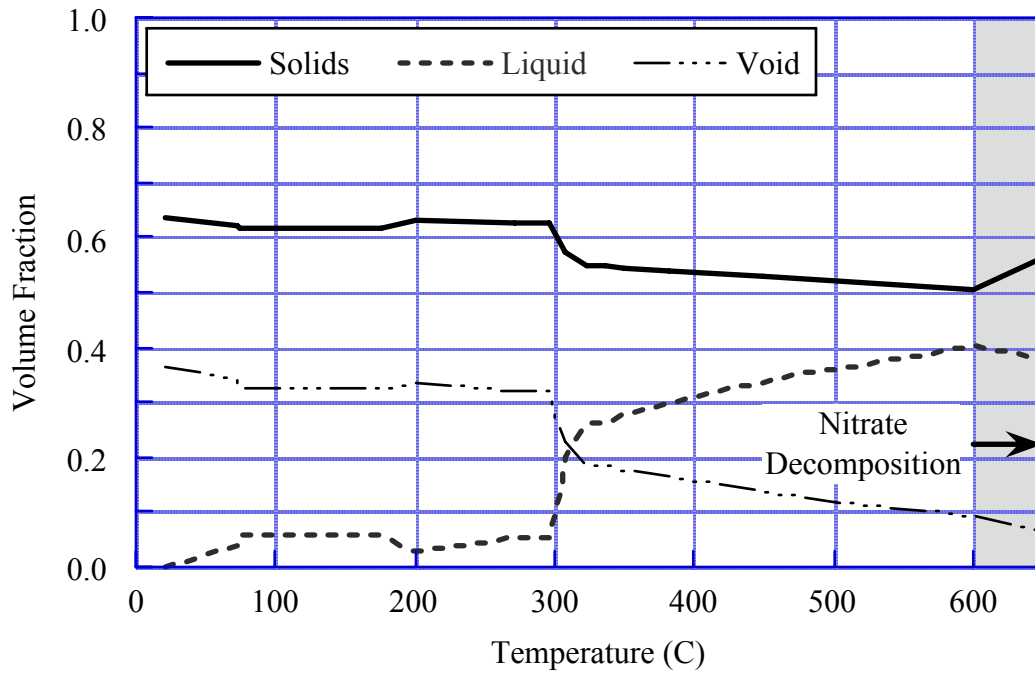


Figure 8.3. Phase Volume Fractions Versus Temperature

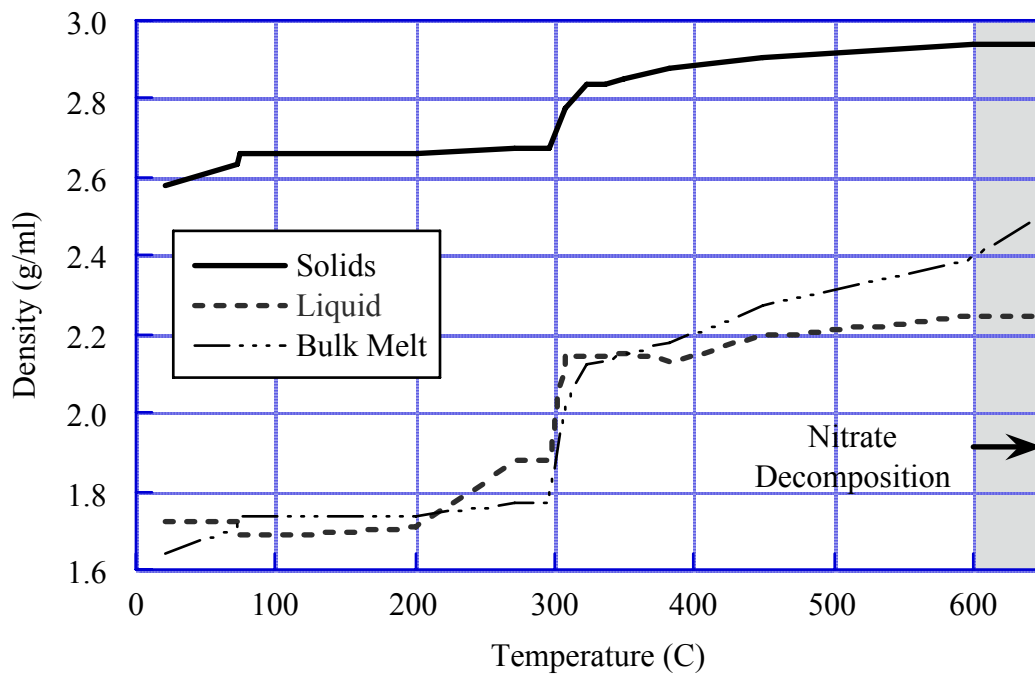


Figure 8.4. Phase Densities Versus Temperature

8.2 Maximum Theoretical Concentration of MIS in the CRB

Figure 8.5 shows the distribution of sodium atoms in a sample of CRB from Engineering Scale Test 31B next to the inside surface exposed to glass (Hrma et al. 2005). The maximum sodium atomic concentration is ~6 atom%. Similar data were obtained from a sample coupon of CRB material immersed in melting glass feed at various temperatures. Because there is little sodium in the CRB material, this indicates penetration of MIS into the CRB. A comparison to the maximum theoretical sodium concentration at different stages of the feed-melting and glass-forming processes gives some insight on which stage is represented and to what extent the molten feed filled the pores in the CRB. The objective of this calculation was to determine whether this amount of sodium represents complete saturation of the available pore space with MIS or some lesser, unsaturated volume.

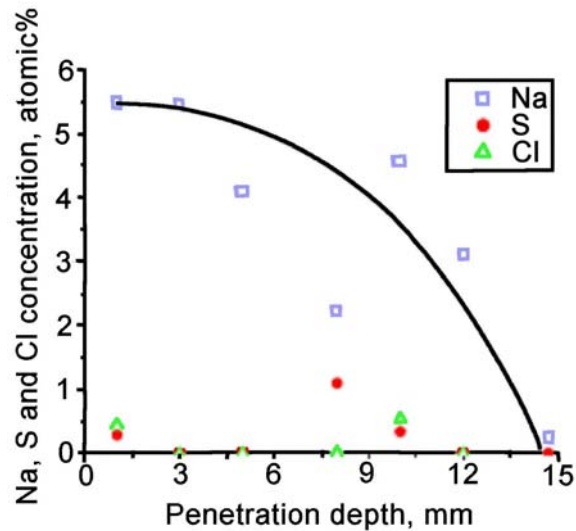


Figure 8.5. Atomic Concentrations in CRB after ES-31B Test
[Figure 5.16 from Hrma et al. (2005)]

To confirm or refute this hypothesis, we need to calculate the theoretical atom% sodium that would occur if all the pore space in the CRB were filled with MIS both before and after nitrate/nitrite decomposition, but before the transition to glass. This range of conditions includes compounds from 1 through 16 in Table 8.2 plus the sodium oxide formed during nitrate/nitrite decomposition. There are no sodium compounds in the CRB material, but the total number of atoms needs to be included. Table 8.3 gives the composition of the CRB solids in terms of metal oxides (Hrma et al. 2005). These oxides do not physically exist in the CRB. However, because the actual mineral content has not yet been determined, we use Table 8.3 as the only approximation available. The number of atoms computed from the oxides should be lower than in the actual mineral composition.

Table 8.3. Composition of Castable Refractory Solids in Terms of Metal Oxides

No.	Component	Name	Molecular Weight	Melting Point (C) ^(a)	Density (g/mL) ^(a)	Mass Fraction ^(b)
1	Al ₂ O ₃	Aluminum oxide	102	2053	3.97	0.608
2	SiO ₂	Silicon oxide	60	1713	2.50	0.345
3	Fe ₂ O ₃	Iron oxide	160	1565	5.25	0.001
4	TiO ₂	Titanium oxide	144	1777	4.49	0.018
5	CaO	Calcium oxide	56	2898	3.34	0.016

(a) CRC Handbook of Chemistry and Physics, 71st Ed., 1990 to 1991.
(b) Mass fractions renormalized to a sum of 1.0 ignoring 0.3 wt% “other.”

8.2.1 Atom Fraction Calculation

Given the porosity and solids density of the CRB, the atom fraction of sodium, A_{Na} , in the MIS-filled CRB is given by:

$$A_{Na} = \frac{a_{Na,S}}{a_S + a_{CRB} \frac{(1-\phi)\rho_{CRB}}{\phi\rho_S}} \quad (8.6)$$

where

- $a_{Na,S}$ = atoms of sodium per unit mass of molten salt (#/g)
- a_S = total number of atoms per unit mass of molten salt (#/g)
- a_{CRB} = total number of atoms per unit mass of CRB material (#/g)
- ϕ = CRB porosity, given as 0.17 by Hrma et al. (2005)
- ρ_S = bulk density of the molten salt (g/mL), Equation (8.3i) at the temperature corresponding to a specific condition (e.g., after initial melting, before nitrate decomposition, etc.)
- ρ_{CRB} = density of the solid material in the CRB (g/mL). Applying Equation (8.3h) to Table 8.3 gives 3.309 g/mL.

Because each mole of a compound contains the same number of molecules, the number of atoms of sodium per unit mass of molten salt is the mass fraction-weighted sum of the number of atoms of sodium per mole of compound over all compounds existing in the MIS. The number of atoms per unit mass of molten salt is the same mass-weighted sum of the total number of atoms per mole. The number of atoms per unit mass of CRB solids is the mass fraction-weighted sum of the number of atoms per mole of each compound over all compounds making up the CRB material. These sums are expressed in terms of mass fractions and molecular weights as follows:

$$a_{Na,S} = \sum_{i=1}^{15} \frac{\omega_i}{M_i} N_{Na,i} + \left[\frac{\omega}{M} N_{Na} \right]_{Na_2O} \quad (8.7a)$$

$$a_S = \sum_{i=1}^{15} \frac{\omega_i}{M_i} N_i + \left[\frac{\omega}{M} N \right]_{\text{Na}_2\text{O}} \quad (8.7b)$$

$$a_{\text{CRB}} = \sum_{i=1}^5 \frac{\omega_i}{M_i} N_i \quad (8.7c)$$

where $N_{\text{Na},i}$ is the number of sodium atoms in one molecule of I, N_i is the total number atoms in one molecule of I, and ω_i and M_i in Equation (8.7a) and (8.7b) are taken from Table 8.2 and those in Equation (8.7c) from Table 8.3.

The various reactions (8.5a) through (8.5f) occurring as the feed temperature increases need to be included in the sodium atomic fraction calculation as they were in the melt progression analysis. The mass fractions of the compounds used in Equations (8.7a) and (8.7b) are adjusted to account for these reactions as described in the preceding section.

8.2.2 Results of Sodium Atom Fraction Analysis

The sodium atom concentrations in the CRB resulting from complete saturation of a liquid salt under several possible conditions are summarized below.

1. 2.6 atom% sodium at 300 to 320°C: molten salt consisting of the compounds through sodium nitrate before any decomposition reactions or loss of water of hydration. Molten salt alone has 19 atom% sodium and a density of 2.15 g/mL.
2. 2.8 atom% sodium at 450 to 500°C: molten salt consisting of compounds through boron oxide after loss of water of hydration and sodium acetate decomposition but before other decomposition reactions. Molten salt alone has 19 atom% sodium and a density of 2.20 g/mL.
3. 5.4 atom% sodium above ~750°C: eutectic liquid consisting of compounds through sodium oxide after decomposition of nitrates, nitrites, and sodium oxalate. Molten salt alone has 47 atom% sodium and a density of 2.28 g/mL.

If the CRB porosity were increased to 0.20, the sodium concentration would increase to 6.4 atom% after decomposition. We conclude that the 6 atom% sodium measured in the CRB from the ES test must represent complete saturation of the pore space by molten salt. The gas generation accompanying nitrate/nitrite decomposition in the molten salt probably does not expel it from the CRB pore space to any measurable degree.

8.3 Physical Concept of the Melting Process

After the started batch has melted, melting should progress upward if feed is added at about the same rate it melts such that a cold cap of roughly constant thickness is maintained in the box. In this case, the dominant temperature gradient in the cold cap is vertical, and the thickness of the layers of feed in different stages of melting remains approximately constant. The time that a point on the CRB wall is exposed to each layer is therefore determined by the feed rate. Figure 8.6 is a sketch of this concept.

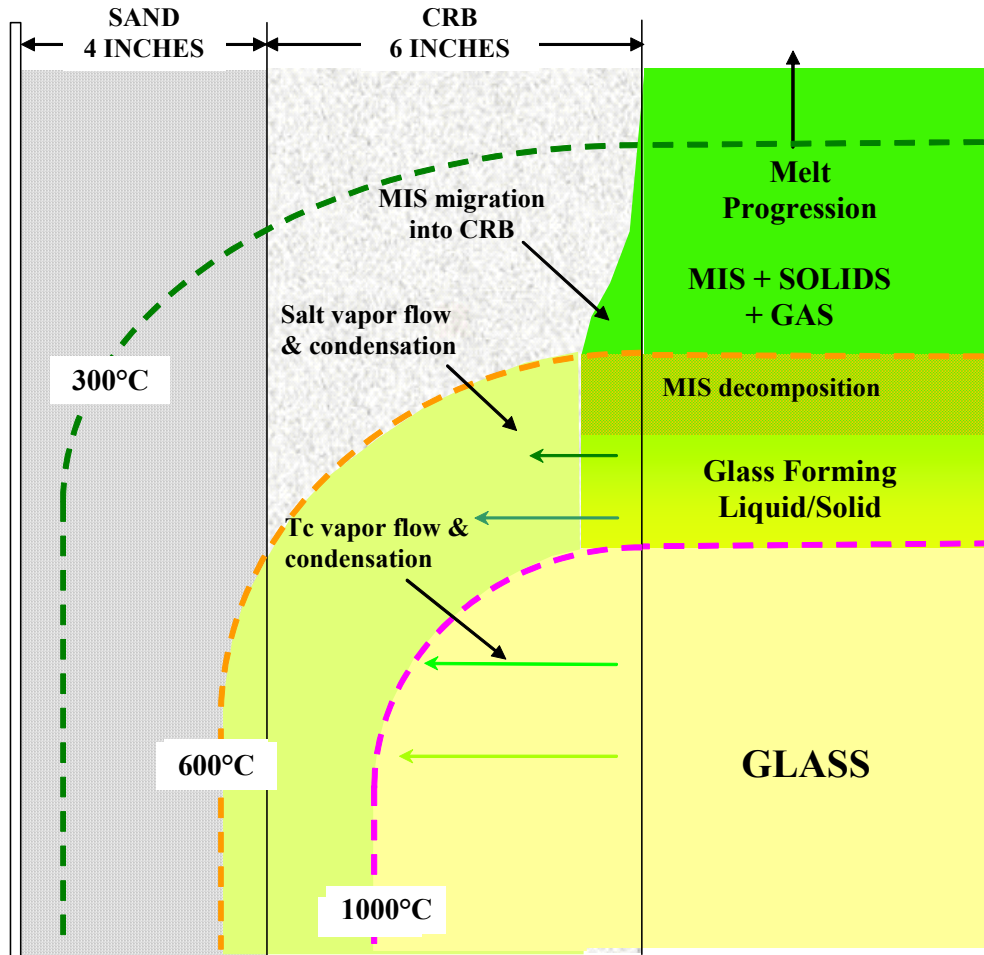


Figure 8.6. Melt Process Concept—Vertical Progression

While this concept is easy to model, it does not explain why the trace amounts of Re in the feed concentrate in the CRB. There is no clear mechanism for lateral transport of perrhenate salts or salt vapors in the vertical progression model to cause such concentration in the side walls. Also, the model does not easily accommodate the mixing effects of the large volume of gas generated during decomposition flowing up through the cold cap. Does this action tend to concentrate or disperse the MIS before decomposition?

An alternative melt progression model that is more lateral than vertical is suggested from the results from a simulation of FS-38A performed with the TEMPEST code. Figure 8.7 shows color contours of temperatures at 48, 59, and 72 h elapsed time on a section of the melter across the width of the melter box at the mid-section. The center line is on the right, and the melter box walls are shown by transparent gray shading. The darker blue oblong on top of the orange-red melt at 48 and 59 h represents feed batches added at 40 and 56 h.

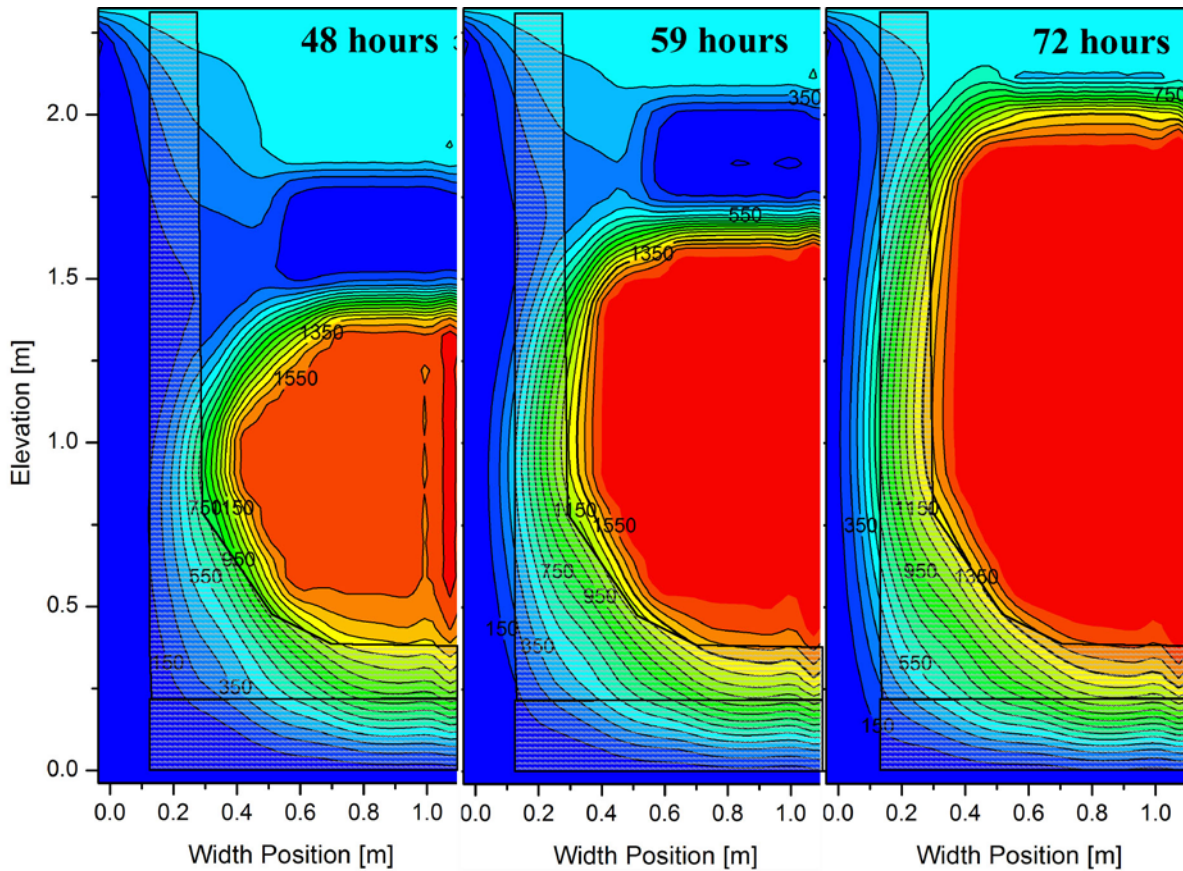


Figure 8.7. Temperature Contours from Simulation of Test 38A

The melt progression shown in Figure 8.7 is as much lateral as vertical most of the time, at least in the upper portion of the melt. This suggests the lateral melt model sketched in Figure 8.8. Rather than a relatively localized process moving up the wall as in the vertical model of Figure 8.6, the reactions may occur in series as the temperature raises more-or-less simultaneously over a large area of the CRB wall. The process might follow a sequence like this: 1) salts begin to melt and move into the CRB at $\sim 450^{\circ}\text{C}$ when sufficient liquid becomes available and continues through the nitrate/nitrite/carbonate decomposition stage beginning at $\sim 600^{\circ}\text{C}$, 2) post-decomposition liquid is replaced by heavier glass-forming liquid/solids at 800 to 1000°C , which halts penetration, and 3) molten salt that has penetrated the CRB reacts with CRB material, forming a durable glass at 1000 to 1200°C .

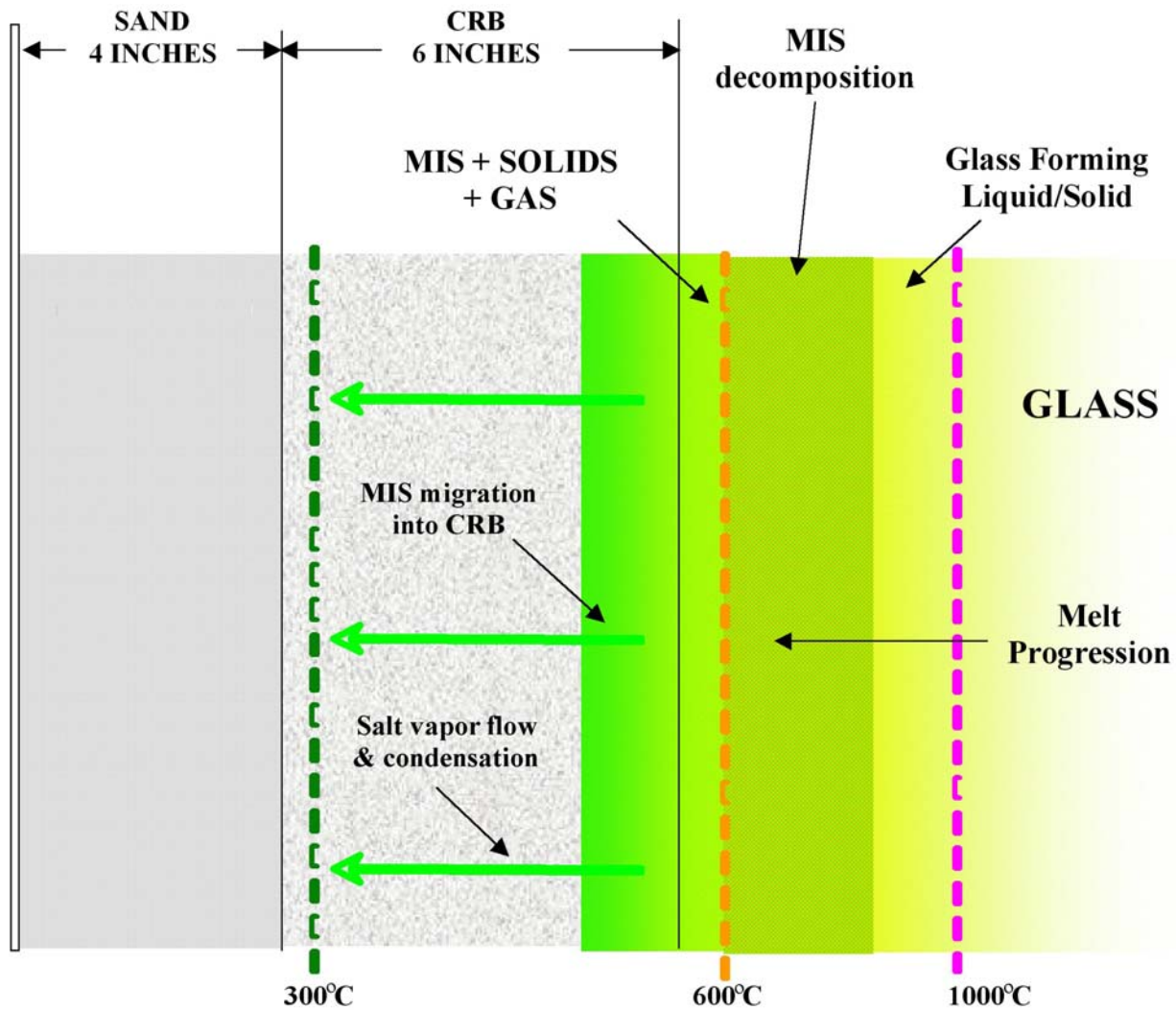


Figure 8.8. Melt Process Concept—Lateral Progression

While there are insufficient data to describe the process very well, the lateral melt progression model is attractive because it provides a clear mechanism for sweeping perhenate salts outward to concentrate at the wall. It also exposes a large volume of liquid salts to the wall over a large depth that helps explain how the CRB pores could saturate with post-decomposition salt.

However, this model probably represents a limiting condition or special case in Test 38 that cannot exist in production. The TEMPEST simulation used a melting criterion where material at less than 1000°C was considered a solid not subject to convection, forcing the colder feed to act as a solid boundary until reaching the specified transition temperature. But the dry, low density (~1.6 g/mL) feed powder would have had little or no strength, and the heavier (density ~2.9 g/mL) liquid glass should have pushed it up out of the way and flowed to the wall. At the same time, later feed batches added on top of the higher-density glass would float with 80 to 90% of their volume submerged. The floating feed would exist in a “trough” located either in the central part of the melter or as a ring around the periphery. A central trough of feed would tend to keep the molten salt in a pool away from the wall, while a peripheral trough would keep the molten salt in contact with the wall more like the horizontal model of Figure 8.8.

It is not possible at this time to conclude which of these scenarios, illustrated in Figure 8.9, is most likely. The actual melt process probably lies somewhere between the vertical and horizontal progression models. The method of feeding probably makes a substantial difference in the mode of MIS-CRB interaction.

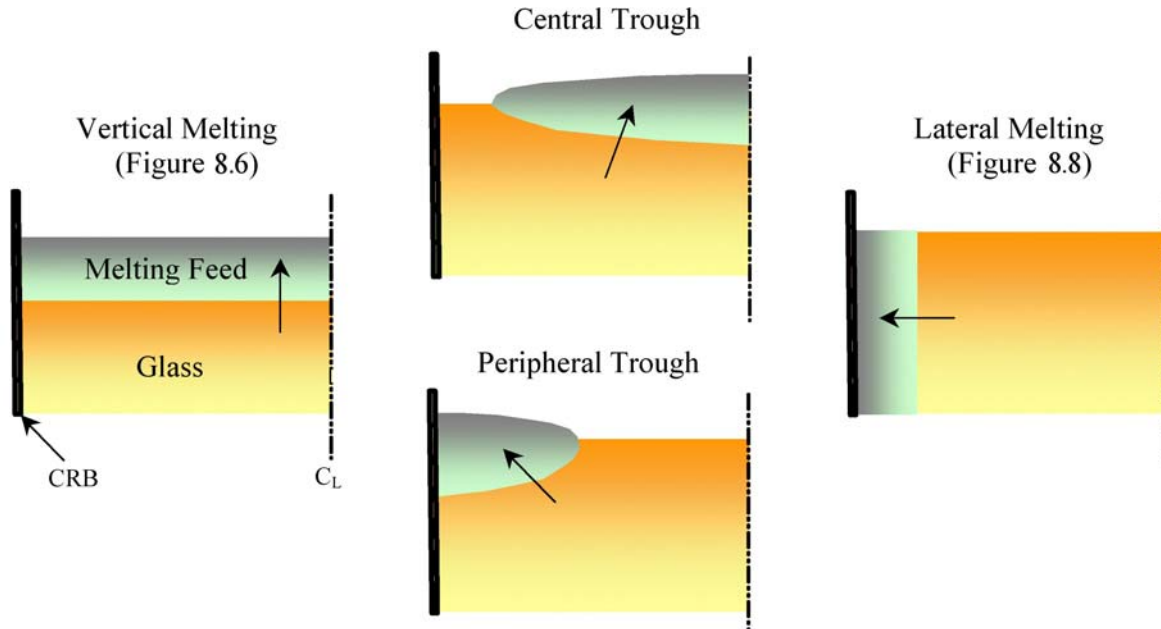


Figure 8.9. Possible Scenarios for the Melt Model

8.4 Mathematical Model for Molten Salt Migration into the CRB

This section describes an initial model for molten salt migration into the CRB based on the vertical melt progression conceptual model expressed in Figure 8.6. As a starting point, the model assumes the following:

- A distinct layer of MIS-saturated feed exists next to the CRB below the “dry” unsaturated feed above and a layer below where nitrates and nitrites decompose, and viscosity increases to prevent further penetration.
- There is both gravity- and capillary-driven MIS migration into the CRB.
- The MIS layer is liquid-saturated, completely wetting the CRB and developing a hydrostatic pressure.
- Isothermal conditions exist within the portion of the CRB where the MIS penetrates.
- There is a transient, one-dimensional Darcy flow.

Figure 8.10 shows an idealized model of the physical problem with its nomenclature. The liquid MIS-saturated layer progresses upward as feed is added and is incorporated into the glass at a rate dependent on the feed rate and melting rate. Within this moving layer, the MIS penetrates the CRB to a distance s as a function of time, dependent on both the capillarity and gravity head of the MIS.

8.4.1 Equations

The Darcy-flow superficial velocity of MIS migration into the CRB in response to a pressure gradient, dp/dx , is described by:

$$u = -\frac{k}{\mu} \frac{dp}{dx} \quad (8.8)$$

where k is the permeability of the CRB, and μ is the liquid viscosity. Assuming incompressible, unsteady flow, the pressure gradient is constrained by:

$$\frac{d^2p}{dx^2} = 0 \quad (8.9)$$

This requires that dp/dx and u are uniform in x , but they may vary with time.

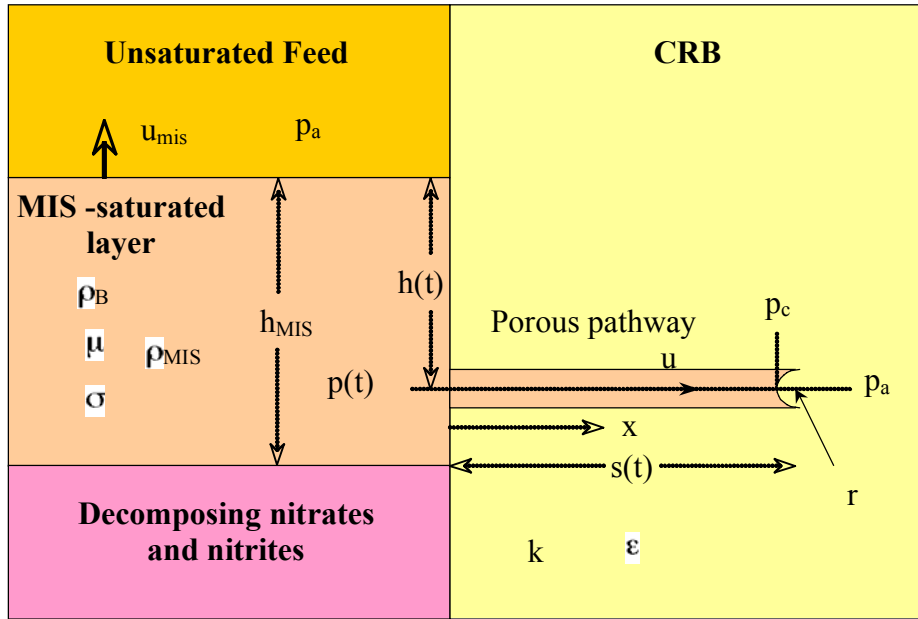


Figure 8.10. Illustrating the MIS Layer and Transport into CRB

The capillary pressure difference across a pore of radius r is given by:

$$\Delta p_c = -2\sigma / r \quad (8.10)$$

where σ is the surface tension. The gravity head in MIS at depth, h , of the MIS-saturated layer is computed from the MIS density, ρ_{MIS} , by:

$$p(t) = p_a + \rho_{MIS}gh(t) \quad (8.11)$$

The uniform pressure gradient in Equation (8.8) is the total pressure difference driving MIS into the CRB (the sum of the gravity pressure difference and capillary pressure) divided by the distance, $s(t)$, as follows

$$\frac{dp}{dx} = \frac{p(t) - p_a - \Delta p_c}{s(t)} = \frac{\rho_{\text{MIS}}gh(t) + 2\sigma/r}{s(t)} \quad (8.12)$$

The position, s , of the MIS front as it penetrates the CRB, which is a function of the liquid superficial velocity, u , and porosity, ε , is described by:

$$\frac{ds}{dt} = u/\varepsilon \quad (8.13)$$

Assuming that h_{MIS} is effectively constant on the average and that there is minimal mass loss during melting, the depth of the MIS-saturated layer at a fixed elevation can be expressed as a function of the average mass feed rate, M_F , the box cross-sectional area, A_B , and the bulk density of the MIS-saturated layer by:

$$h(t) = \frac{M_F}{\rho_F A_B} t \quad (8.14)$$

Combining Equations (8.8), (8.12), and (8.13) and substituting Equation (8.14) for the depth gives

$$s(t) = \sqrt{\frac{2k}{\varepsilon\mu} \left(\frac{\rho_{\text{MIS}}}{\rho_F} \frac{gM_F}{2A_T} t^2 + \frac{2\sigma}{r} t \right)} \quad (8.15)$$

The maximum penetration distance of MIS into the CRB, achieved at the point where the MIS-saturated layer passes, is given by Equation (8.15) at time $t = h_{\text{MIS}}\rho_B A_B / M_F$:

$$s_{\text{max}} = \rho_{\text{MIS}} h_{\text{MIS}} \sqrt{\frac{\rho_F}{\rho_{\text{MIS}}} \frac{kgA_T}{\varepsilon\mu M_F} (1 + F_\sigma)} \quad (8.16)$$

where $F_\sigma = \frac{4\sigma}{\rho_{\text{MIS}}gh_{\text{MIS}}r}$.

Evaluating Equation (8.16) for the conditions and property values listed in Table 8.4, the predicted MIS penetration layer thickness in the CRB for a full-scale operation is ~540 mm. This estimate is far greater than the ~15-mm penetration implied from the CRB sodium atom fraction analysis in Section 8.2.2. The extremely small pore radius observed in the recent PNNL capillary rise tests (see note in Table 8.4), makes capillary wicking the dominant mechanism of penetration with $F_\sigma = 4 (10^4)$. This means that any MIS exposed to the inner surface will penetrate the full thickness of the CRB without regard to available gravity head.

Table 8.4. Values Used for Evaluating MIS Penetration Model

Variable/Symbol/Units	Value	Source
permeability, k (m^2)	$3 (10^{-17})$	Hrma et al. (2005)
porosity, ϵ	0.18	Hrma et al. (2005)
viscosity of MIS, μ ($N\cdot s/m^2$)	$7 (10^{-3})$	Section 5.3
density of MIS, ρ_{MIS} (kg/m^3)	2,200	Section 8.1.4
bulk density of feed, ρ_F (kg/m^3)	1,600	PNNL measurements ^(a)
surface tension of MIS, σ (N/m)	0.1	Hrma et al. (2005)
CRB pore radius, r (m)	$1.7 (10^{-9})$	Section 5.3
thickness of MIS-saturated layer, h_{MIS} (m)	0.3	Est. from temperature transients ^(b)
mass feed rate, M_F (kg/s)	0.121	AMEC test instruction ^(c)
box cross-sectional area, A_B (m^2)	120	Approx. as length x width
(a) Memo from Renee Russell, PNNL, February 22, 2006, reporting measurements obtained under Test Instruction AMEC-TI-06-02. (b) Draft report by Pat Lowery (ARES), February 7, 2006, <i>TEMPEST Simulation of a Bulkvit Feed-While-Melt ICV Process: Comparison of Computation with Experiment</i> . (c) <i>Large Scale Test Instruction: Test LS38C</i> , 34006-TI-001, Rev. A (draft), March 2006, AMEC Earth & Environmental, Inc., Richland, WA.		

8.4.2 Scaling

If we assume simple geometric scaling with the length scale, L , Equation (8.14) identifies the main scalable parameters as:

- Container cross-section A_T : This scales with the linear dimension squared (L^2). Hence, all else being equal, $s \sim L$.
- Mass feed rate M_F : This is an operationally controlled parameter for which is difficult to assign a functional dependency. If the feed rate is volumetrically scaled, then the penetration scales with $s \sim L^{3/2}$. If the operators hold M_F/A_T constant by varying the power, the penetration distance is also constant with the scale, $s \sim L^0$.
- Thickness of MIS layer h_{mis} : This term appears twice in Equation (8.14) because it affects capillary and gravity action differently. If the gravity head dominates ($F_\sigma \ll 1$), then $s \sim h_{mis}$. If capillary action dominates ($F_\sigma \gg 1$), then $s \sim h_{mis}^{1/2}$. From above, the latter case appears most probable.

How h_{MIS} scales is quite important. On the average, it must scale as a balance of the melt and feed rates. The melt rate would, in turn, be proportional to net power input according to

$$h_{MIS} = C \frac{P - P_{loss}}{\Delta E_{MIS} M_F} \quad (8.17)$$

where P = power to the melter
 P_{loss} = heat loss rate
 ΔE_{MIS} = energy required to convert 1 kg of bulk feed to the material of the MIS-saturated layer
 C = a constant.

If the heat loss is minor, the net power to the melter likely scales with $P \sim L^3$. But M_F should also scale with L^3 , and ΔE_{MIS} should be constant. Hence, the MIS thickness must also be a constant, or it depends on other factors. It is also subject to operator intervention, and, since the feed is added in batches, it varies over some significant range. All things considered, it would be logical if the MIS thickness varied directly with L on the average.

Combining all these factors, the MIS penetration thickness may scale with: $s \sim L^a$, where $a = 0$ for capillary-driven MIS migration and $a = 0.5$ for gravity-driven MIS migration. Based on the small pore size of the CRB, the MIS penetration process is completely dominated by capillary action, and neither the MIS layer thickness nor any other scaled parameter has a significant effect.

8.5 Summary

The main purpose of the modeling effort described in this section was to check if the modeling can identify additional mechanisms for MIS transport that have not been thought of. The present modeling result supports the conclusion from capillary experiments in Section 5.0 that the MIS penetration process is dominated by capillary action, without any indication of other parameters that have significant effects.

9.0 Re Migration Tests

This subtask extended the previous cold-finger tests (Kim et al. 2005) to investigate specific aspects of early melting reactions and Re volatilization from molten glass. The cold-finger test setup was redesigned to provide data with higher confidence by improving the Re mass balance closure. Unlike the previous study, the present work was performed in a non-radioactive laboratory using only Re, which previous work indicated to be a good surrogate for Tc. Modified cold-finger tests were used to 1) establish the rate of Re release and condensation from pre-melted glass held at temperatures below the 1200°C tested earlier, 2) determine the effect of change in the waste and glass composition on the Re release and condensation during feed melting, and 3) perform screening tests to evaluate the effectiveness of alternate feed materials to reduce Re release as discussed in Task 30.

9.1 Feeds and Pre-Melted Glass Preparation

The LAW simulant described in Section 4.0 (Table 4.1) was used to prepare the feeds. The feed variations tested in this study were:

- Case 1—Baseline: A baseline feed with a target concentration of 8.1 mg/kg Re in glass. The target glass was the current baseline composition (Kim et al. 2003) used in a previous study (Kim et al. 2005) as summarized in Table 4.2.
- Case 2—High Cl/F: A feed with a simulant modified by chlorine and fluorine spiking to simulate the high-Cl/F waste. NaCl and NaF were added to the feed to provide target concentrations of 0.37 wt% Cl and 0.62 wt% F in glass (compared to 0.18 wt% Cl and 0.07 wt% F in the baseline glass supplied from 6-tank composite simulant only), which were expected to be maximum based on a recent study.^(p) The target glass composition was basically the same as the baseline case except for Cl and F concentrations. This case was to determine the effect of Cl and F in the waste on the migration of Re.
- Case 3—High CaO/MgO: A feed with the same simulant as in the baseline case but with a modified target glass composition with higher concentrations of CaO and MgO that were expected to increase the sulfur loading in LAW glass (Vienna et al. 2004). The concentration of CaO and MgO in glass was increased by ~2 wt% CaO (from 2.95 to 5.0 wt%) and by ~1 wt% MgO (from 1.44 to 2.5 wt%). This test was to determine the effectiveness of changing the glass composition on sulfur loading and the migration of Re.
- Case 4—Crushed soil: The same baseline feed as Case 1 but with crushed soil. Task 30 identified that crushing the soil to provide a higher surface area is the most promising method to decrease the MIS penetration into the CRB. The soil was ground in a tungsten carbide mill for 2 min. This case was to determine the effect of crushed soil on the migration of Re.

Table 9.1 summarizes the recipe to produce the 800 grams of each feed required for the four test runs necessary for each test case. Table 9.1 also includes oxide loading for each recipe material in terms of mass fraction of oxides and halogens, assuming the glass retains 100% of all components. Table 9.2 summarizes the target glass composition for each test feed. The modification of waste simulant in Case 2 and of glass composition in Case 3 resulted in a small difference in the amount of simulant per unit mass

(p) LA Mahoney. 2005. Letter Report: *Development of Waste Simulants for Series 33 Bulk Vitrification Tests*. ST05.013, Pacific Northwest National Laboratory.

of glass and therefore there were different concentrations for components supplied from the simulant, especially for S and Re. For Case 2, Na₂SO₄ was spiked in addition to NaCl and NaF to compensate for the decreased S because it was found from a previous study (Kim et al. 2005) that the concentration of S in the feed had a strong effect on the migration of Re. However, no adjustment was made for Re.

Table 9.1. Feed Recipe and Oxide Loading

Materials	Recipe for 800 g glass (g)			Oxide Loading ^(a) (mass fraction)		
	Cases 1 and 4 ^b	Case 2	Case 3	Cases 1 and 4 ^b	Case 2	Case 3
6-tank composite simulant (Liquid simulant volume)	356.7 (938.9 mL)	335.1 (882.1 mL)	358.5 (943.7 mL)	0.2024	0.1901	0.2034
NaCl	-	2.621	-	-	0.0037	-
NaF	-	9.789	-	-	0.0146	-
Na ₂ SO ₄	-	0.791	-	-	0.0010	-
CaCO ₃	-	-	31.34	-	-	0.0219
MgCO ₃	-	-	18.88	-	-	0.0113
HRTS0 ₅	553.8	548.1	525.8	0.6776	0.6706	0.6434
ZrO ₂	56.00	56.00	56.00	0.0700	0.0700	0.0700
B ₂ O ₃	41.95	41.95	41.95	0.0500	0.0500	0.0500
Total	1008.4	994.3	1032.5	1.0000	1.0000	1.0000

(a) Expressed in terms of oxides and halogens that are assumed to remain in glass with 100% retention.
(b) Case 4 had the same recipe as the baseline (Case 1), but used the crushed soil.

Table 9.2. Target Glass Compositions (in mass fraction except for Re metal in mg/kg)

Component	Cases 1 and 4	Case 2	Case 3
Al ₂ O ₃	0.0878	0.0867	0.0836
B ₂ O ₃	0.0500	0.0500	0.0500
BaO	0.0005	0.0005	0.0005
CaO	0.0295	0.0292	0.0500
Cl	0.0018	0.0037	0.0018
Cr ₂ O ₃	0.0010	0.0010	0.0010
F	0.0007	0.0062	0.0007
Fe ₂ O ₃	0.0462	0.0457	0.0439
K ₂ O	0.0223	0.0220	0.0212
MgO	0.0144	0.0143	0.0250
MnO	0.0007	0.0007	0.0007
Na ₂ O	0.2000	0.2000	0.2000
P ₂ O ₅	0.0057	0.0054	0.0056
SiO ₂	0.4531	0.4484	0.4302
SO ₃	0.0085	0.0085	0.0085
SrO	0.0003	0.0003	0.0003
TiO ₂	0.0074	0.0073	0.0070
ZrO ₂	0.0700	0.0700	0.0700
Total	1.0000	1.0000	1.0000
Re, mg/kg	8.10	7.61	8.14

For each test, the simulant solution was mixed with various additive materials as given in Table 9.1. The slurry feed mix was dried before crucible testing. Initially, the water from the wet feed was evaporated by mechanically stirring the feed contained in a stainless steel beaker placed on hot plate. This process continued until the feed became dry. The resulting dried feed was analyzed for Re via ICP-MS and for major glass components via ICP-AES.

The pre-melted glass was prepared according to the PNNL procedure Glass Development Laboratory-Glass Batching and Melting (GDL-GBM) using raw chemicals that achieve the same baseline glass composition as prepared from the dried feed. The baseline pre-melted glass was fabricated in Pt-10%Rh crucibles following a two-step melting process: melt raw materials for 1 h at 1300°C, quench on a steel plate, grind glass for homogeneity, and re-melt glass for 1 h at 1300°C. The glass batch was spiked with twice the Re required for the current target (8.1 mg/kg in glass) to compensate for the volatile loss during glass fabrication. The glass was prepared in three separate batches, and all the resulting glass was homogenized before taking three samples for chemical analysis. The glass was analyzed for Re via ICP-MS and Na and S via ICP-AES in three samples and for major glass components via ICP-AES in one sample.

9.2 Experimental Methods

The cold-finger test setup used in a previous study (Kim et al. 2005), shown in Figure 9.1, was very useful to obtain the information on the relative effect of feed variation on the volatilization of Re and Tc from melting feed or molten glass.

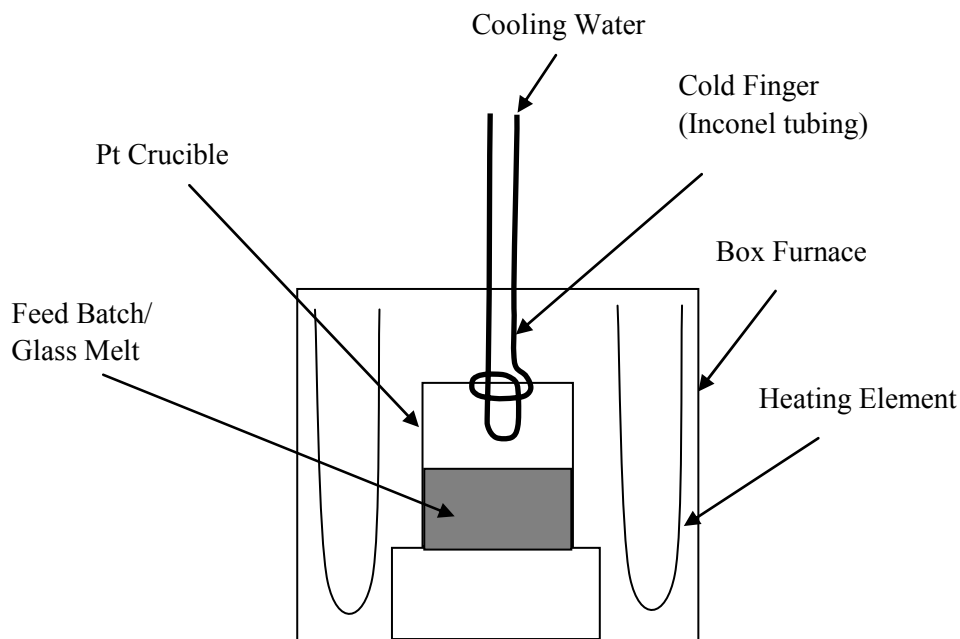


Figure 9.1. Schematic of Experimental Setup for Cold Finger Crucible Tests Used in the Previous Study (Kim et al. 2005)

The tests conducted using this cold-finger test setup were not intended to supply a full Tc and Re mass balance, mainly because the setup was not designed to capture all the volatiles. In a previous study (Kim et al. 2005), it was assumed that the condensation efficiency (fraction collected on the cold finger to the total volatilized) is roughly constant without a significant variation to test. Although these test methods were good enough to provide information on the major effect of feed variations, the application of these tests is limited because of high data uncertainties caused by the poor mass balance. The total Re or Tc mass accounted for by chemical analyses in crucible rinse, condensate, and residual glass samples was 48 to 71% for Re and 48 to 77% for Tc relative to the mass added to the feed. Therefore, a new setup was developed, and preliminary tests were conducted to evaluate the feasibility of mass balance tests and the effectiveness of the setup.

In addition, two other factors that contributed to high data uncertainties in the previous study were modified:

- The sample for glass retention measurement was taken after fully homogenizing the entire remaining glass materials, which was not performed in the previous study because of constraints associated with handling radioactive samples. The glass melt heated to just 1200°C (the highest temperature used in a previous study) is expected to be inhomogeneous as collected.
- The Re partition calculation will be based on measured concentrations in the feed instead of target values used in the previous study to minimize errors associated with analytical bias.

Figure 9.2 is a schematic of a new experimental setup developed to improve system mass balance. The new setup was designed to capture all the volatiles by condensing them inside a stainless steel tube or dissolving them in a pair of scrub solutions. The first scrub solution was kept at 10°C using a water bath equipped with a chiller to facilitate capturing the volatiles. The container for the second scrub solution was kept at a slightly lower pressure than the ambient pressure to minimize the leakage of volatiles through the gap between the Pt crucible and the lid. After each experiment, the tubes were washed with DIW and mixed with scrub solutions to analyze for total volatilized materials. The initial test of the system included washing the tube with a more aggressive rinse that used a tube brush to check if the DIW wash alone was enough to remove all the condensates. The fritted pipe end was used to reduce the bubble size so the volatiles would dissolve faster into the solution.

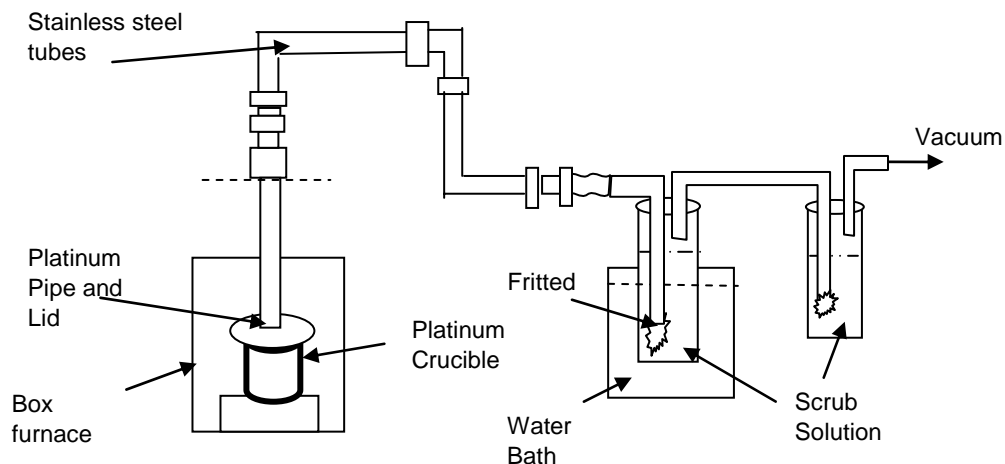


Figure 9.2. Schematic of New Experimental Setup Proposed for Re Migration Tests

The dried feeds were tested by heating in a Pt-10%Rh crucible at 5°C/min starting from 80°C and terminating at the following temperatures right after each temperature is reached: 800, 900, 1000, and 1200°C (four test runs per each feed). The pre-melted glass was ramp heated at 5°C/min starting from 500°C to three different temperatures of 1000, 1100, and 1200°C and held at the final temperature for 1 and 5 h. In addition, the test run at 1100°C for 5 h was repeated for reproducibility.

The test with pre-melted glass used ~200 g of pre-melted glass. For tests with dried feed, the mass required for ~200 g glass was used for each run. However, in Case 3, the feed at 1000°C foamed more severely than with the previous two feeds and overflowed the crucible. The foam at the center of the crucible touched the lid and clogged the pipe entrance connected to the lid, suggesting that a bigger crucible or a smaller amount of feed is needed. Meanwhile, in the tests with crushed soil performed under Task 30, we discovered that the crushed soil feed foams to more than twice the volume of feed prepared with uncrushed soil. It was decided to reduce the mass of the batches for the remaining Case 3 and Case 4 feeds. Preliminary melting experiments were performed with crushed soil feed to determine the maximum amount of feed that can be used without having the foaming that can clog the pipe. It was found that the batch size should be decreased approximately by a half. Therefore, the subsequent tests, starting from Case 3 1000°C tests, used the feed mass required to make ~100 g glass. To evaluate the effect of using a smaller batch size, two tests with Case 1 feed at 1000 and 1200°C were repeated with half-size feed batches.

The heat-treated samples were air cooled after reaching the preset temperature (for the tests with dried feed) or after the preset time at each test temperature (for tests with pre-melted glass). The following samples were analyzed:

- Crucible rinse samples: All the partly reacted feed and glass materials remaining in the Pt crucible were collected, crushed, and washed with a dilute (0.001 M) nitric acid (HNO₃). The rinse solutions from the tests with dried feed were filtered and analyzed for Re via ICP-MS, Na, and S via ICP-AES, and for anions via ion chromatography (IC). The rinse solutions from the tests with pre-melted glass were prepared but were not analyzed. The solutions were archived in case it was determined that the analyses were necessary based on the evaluation of other test results. The solid materials collected after the crucible rinse were washed with DIW two or three times to remove any residual soluble components.
- Condensate samples: The condensate materials were collected from the tubes by washing with DIW and mixed with the two scrub solutions. The condensate samples from all tests were analyzed for Re via ICP-MS, for Na and S via ICP-AES, and for anions via IC.
- Glass samples: The glass samples from 1200°C tests performed with dried feed and from all tests with pre-melted glass were analyzed for Re via ICP-MS and for Na and S via ICP-AES.

Table 9.3 summarizes the chemical analyses of all the samples collected from the tests described in this section.

Table 9.3. Summary of Chemical Analyses To Be Performed for Various Samples

Sample	ICP-MS (Re) and ICP-AES (Na, S)	ICP-AES (major glass components)	IC (Cl, F, NO ₃ , NO ₂ , PO ₄ , SO ₄)
Dried feed and pre-melted glass	Yes	Yes	No
Crucible rinse solution from tests with dried feed	Yes	No	Yes
Crucible rinse solution from tests with pre-melted glass	Archive only		
Condensate rinse solutions from all tests with dried feed and pre-melted glass	Yes	No	Yes
Glass sample from 1200°C tests with dried feed and all tests with pre-melted glass	Yes	No	No

The preliminary test was performed with the baseline feed following the procedure described above with an initial setup that was slightly different from Figure 9.2 as discussed below. The final temperature was 1200°C. Table 9.4 summarizes the Re wt% of total found in each sample from the preliminary test. The mass balance closure was 82.4 wt% compared to 57.2 wt% for the same baseline feed from a previous study (Kim et al. 2005). This indicated that the initial setup helped to improve the Re mass balance, but in an effort to further improve the Re mass balance, the initial setup was modified in two areas: 1) a taller container was used for scrub solution to provide a longer time for the bubbles to be in contact with the solution, and 2) a second scrub solution was added to the setup as shown in Figure 9.2 to capture the volatiles that escape from the first scrub solution. Table 9.4 also suggests that the contribution of an aggressive pipe rinse is negligible. Therefore, the main tests did not include the aggressive pipe rinse step.

Table 9.4. Summary of Re Mass Balance Closure from Preliminary Tests

Sample	Concentration of Re (mg/kg)	Sample Mass (g)	Re mass (mg)	Wt% of Total
Crucible rinse	0.239	100	0.0239	1.47
Condensate solution including pipe rinse	0.684	819	0.560	34.60
Aggressive pipe rinse	0.024	105	0.00254	0.16
Glass	3.740	200	0.748	46.17
Total				82.40

9.3 Results and Discussion

The tests used two batches of liquid simulant: the second batch was prepared after the first batch was depleted. Table 9.5 summarizes the analyzed composition of 6-tank composite simulant compared with the target composition calculated from Table 4.1. Table 9.5 also includes the RPD between the target and analyzed compositions. Table 9.5 shows that the analyzed simulant composition agrees well with the target composition for major components with at least 1000 mg/kg. The large difference for K is not of concern considering its low concentration in the simulant and in glass (0.34 wt% K₂O in simulant and

0.07 wt% in glass from simulant at 20.24 wt% simulant oxide loading). There was no practical difference between the first and second batches of simulant.

Table 9.5. Analyzed Composition of 6-Tank Composite Simulant Compared to Target

Component	Analyzed, mg/kg		Target, mg/kg	RPD (%)	
	6-Tank Simulant (2/15/06)	6-Tank Simulant (4/10/06)		6-Tank Simulant (2/15/06)	6-Tank Simulant (4/10/06)
Al	1390	1380	1398	-0.5	-1.3
Cl	NA	NA	1263	-	-
Cr	394	402	438	-10.1	-8.4
F	NA	NA	489	-	-
K	471	721	393	19.7	83.5
Na	87000	88100	93453	-6.9	-5.7
P	1180	1220	1239	-4.7	-1.5
Re	5.62	5.37	5.62	0.0	-4.4
S	2290	2260	2346	-2.4	-3.6

NA: not analyzed.
 RPD: relative percent difference, $([\text{Analyzed}] - [\text{Target}])/[\text{Target}]$

Table 9.6 summarizes the analyzed composition of dried feeds compared with target compositions calculated from Table 9.1. Table 9.7 gives the relative percent difference between target and analyzed concentration. The analyzed compositions agreed well with the target compositions with a relative difference between target and analyzed compositions within 10% for major components with at least 2 wt% in the feed. There were two exceptions: Fe₂O₃ had a relative difference of 14% only in the Case 2 feed, and ZrO₂ had a relative difference from 11 to 19%, which is a troublesome component for chemical analyses because it is difficult to completely dissolve. The Re showed a good agreement with a relative difference ranging from 3 to 5%. The analyzed composition is used for Re and S mass balance calculations.

**Table 9.6 Analyzed Composition of Dried Feeds Compared to Target Compositions
(in mass fraction for oxides/halogens and mg/kg for Re metal)**

Component	Case 1 (Baseline) and Case 4 (Crushed soil)			Case 2 (High Cl/F)		Case 3 (High Ca/Mg)	
	Analyzed, Case 1	Analyzed, Case 4	Target	Analyzed	Target	Analyzed	Target
Al ₂ O ₃	0.0693	0.0726	0.0696	0.0712	0.0697	0.0648	0.0647
B ₂ O ₃	0.0383	0.0419	0.0397	0.0402	0.0402	0.0386	0.0387
BaO	0.0005	0.0005	0.0004	0.0005	0.0004	0.0005	0.0004
CaO	0.0238	0.0238	0.0234	0.0248	0.0235	0.0385	0.0387
Cl	NA	NA	0.0014	NA	0.0030	NA	0.0014
Cr ₂ O ₃	0.0008	0.0009	0.0008	0.0009	0.0008	0.0008	0.0008
F	NA	NA	0.0006	NA	0.0050	NA	0.0006
Fe ₂ O ₃	0.0382	0.0380	0.0366	0.0417	0.0368	0.0366	0.0340
K ₂ O	0.0129	0.0133	0.0177	0.0130	0.0177	0.0116	0.0164
MgO	0.0112	0.0114	0.0115	0.0119	0.0115	0.0179	0.0194
MnO	0.0006	0.0006	0.0006	0.0007	0.0006	0.0008	0.0005
Na ₂ O	0.1570	0.1604	0.1587	0.1645	0.1609	0.1631	0.1550
P ₂ O ₅	0.0045	0.0042	0.0045	0.0048	0.0044	0.0043	0.0044
SiO ₂	0.3359	0.3337	0.3595	0.3359	0.3608	0.3038	0.3334
SO ₃	0.0071	0.0077	0.0067	0.0073	0.0068	0.0069	0.0066
SrO	0.0002	0.0002	0.0002	0.0002	0.0002	0.0002	0.0002
TiO ₂	0.0068	0.0066	0.0059	0.0073	0.0059	0.0084	0.0054
ZrO ₂	0.0465	0.0492	0.0555	0.0455	0.0563	0.0442	0.0542
LOI	0.2360	0.2310	0.2067	0.2140	0.1954	0.2510	0.2251
SUM	0.9897	0.9959	1.0000	0.9844	1.0000	0.9920	1.0000
Re, mg/kg	6.61	6.66	6.43	6.44	6.12	6.61	6.31
NA: not analyzed.							
LOI: loss on ignition measured after heat treating the feed at 1050°C for 2 h.							

Table 9.7. Relative Percent Difference¹⁾ between Target and Analyzed Compositions in Dried Feeds

Component	Case 1	Case 2	Case 3	Case 4
Al ₂ O ₃	-0.4	4.2	2.1	0.1
B ₂ O ₃	-3.4	5.5	0.0	-0.3
BaO	9.2	15.9	14.7	28.7
CaO	1.5	1.5	5.3	-0.7
Cl	-	-	-	-
Cr ₂ O ₃	0.7	6.1	12.0	5.7
F	-	-	-	-
Fe ₂ O ₃	4.2	3.8	13.5	7.7
K ₂ O	-26.6	-24.9	-26.5	-29.6
MgO	-1.9	-0.6	3.5	-7.5
MnO	8.2	1.4	14.3	42.4
Na ₂ O	-1.0	1.1	2.2	5.2
P ₂ O ₅	-0.7	-7.5	9.8	-1.2
SiO ₂	-6.6	-7.2	-6.9	-8.9
SO ₃	6.2	14.6	6.9	4.6
SrO	-0.9	-0.7	0.4	-3.7
TiO ₂	15.5	13.1	23.4	54.2
ZrO ₂	-16.3	-11.4	-19.2	-18.5
Re	2.9	3.6	5.2	4.8

1) calculated as $([\text{Analyzed}] - [\text{Target}]) / [\text{Target}]$

Table 9.8 summarizes the concentration of Re, Na, and S in three samples of pre-melted glass. Table 9.9 compares the analyzed composition of one pre-melted glass (Glass A) with the target composition. There was a good agreement between analyzed and target for all the major components with a target of at least 1 wt%. The Re retention was low at 28.7 wt% on average (based on 16.2 mg/kg Re target), and S retention was relatively high at 84.6 wt% on average.

Table 9.8. Re, Na, and S Concentration in Pre-melted Glass Samples (in mg/kg)

Sample	Re	Na	S
Glass A	4.58	154000	2865
Glass B	4.71	153000	2835
Glass C	4.66	156000	2660
Average	4.65	154333	2787
% relative standard deviation	1.36	0.99	3.97

Table 9.9. Analyzed Composition of Pre-melted Glass Compared with Target Composition (in mass fraction)

Oxide	Analyzed	Target	RPD (%)
Al ₂ O ₃	0.0895	0.0878	1.9
B ₂ O ₃	0.0504	0.0500	0.8
BaO	0.0007	0.0005	22.4
CaO	0.0291	0.0295	-1.5
Cl	-	0.0018	-
Cr ₂ O ₃	0.0011	0.0010	10.3
F	-	0.0007	-
Fe ₂ O ₃	0.0430	0.0462	-7.0
K ₂ O	0.0230	0.0222	3.2
MgO	0.0132	0.0144	-9.0
MnO	0.0008	0.0007	11.9
Na ₂ O	0.2076	0.2000	3.8
P ₂ O ₅	0.0056	0.0057	-0.9
SiO ₂	0.4567	0.4531	0.8
SO ₃	0.0072	0.0085	-15.4
SrO	0.0003	0.0003	0.0
TiO ₂	0.0081	0.0074	9.2
ZrO ₂	0.0647	0.0700	-7.6
SUM	1.0007	1.0000	

Table 9.10 summarizes the analyses of crucible rinse and condensate solutions. For tests with dried feed, the sample ID denotes Case #, final temperature, and crucible rinse (“1”) or condensate solution (“2”). The condensate solution includes all the scrub 1, scrub 2, and pipe wash solutions. The exception was for tests at 800 and 900°C with Case 1 feed that had separate samples for the aggressive rinse (denoted as “4”) and scrub 2 (“5”). For tests with pre-melted glass, the sample ID starts with “PMG” (for pre-melted glass) and provides information on test temperature, duration at a test temperature, and “2” for condensate solution (note that the crucible rinse samples were not analyzed). The additional note “1/2B” specifies that the test was performed with a half size batch (~100 g glass instead of ~200 g glass) and “2nd” denotes a repeated run. Table 9.10 shows that the 2nd solution (“5”) resulted in a negligibly small concentration or below the reporting limit for Re in both tests. However, for the aggressive pipe wash (“4”), one test resulted in a small but non-negligible Re concentration while another had Re below the reporting limit. The non-negligible Re concentration found in one sample suggests that skipping the aggressive rinsing step can partially contribute to the mass balance closure of less than 100%.

Table 9.10 Analyzed Concentrations in Crucible Rinse and Condensate Solutions (in mg/L)

Sample ID	Re	Na	S	Cl ⁻	F ⁻	NO ₃	NO ₂ ⁻	PO ₄ ³⁻	SO ₄ ²⁻
Case 1—Baseline									
C1-800-1	2.02	34300	1560	623	181	12749	2220	2318	4570
C1-900-1	0.294	1660	444	50.9	5.34	447	35.1	702	1340
C1-1000-1	0.803	1110	630	84.8	5.21	71.5	3.88	172	1940
C1-1000-1-1/2B	0.347	744	422	39.7	3.84	46.7	<6.57	138	1280
C1-1200-1	0.112	1820	1170	35.2	6.92	59.8	<6.57	130	3600
C1-1200-1-1/2B	0.0373	696	437	7.33	2.75	73.9	7.00	46.9	1330
C1-800-2	0.0121	8.05	<0.400	32.5	<10.0	27977	<32.8	<30.7	25.3
C1-800-4	<0.00100	<5.00	<0.400	0.34	<0.1	10.9	<0.328	<0.307	0.505
C1-800-5	<0.00050	<5.00	<0.400	6.45	<2	4604	<6.57	<6.13	5.48
C1-900-2	0.0761	8.06	<0.400	40.4	<10.0	31297	<32.8	<30.7	45.6
C1-900-4	0.00395	<5.00	<0.400	0.388	0.108	3.76	<0.328	<0.307	0.554
C1-900-5	0.00053	<5.00	<0.400	10.7	<2	7835	13.2	<6.13	7.7
C1-1000-2	0.320	14.6	<0.400	41.3	<10.0	24923	<32.8	<30.7	57.3
C1-1000-2-1/2B	0.160	9.49	0.409	16.9	3.62	7747	<6.57	<6.13	9.56
C1-1200-2	0.537	39.1	7.61	63.7	11.6	20186	<32.8	<30.7	96.7
C1-1200-2-1/2B	0.272	23.0	8.42	35.6	8.15	8544	<6.57	<6.13	42.8
Case 2—High Cl/F									
C2-800-1	3.02	30500	1840	1830	1800	25764	4401	1637	5310
C2-900-1	1.48	1770	798	348	94.0	415	52.2	145	2470
C2-1000-1	1.53	2300	1260	428	88.9	96.5	<32.8	128	3810
C2-1200-1	0.0539	2110	1360	106	50.0	85.0	<32.8	69.3	4090
C2-800-2	0.0119	<5.00	<0.400	18.8	<10.0	11908	<32.8	<30.7	29.2
C2-900-2	0.0596	<5.00	<0.400	29.9	10.2	15228	<32.8	<30.7	38.3
C2-1000-2	0.282	30.6	5.39	58.4	16.7	14011	<32.8	<30.7	76.5
C2-1200-2	0.475	69.5	9.58	111	44.9	13502	<32.8	<30.7	93.4
Case 3—High CaO/MgO									
C3-800-1	4.61	51800	2410	1630	458	72599	12251	1033	7480
C3-900-1	0.208	596	297	68.1	3.33	69.1	8.93	69.0	922
C3-1000-1-1/2B	0.364	673	411	36.9	4.04	103	6.32	25.4	1280
C3-1200-1-1/2B	0.0155	532	348	10.8	7.05	57.1	<3.28	15.05	1130
C3-800-2	0.00294	<5.00	<0.400	5.55	2.51	4471	<6.57	<6.13	6.95
C3-900-2	0.0456	<5.00	<0.400	34.0	<10.0	20894	<32.8	<30.7	31.0
C3-1000-2-1/2B	0.206	63.2	1.61	37.5	80.8	10314	<32.8	<30.7	44.3
C3-1200-2-1/2B	0.238	49.4	2.25	18.2	690	4307	<6.57	<6.13	10.8
Case 4—Crushed Soil									
C4-800-1-1/2B	0.0293	9080	450	109	20.6	122	14.3	1018	1380
C4-900-1-1/2B	0.0860	406	166	27.4	1.97	113	5.06	111	521
C4-1000-1-1/2B	0.239	602	364	29.5	2.41	49.1	<6.57	62.2	1090
C4-1200-1-1/2B	0.0133	684	436	3.94	2.40	44.1	<6.57	43.8	1320
C4-800-2-1/2B	0.00374	7.63	<0.400	12.5	16.5	8455	<32.8	<30.7	21.7
C4-900-2-1/2B	0.0335	4.33	<0.400	15.8	9.41	9075	28.6	13.1	20.5
C4-1000-2-1/2B	0.180	12.9	<0.400	24.0	5.39	5976	<6.57	<6.13	6.62
C4-1200-2-1/2B	0.346	48.2	18.2	66.0	14.5	8057	<6.57	<6.13	71.1

Table 9.10 (Contd)

Sample ID	Re	Na	S	Cl ⁻	F ⁻	NO ₃	NO ₂ ⁻	PO ₄ ³⁻	SO ₄ ²⁻
Pre-melted Glass									
PMG-1000-1-2	0.00715	<5.00	0.506	2.65	1.60	1.27	<0.657	<0.613	0.775
PMG-1000-5-2	0.0147	10.3	2.04	6.27	4.46	1.21	<0.657	<0.613	5.54
PMG-1100-1-2	0.0287	8.25	2.39	11.6	2.58	0.978	<0.657	<0.613	6.51
PMG-1100-5-2	0.129	45.7	13.9	48.3	12.5	1.09	<0.657	<0.613	41.5
PMG-1100-5-2 2nd	0.179	68.5	21.6	71.0	17.0	12.0	<3.28	<3.07	65.0
PMG-1200-1-2	0.214	76.2	44.6	68.1	13.7	5.67	<3.28	<3.07	137
PMG-1200-5-2	0.443	141	88.6	123	20.2	<4.43	<3.28	<3.07	266

Table 9.11 summarizes the wt% of the total mass added to the feed (or glass) found in each crucible rinse or condensate solution for all the components analyzed. The concentration of SO₄ ion was converted to elemental S. For the tests with feeds, the mass of each component was calculated by multiplying the volume of solution collected by the analyzed concentration. The total mass used in each test was obtained from either analyzed concentrations (for Re, Na, S, and PO₄) for the feeds or target concentrations (for Cl, F, NO₃, NO₂) and the mass of feed or glass used in each test.

For pre-melted glass, NO₃ and NO₂ are not applicable, and PO₄ concentration was below reporting limits for all samples. The analyzed concentrations were used for Re, Na, and S, and target concentrations were used for Cl and F. The actual Cl and F concentrations in the pre-melted glass will be lower than the target value because of volatilization, but this analysis is still valid for a relative comparison between tests.

The S results by ICP-AES showed good agreement with IC results for all crucible rinse solutions; however, there were some cases of discrepancy for condensate samples with a low concentration. The IC results will be used for data evaluation because the IC methods provided lower reporting limits for those samples with a low concentration. The sample results for low concentrations do not make any practical difference in evaluating results.

For PO₄ and NO₂, the wt% of total in the crucible rinse decreases as the temperature increases because of decomposition (NO₂) and/or reaction into glass-forming melt (PO₄), but they are not found in the condensate samples in any significant amount. For NO₃, similarly to NO₂ and PO₄, the wt% of the total analyzed in the crucible rinse decreases as temperature increases; however, NO₃ is captured in the condensate. The NO₃ results will be used for the main evaluation. For Cl and F, Cl is used for further evaluation to analyze the behavior of halogens because the change of F is overall similar to Cl. In summary, data are evaluated on Re, Na, S, Cl, and NO₃ results.

Table 9.11. Wt% of Total Analyzed in Crucible Rinse or Condensate Solution

Samples	Test Condition	Re	Na	S	Cl	F	NO ₃	NO ₂	PO ₄	S
Case 1: Crucible Rinse	800°C	24.37	23.48	43.57	34.38	25.69	7.01	9.75	30.84	42.61
	900°C	3.54	1.14	12.39	2.81	0.76	0.25	0.15	9.33	12.49
	1000°C	10.07	0.79	18.29	4.86	0.77	0.04	0.02	2.37	18.81
	1000°C-1/2B	9.02	1.10	25.40	4.72	1.17	0.06	-	3.95	25.74
	1200°C	1.35	1.24	32.59	1.94	0.98	0.03	-	1.73	33.48
	1200°C-1/2B	0.91	0.97	24.77	0.82	0.79	0.08	0.06	1.27	25.16
Case 1: Condensate Solution	800°C	0.72	0.03	-	9.64	-	81.14	-	-	1.28
	900°C	4.68	0.03	-	12.41	0.04	94.85	0.13	-	2.28
	1000°C	25.86	0.07	-	15.27	-	91.84	-	-	3.58
	1000°C-1/2B	27.73	0.09	0.16	13.40	7.38	61.23	-	-	1.28
	1200°C	52.02	0.21	1.71	28.23	13.22	89.16	-	-	7.24
	1200°C-1/2B	44.23	0.21	3.17	26.48	15.59	63.35	-	-	5.38
Case 2: Crucible Rinse	800°C	38.40	20.47	51.42	50.35	29.54	15.27	20.82	20.92	49.53
	900°C	19.26	1.22	22.82	9.80	1.58	0.25	0.25	1.90	23.58
	1000°C	19.48	1.55	35.25	11.79	1.46	0.06	-	1.64	35.58
	1200°C	0.69	1.42	38.05	2.92	0.82	0.05	-	0.89	38.19
Case 2: Condensate Solution	800°C	1.22	-	-	4.15	-	56.70	-	-	2.19
	900°C	6.29	-	-	6.83	1.39	74.98	-	-	2.97
	1000°C	32.49	0.19	1.37	14.57	2.48	75.39	-	-	6.48
	1200°C	58.16	0.45	2.58	29.41	7.10	77.08	-	-	8.39
Case 3: Crucible Rinse	800°C	58.41	35.85	73.12	96.24	69.54	42.73	57.53	15.01	75.76
	900°C	2.51	0.39	8.57	3.82	0.48	0.04	0.04	0.95	8.88
	1000°C	7.91	0.80	21.36	3.73	1.05	0.10	0.05	0.63	22.23
	1200°C	0.38	0.71	20.24	1.22	2.05	0.06	-	0.42	21.94
Case 3: Condensate Solution	800°C	0.29	-	-	2.55	2.97	20.47	-	-	0.55
	900°C	4.30	-	-	14.93	-	91.43	-	-	2.33
	1000°C	33.41	0.56	0.63	28.34	157 ^(a)	77.71	-	-	5.74
	1200°C	38.32	0.43	0.87	13.66	1331 ^(a)	32.22	-	-	1.39
Case 4: Crucible Rinse	800°C	0.74	12.85	24.60	12.70	6.17	0.14	0.13	30.71	25.18
	900°C	2.19	0.58	9.13	3.21	0.59	0.13	0.05	3.36	9.56
	1000°C	6.06	0.85	19.95	3.45	0.72	0.06	-	1.88	19.94
	1200°C	0.35	1.01	24.82	0.48	0.75	0.05	-	1.38	25.08
Case 4: Condensate Solution	800°C	0.70	0.08	-	10.82	36.71	72.92	-	-	2.94
	900°C	6.07	0.04	-	13.19	20.20	75.52	1.90	2.83	2.68
	1000°C	31.09	0.12	-	19.11	11.03	47.42	-	-	0.83
	1200°C	61.32	0.48	6.97	53.92	30.46	65.60	-	-	9.10
Premelted Glass: Condensate Solution	1000°C 1h	1.05	-	0.12	0.99	1.54	-	-	-	0.06
	1000°C 5h	2.01	0.04	0.47	2.19	4.02	-	-	-	0.42
	1100°C 1h	4.26	0.04	0.59	4.39	2.52	-	-	-	0.54
	1100°C 5h	17.67	0.19	3.18	16.88	11.27	-	-	-	3.17
	1100°C 5h 2nd	27.35	0.32	5.51	27.67	17.09	-	-	-	5.53
	1200°C 1h	30.64	0.33	10.65	24.86	12.91	-	-	-	10.92
1200°C 5h	59.92	0.57	19.99	42.43	17.98	-	-	-	20.03	

The blank cells indicate that the analytical results were below the reporting limit.
(a) The data are in error—source of error unknown.

Table 9.12. Analyzed Concentration and Wt% of Total Retained in Glass for Re, Na, and S

Sample	Concentration, mg/kg			Wt% of Total Retained in Glass		
	Re	Na	S	Re	Na	S
Tests with Dried Feeds at 1200°C Final Temperature						
Case 1	3.40	146000	2390	38.8	94.5	63.1
Case 1-1/2B	3.45	142500	2375	39.3	92.2	62.7
Case 2	2.33	147000	2100	27.9	92.8	55.2
Case 3	3.56	149000	2710	39.9	91.2	72.8
Case 4	3.25	142000	2180	37.3	91.3	54.1
Tests with Pre-melted Glass						
1000°C 1h	4.34	144000	2640	93.4	93.3	94.7
1000°C 5h	4.16	144000	2620	89.5	93.3	94.0
1100°C 1h	3.89	142000	2470	83.7	92.0	88.6
1100°C 5h	3.08	143000	2490	66.3	92.7	89.4
1100°C 5h 2nd	3.10	143000	2490	66.7	92.7	89.4
1200°C 1h	3.10	140000	2360	66.7	90.7	84.7
1200°C 5h	1.61	144000	1970	34.6	93.3	70.7

Table 9.13 summarizes the analytical results of Re, Na, and S concentrations for those samples with duplicate analyses. Table 9.13 shows that the reproducibility of analyses is good with a RPD of 10% or smaller for all samples.

There was only one duplicate test that was performed under exactly the same condition (test with pre-melted glass at 1100°C for 5 h), and there were two duplicate tests that were performed under the same condition except for the batch size (tests with Case 1 feed at final temperatures of 1000 and 1200°C). Table 9.14 summarizes the results from these duplicate tests. Table 9.14 shows that there was no apparent bias between tests with different batch sizes (i.e., ½ batch size was obtained, depending both upon test condition and component) and that the reproducibility of duplicate tests was in general poor with the RPD of up to 43% for Re. This poor reproducibility, although based on very limited data, suggests that one should be cautious when evaluating the present results.

Table 9.13. Summary of Duplicate Analytical Results

Solution Samples							
Sample ID	Sample Description	Analyzed Concentration			RPD, %		
		Re (mg/L)	Na (mg/L)	SO ₄ (mg/L)	Re	Na	SO ₄
C1-1000-1	Case 1, 1000°C run, crucible rinse	0.803	1110	1930	0.1	0.0	1.0
Duplicate		0.802	1110	1950			
C2-1000-2	Case 2, 1000°C run, condensate	0.285	29.8	73.1	2.5	4.9	8.9
Duplicate		0.278	31.3	79.9			
C3-1000-1	Case 3, 1000°C run, crucible rinse	0.363	670	1280	0.5	0.7	0.0
Duplicate		0.365	675	1280			
C1-1000-1-1/2 BATCH	Case 1 with 1/2 batch, 1000°C run, crucible rinse	0.35	743	1280	2.0	0.1	0.0
Duplicate		0.343	744	1280			
Glass samples							
Sample ID	Sample Description	Analyzed concentration			RPD, %		
		Re (mg/kg)	Na (mg/kg)	S (mg/kg)	Re	Na	S
Re Glass A	Pre-melted glass, sample A	4.55	155000	2850	1.3	1.3	1.0
Duplicate		4.61	153000	2880			
Re Glass B	Pre-melted glass, sample B	4.75	153000	2830	1.9	0.0	0.4
Duplicate		4.66	153000	2840			
C1-1200-3-1/2 BATCH	Case 1 with 1/2 batch, 1200°C run, glass	3.57	144000	2370	7.0	2.1	0.4
Duplicate		3.33	141000	2380			
The SO ₄ concentration in solution samples was from IC, and the S concentration in glass samples was from ICP-MS.							
RPD: relative percent difference (the absolute value of difference was divided by the average of two)							

Table 9.14. Comparison of Results from Duplicate Tests

Samples	Test Condition	Wt% of Total Analyzed in each Sample			RPD, %		
		Re	Na	S	Re	Na	S
Crucible rinse	Case 1, 1000°C	10.07	0.79	18.81	-11.0	32.8	31.1
	Case 1, 1000°C-1/2B	9.02	1.1	25.74			
	Case 1, 1200°C	1.35	1.24	33.48	-38.9	-24.4	-28.4
	Case 1, 1200°C-1/2B	0.91	0.97	25.16			
Condensate solution	Case 1, 1000°C	25.86	0.07	3.58	7.0	25.0	-94.7
	Case 1, 1000°C-1/2B	27.73	0.09	1.28			
	Case 1, 1200°C	52.02	0.21	7.24	-16.2	0.0	-29.5
	Case 1, 1200°C-1/2B	44.23	0.21	5.38			
	PMG, 1100°C 5h	17.67	0.19	3.17	43.0	51.0	54.3
	PMG, 1100°C 5h 2nd	27.35	0.32	5.53			
Glass	Case 1, 1200°C	38.8	94.5	63.1	1.3	-2.5	-0.6
	Case 1, 1200°C-1/2B	39.3	92.2	62.7			
	PMG, 1100°C 5h	66.3	92.7	89.4	0.6	0.0	0.0
	PMG, 1100°C 5h 2nd	66.7	92.7	89.4			
RPD: relative percent difference, $([duplicate] - [original])/[average]$							

9.3.1 Tests with Pre-Melted Glass

Figure 9.3 displays the wt% of total Re, S, and Cl analyzed in condensate, and Figure 9.4 shows Re and S retained in glass from tests with pre-melted glass as a function of temperature. The overall volatilization of Re, S, and Cl strongly increased as the temperature increased, starting from a negligible extent at 1000°C. At 1200°C, ~30% of Re was lost through volatilization after 1 h and ~60% after 5 h. As seen in Figure 9.4, retention of Re and S in glass is inversely proportional to the observed volatilization. Figure 9.3 shows that Re had the highest volatility among three components whereas S had the lowest volatility.

Figure 9.5 and Figure 9.6 display the wt% of total Re (Figure 9.5) and S (Figure 9.6) analyzed in condensate solutions and retained in glass from tests with pre-melted glass, showing the trend of increasing volatilization as the temperature and the time increase. Figure 9.5 and Figure 9.6 show that the modified experimental setup developed in this study successfully achieved a high mass balance closure, which was ~93% on average for both Re and S, not including the contribution from the crucible rinse. This result is encouraging considering the typical analytical uncertainty of ±10%.

Figure 9.7 and Figure 9.8 (same as Figure 9.7 in log scale) plot the average volatilization rate, $r_{a,i}$ (in wt%/h obtained as an average rate between 1 and 5 h), of Re, S, and Cl as a function of temperature. Figure 9.8 is the same as Figure 9.7 but in logarithm of $r_{a,i}$ versus reciprocal temperature to fit the Arrhenius form

$$r_{a,i} = r_{a,i0} \exp(-E_{a,i}/RT) \quad (9.1)$$

where $r_{a,i0}$ = a constant

$E_{a,i}$ = an experimental activation energy for average volatilization

R = a gas constant (8.314 J/mol K)

T = the absolute temperature.

Figure 9.8 shows that the experimental data do not fit the Arrhenius equation well, which is understandable because the $r_{a,i}$ was based on the initial concentration whereas the volatilization rate should be adjusted as the concentration of volatiles in the melt decreases, especially in the case of the extremely high volatilization rate in this study. The activation energy values directly obtained from Figure 9.8 (simple linear fit) were 270, 254, and 214 kJ/mole for Re, S, and Cl, respectively.

A more rigorous analysis was performed for Re to obtain the activation energy based on the volatilization rate adjusted for the concentration of volatiles in the melt. The accumulated wt% of Re volatilized, w , for the test conditions in this study is given as

$$w_{\theta,\tau} = \int_{773}^{\frac{\theta-773}{5}} r(1-w)dt + \int_{\frac{\theta-773}{5}}^{\frac{\theta-773}{5}+\tau} r_{T=\theta}(1-w)dt \quad (9.2)$$

where θ is the final temperature (1273, 1373, or 1473 K), τ is the time (60 or 300 min) at the final temperature, and r is the volatilization rate of Re, which is defined as:

$$r = \frac{dw}{(1-w)dt} \quad (9.3)$$

The temperature dependence of r is given as

$$r = r_0 \exp(-E/RT) \quad (9.4)$$

where r_0 is a constant. During ramp heating from 500°C to the final temperature, $T = 773 + 5t$, then Equation (9.2) can be rewritten as

$$w_{\theta,\tau} = \int_{773}^{\frac{\theta-773}{5}} r_0 \exp\left(-\frac{E}{R(773+5t)}\right) (1-w) dt + \int_{\frac{\theta-773}{5}}^{\frac{\theta-773}{5}+\tau} r_{T=\theta} (1-w) dt \quad (9.5)$$

Because there is no analytical solution to Equation (9.5), a simple numerical calculation was performed to obtain the constants r_0 and E . Using the w (equivalent to the wt% of total analyzed in condensate) data given in Table 9.11, we obtain $r_0 = 4,998,969 \text{ min}^{-1}$ and $E = 258 \text{ kJ/mole}$. Table 9.15 summarizes the volatilization rate calculated from Equation (9.4). Figure 9.9 shows the measured and calculated values of the accumulated Re wt% volatilized.

Table 9.15. Calculated Re Volatilization Rate

Temperature (°C)	Re volatilization rate (r), wt%/hr
1000	0.7
1100	4.4
1200	20.4

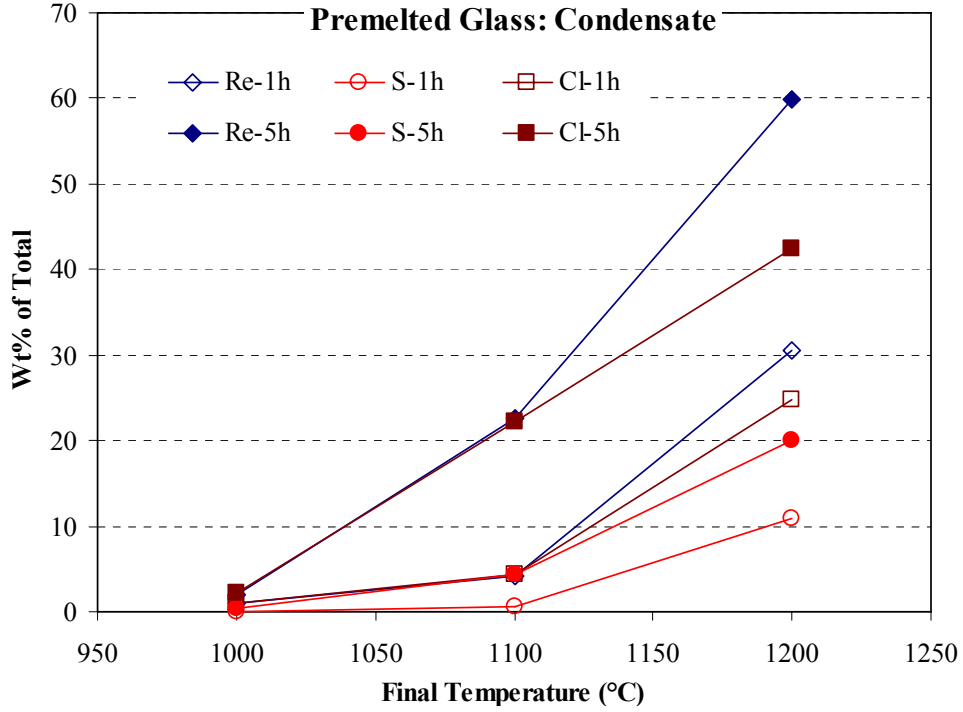


Figure 9.3. Wt% of Total Analyzed in Condensate Solutions from the Tests with Pre-melted Glass

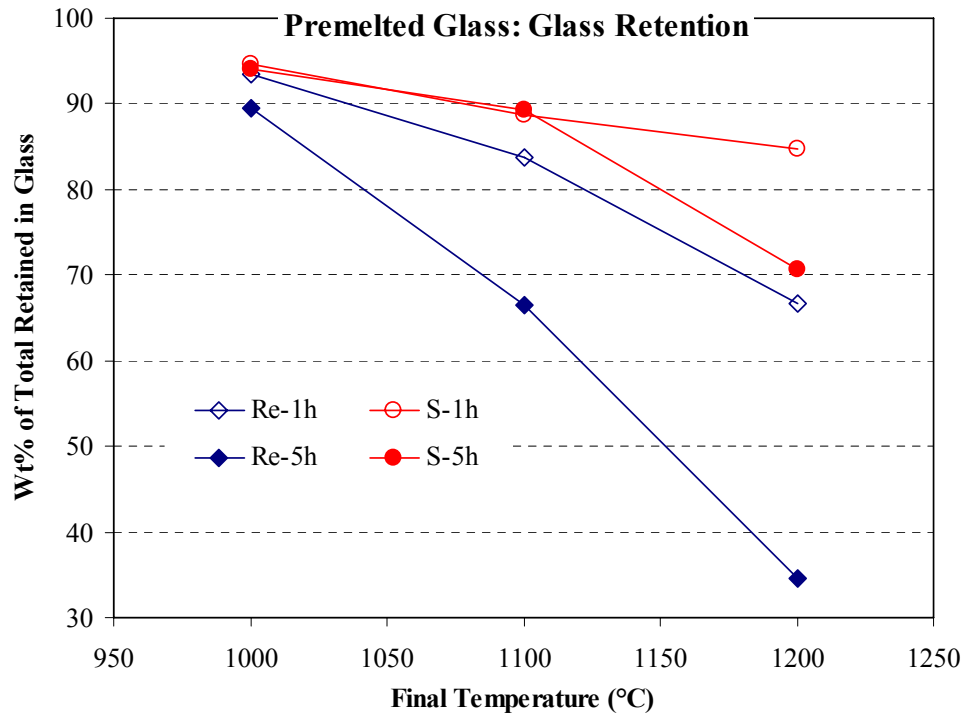


Figure 9.4. Wt% of Total Retained in Glass from the Tests with Pre-melted Glass

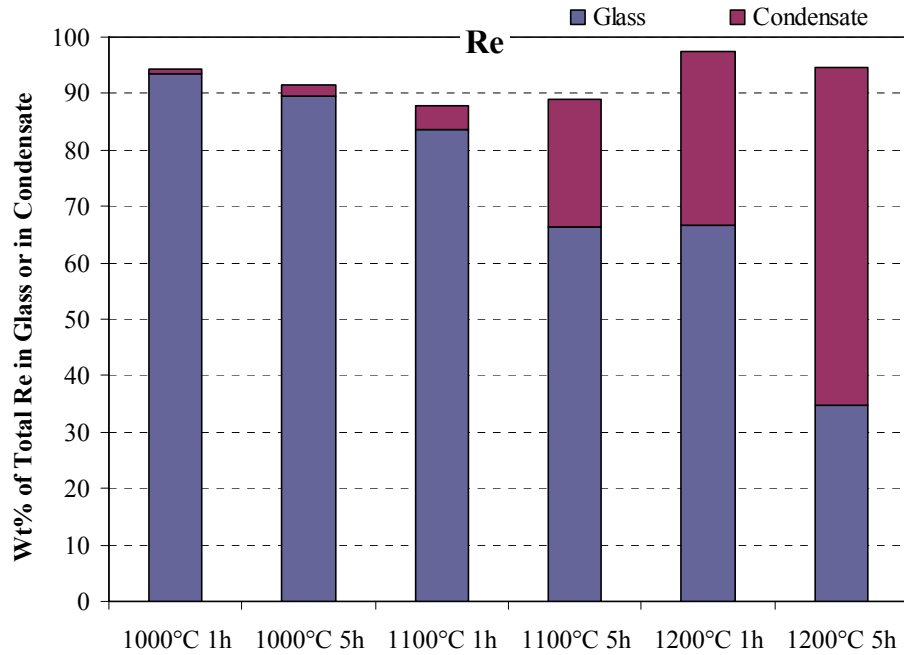


Figure 9.5. Wt% of Total Re Retained in Glass and Analyzed in Condensate Solutions from the Tests with Pre-melted Glass

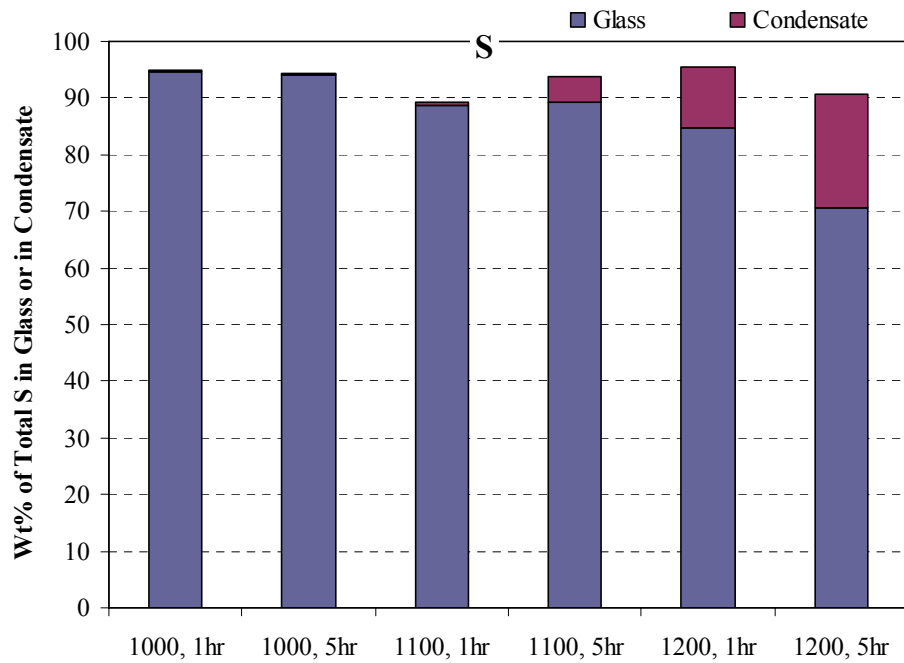


Figure 9.6. Wt% of Total S Retained in Glass and Analyzed in Condensate Solutions from the Tests with Pre-melted Glass

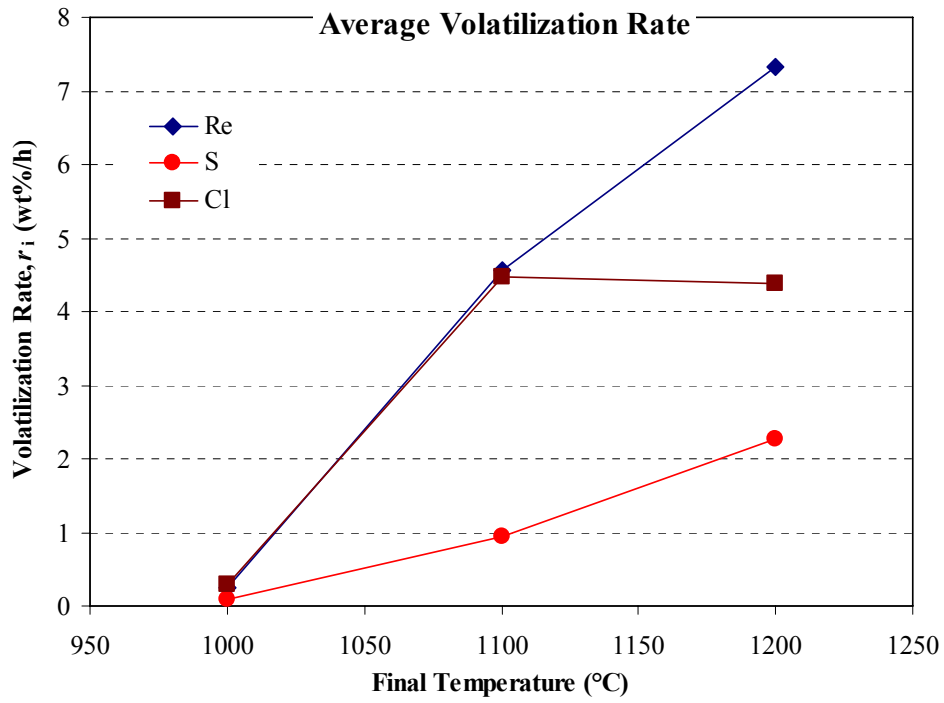


Figure 9.7. Average Volatilization Rate of Re, S, and Cl from Pre-melted Glass

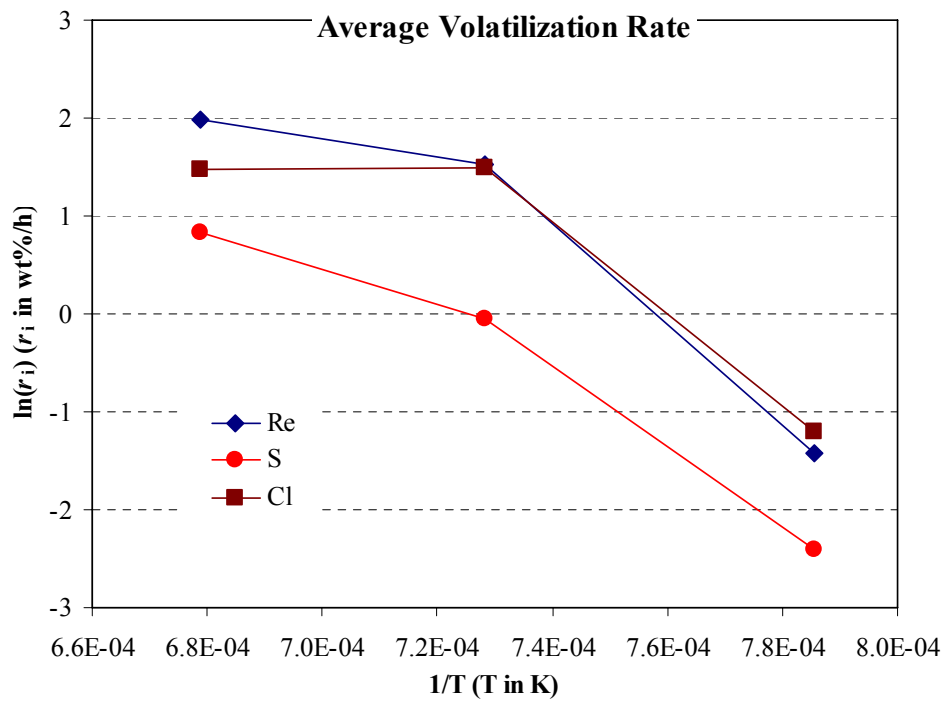


Figure 9.8. Natural Log of Average Volatilization Rate of Re, S, and Cl from Pre-melted Glass

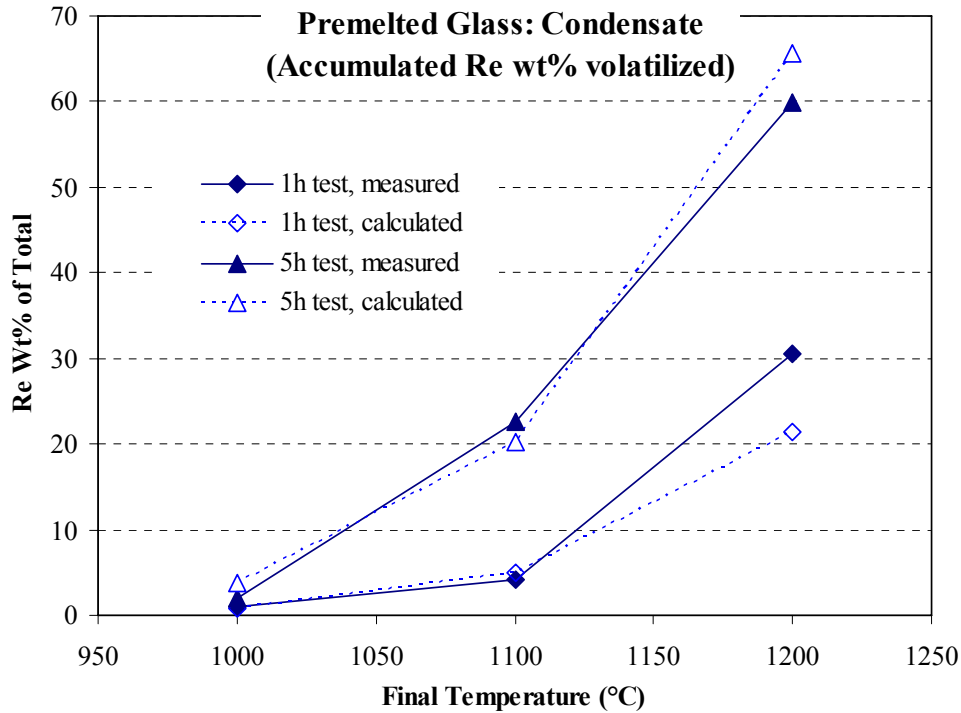


Figure 9.9. Measured Versus Calculated Accumulated Re wt% Volatilized

9.3.2 Tests with Dried Feed

Figure 9.10 and Figure 9.11 display the wt% of total Re, Na, S, Cl, and NO₃ analyzed in the crucible rinse (Figure 9.10) and in the condensate (Figure 9.11) from tests with Case 1 (baseline) feed. The same plots from the tests with Case 2 (high Cl/F) feed are in Figure 9.12 (crucible rinse) and Figure 9.13 (condensate), Case 3 (high CaO/MgO) feed in Figure 9.14 (crucible rinse) and Figure 9.15 (condensate), and Case 4 (crushed soil) feed in Figure 9.16 (crucible rinse) and Figure 9.17 (condensate). The plots of the wt% of total Re, S, and Cl analyzed in both crucible rinse and condensate for all test cases are in Figure 9.18 (Re), Figure 9.19 (S), and Figure 9.20 (Cl).

Figure 9.10 shows that Na and NO₃ in the crucible rinse decrease to close to zero at 900°C. The concentration of Cl and Re decreases between 800 and 900°C, increases between 900 and 1000°C, and then decreases as the temperature increases from 1000 to 1200°C, whereas S decreases between 800 and 900°C and then increases between 900 and 1200°C.

The decrease of Na and NO₃ to close to zero at 900°C suggests that most NaNO₃ and (other salts) reacted with additives (mainly soil) to form glass-forming melt and generated NO₃ by 900°C. Starting from ~900°C, the remaining MIS was highly concentrated with sulfate as the nitrate decomposition was completed. It is likely that the salt phase at 900°C is distributed as droplets throughout the glass-forming melt. Then a separated salt layer started to form as the temperature increased, transported by rising bubbles (Hrma et al. 2005), which can be inferred from the increase of sulfate between 900 and 1200°C shown in Figure 9.10. The method of crucible rinse used in this study did not dissolve the salt phases that were distributed in small closed pores or as small inclusions. The decrease of Re and Cl in the crucible

rinse is explained by the volatilization of Re and Cl from this separated sulfate salt. This means that the Re and Cl that did not become incorporated into glass-forming melt during initial melting was lost through volatilization below 1200°C.

Figure 9.11 shows that NO₃ in the crucible rinse increased to ~80 wt% at 800°C and was constant—it is likely that the difference measured between 900 and 1200°C is within experimental variation. No measurable volatilization was observed for Na. The volatilization of Re, S, and Cl increased as the temperature increased with the highest rate for Re.

Figure 9.12 shows that the crucible rinse from the Case 2 feed with spiked Cl and F had a general behavior similar to the baseline feed. One noticeable difference was that the crucible rinse from the Case 2 feed had an overall higher wt% of Re, S, and Cl rinse at 900 and 1000°C. Figure 9.13 also shows that the condensate from the Case 2 feed showed a trend similar to the baseline feed, but with significantly lower NO₃ at 800°C and slightly higher Re than the baseline feed.

Figure 9.14 shows that the crucible rinse from the Case 3 feed with higher CaO and MgO also showed an overall trend similar to that shown by the baseline feed. A noticeable difference was seen in the 800°C crucible rinse results where all five components from the Case 3 feed had higher concentrations than the baseline feed. For condensate, Figure 9.15 shows that there was a major decrease in the NO₃ for 800 and 1200°C tests for Case 3, relative to the baseline feed. Another noticeable difference was that the increase of Re in the condensate between 1000 and 1200°C was smaller for the Case 3 feed than for the baseline feed. The low NO₃ level in the Case 3 condensate agrees well with the high NO₃ in the crucible rinse at 800°C. Overall, the high wt% of MIS components in the crucible rinse and low NO₃ in the condensate at 800°C compared to the baseline suggests that the incorporation of MIS into glass-forming melt was delayed in the Case 3 feed. However, the low NO₃ at 1200°C is not understood.

Figure 9.16 shows that crucible rinses for the Case 4 (crushed soil) feed also behave similarly to the baseline feed. The main difference was that the 800°C Case 4 test showed an overall lower concentration of MIS components in the crucible rinse, especially NO₃, which was zero at 800°C. This suggests that nitrate decomposition is complete below 800°C for the Case 4 feed, whereas the nitrate decomposition is complete between 800 and 900°C for the baseline feed. The finer particle size of crushed soil seemed to accelerate the reaction between MIS and soil. However, this early reaction had no noticeable effect on the volatilization of the MIS components. Figure 9.17 shows that the Case 4 feed condensate had results comparable to the baseline feed. The only difference was that the NO₃ wt% in the condensate was lower than the baseline, especially at 1000°C.

Figure 9.21 shows the wt% of Re and S retained in the glass for the tests with dried feeds at a final temperature of 1200°C. Figure 9.21 shows that Re retention in the glass is 29% lower than the baseline for Case 2 feed while Case 3 and 4 feeds had Re retentions within ±5% of the baseline. The S retention was higher in Case 3 by 16% and lower in Case 2 and Case 4 by 12% and 14%, respectively. Figure 9.22 and Figure 9.23 show the combined wt% of Re (Figure 9.22) and S (Figure 9.23) present in the glass, crucible rinse, and condensate samples at a final temperature of 1200°C. The total mass balance closure ranged from 79 to 99 wt% with an average of 88 wt% for Re and 88 to 102 wt% with an average of 96 wt% for S. The high variation of mass balance closure for tests with feeds compared to the tests with pre-melted glass is likely caused by larger quantities of gas generated with the feeds. Overall, there was no correlation between the mass balance closures for Re and S—Case 3 feed had lowest mass-balance

closure of 79% for Re, but the S mass balance closure was comparable to other feeds, and Case 4 had the highest mass balance closure for Re whereas it had the lowest for S. This may indicate that the case-to-case variation was not simply related to the materials lost through the Pt crucible and lid gap. Overall, the mass balance for Re was significantly better than that obtained in earlier tests (Kim et al. 2005). However, these tests show that even in well controlled laboratory tests, it is difficult to consistently close the mass balance for Re to better than 90%.

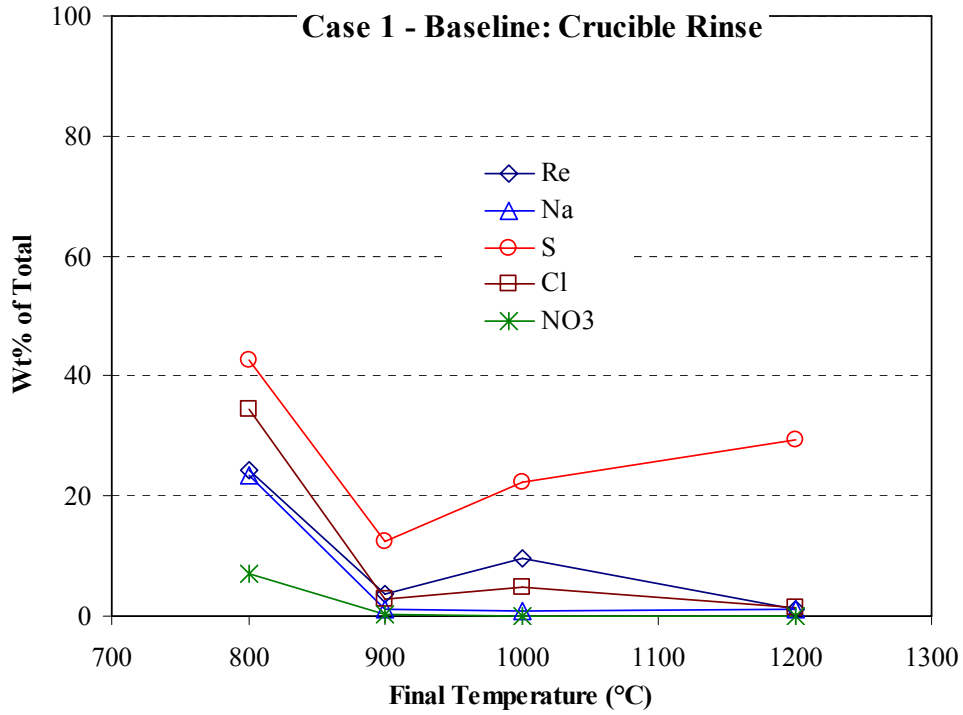


Figure 9.10. Wt% of Total Analyzed in Crucible Rinse from Case 1 (Baseline Feed)

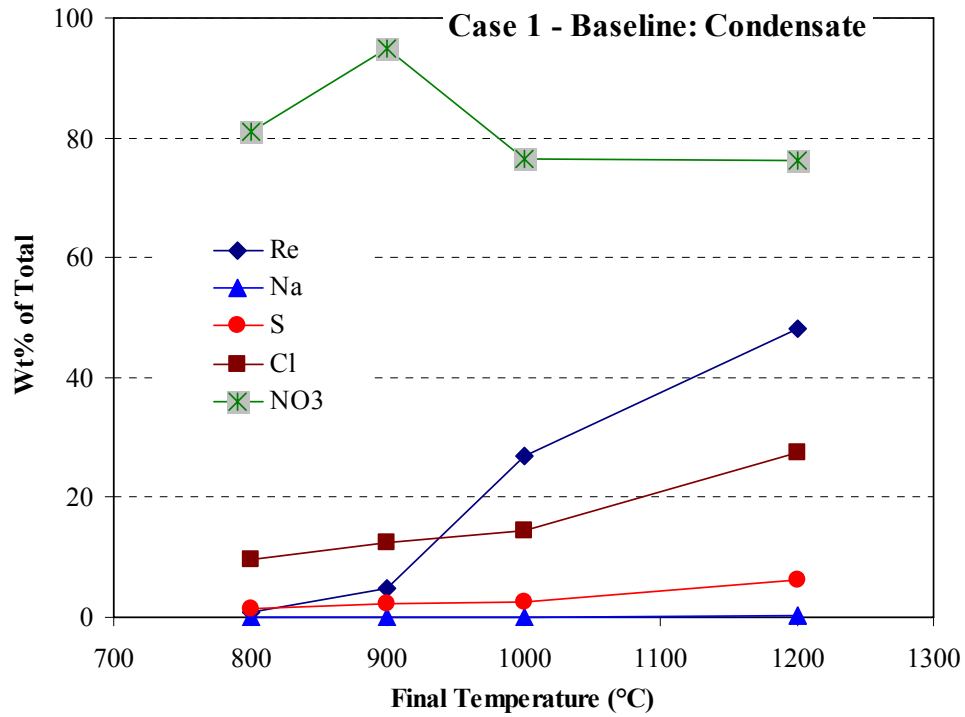


Figure 9.11. Wt% of Total Analyzed in Condensate Solutions from Case 1 (Baseline Feed)

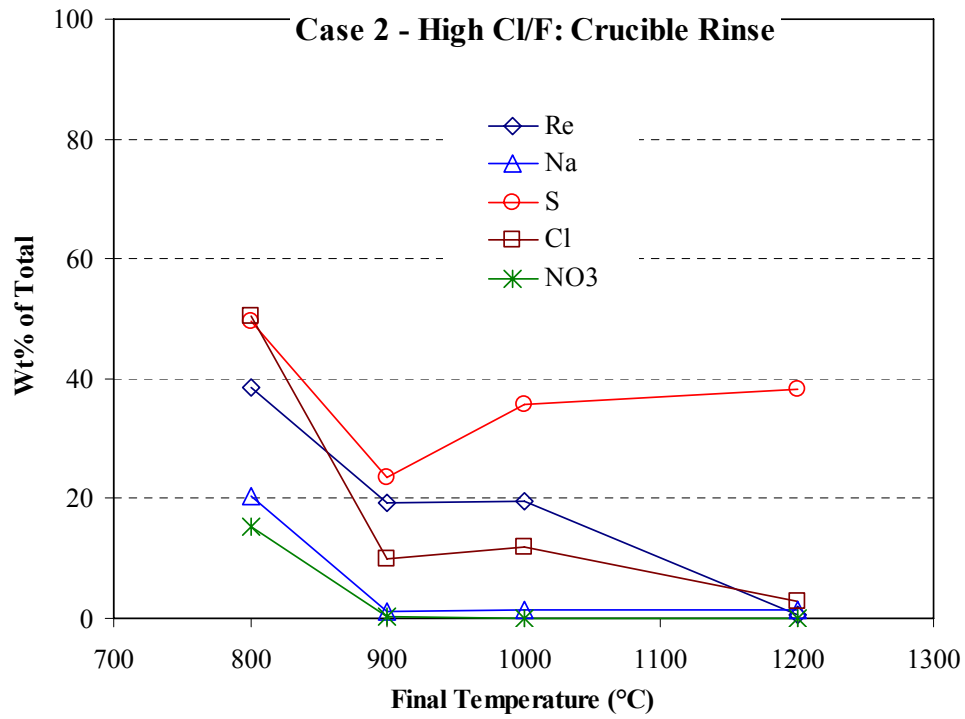


Figure 9.12. Wt% of Total Analyzed in Crucible Rinse from Case 2 (High Cl/F Feed)

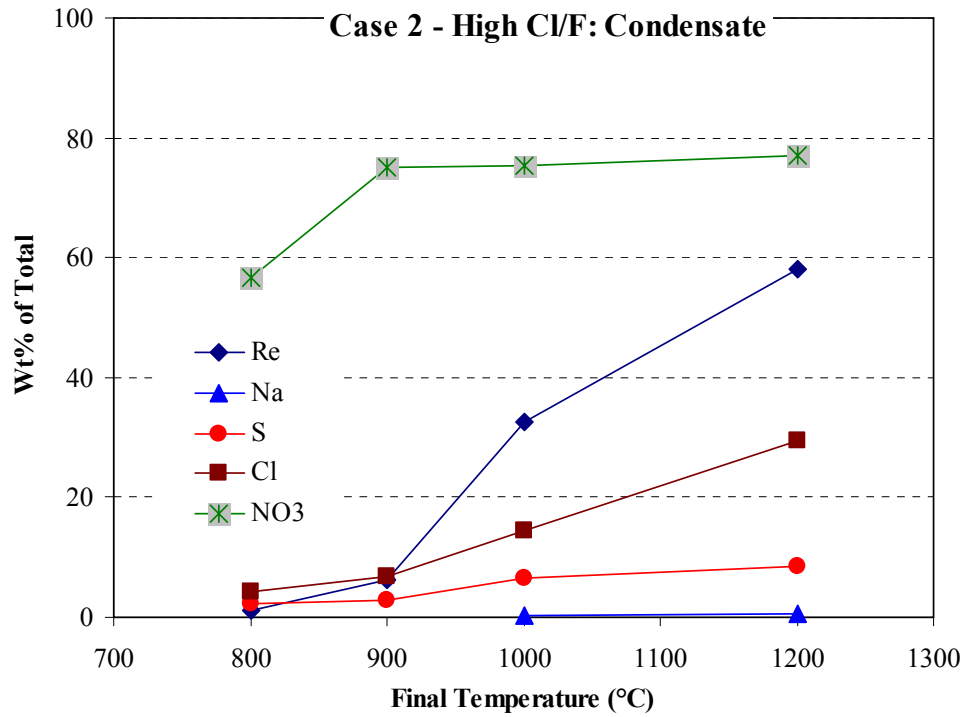


Figure 9.13. Wt% of Total Analyzed in Condensate Solutions from Case 2 (High Cl/F Feed)

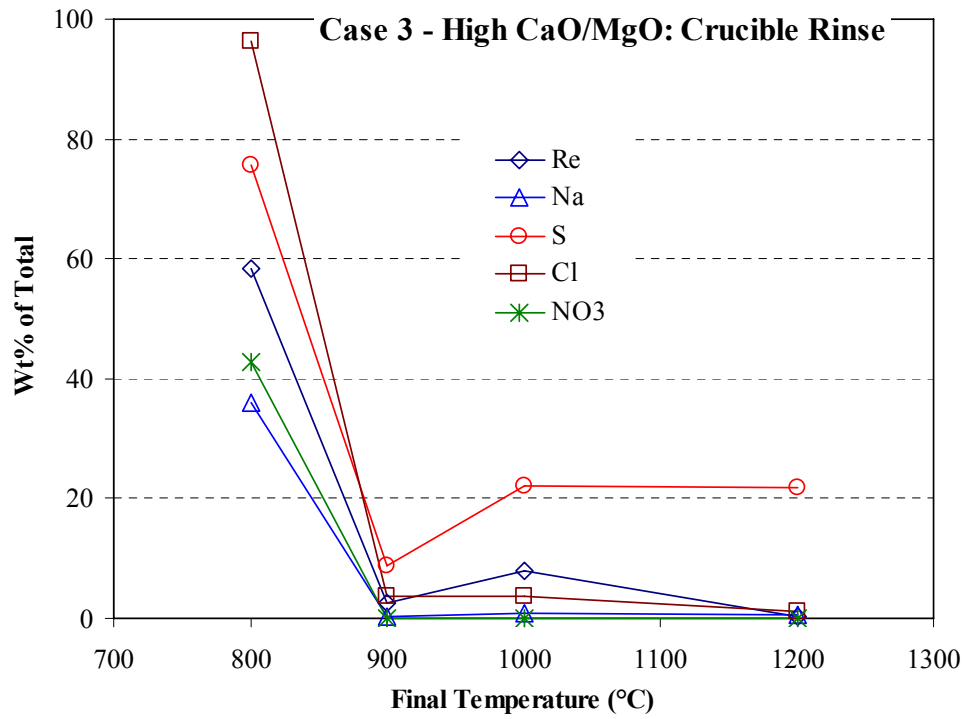


Figure 9.14. Wt% of Total Analyzed in Crucible Rinse from Case 3 (High CaO/MgO Feed)

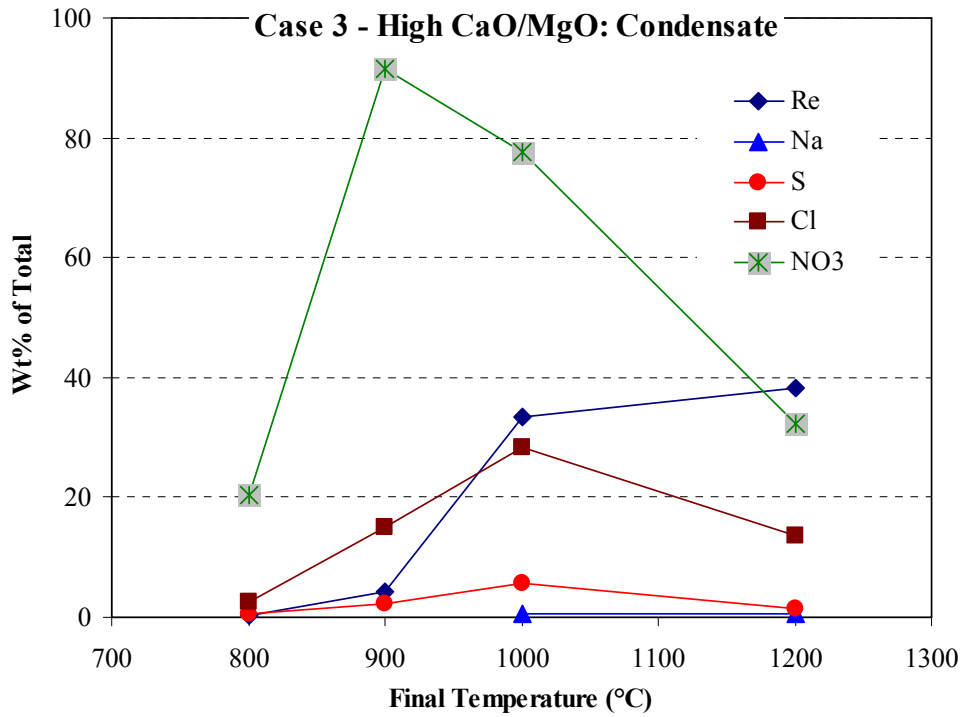


Figure 9.15. Wt% of Total Analyzed in Condensate Solutions from Case 3 (High CaO/MgO Feed)

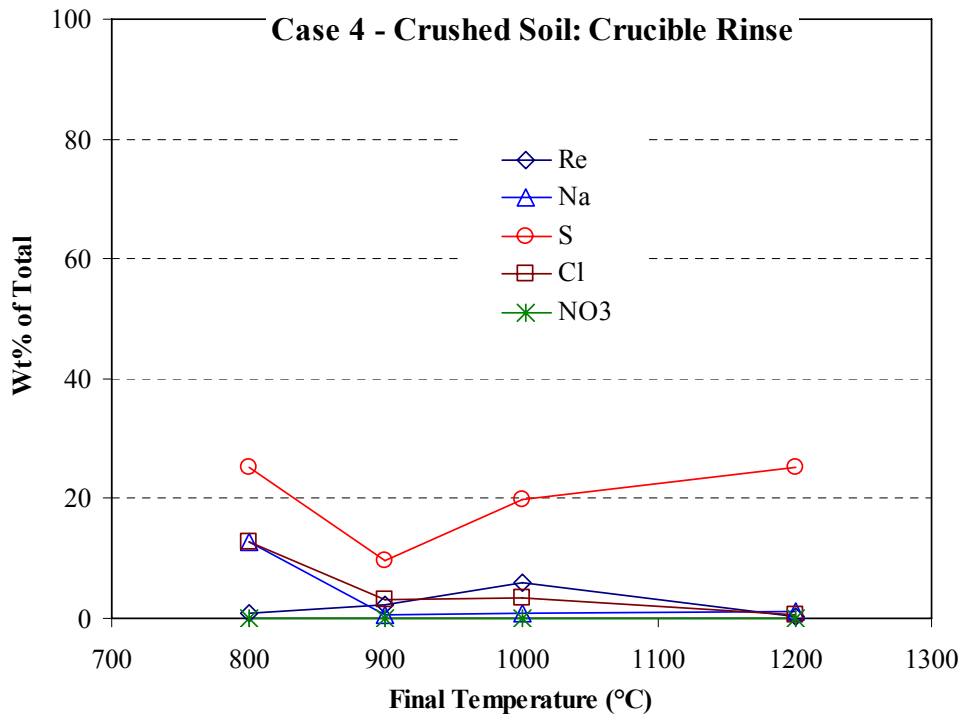


Figure 9.16. Wt% of Total Analyzed in Crucible Rinse from Case 4 (Crushed Soil Feed)

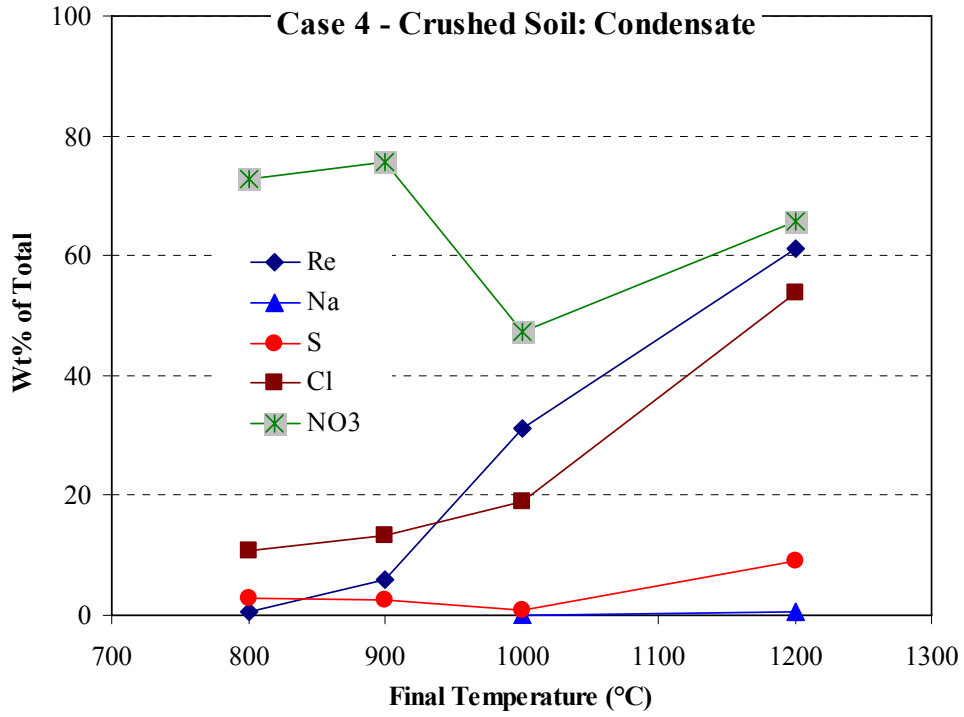


Figure 9.17. Wt% of Total Analyzed in Condensate Solutions from Case 4 (Crushed Soil Feed)

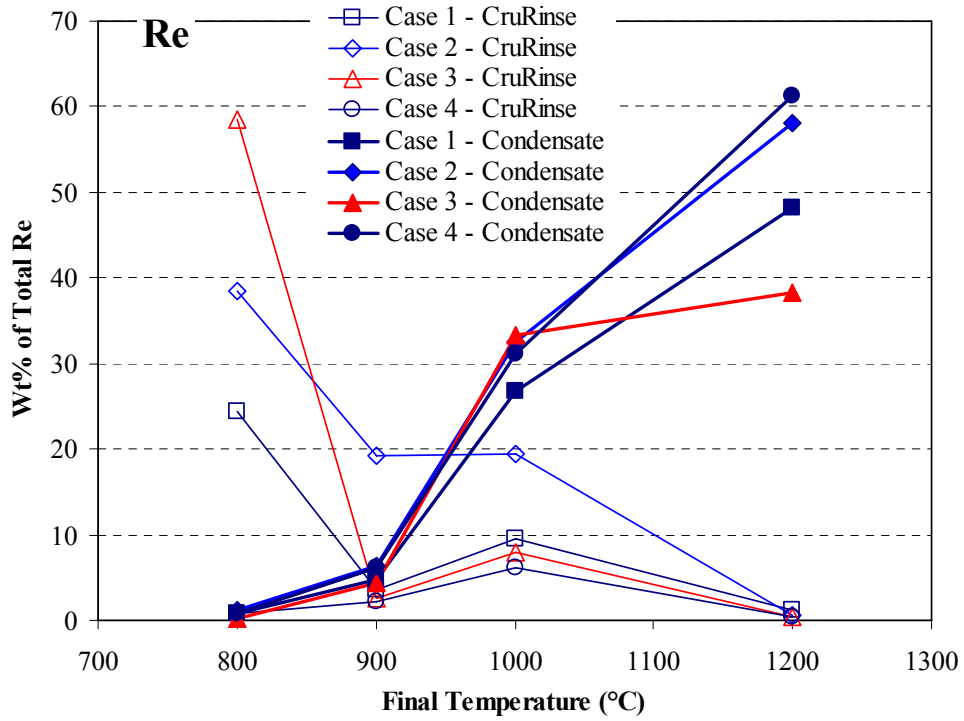


Figure 9.18. Wt% of Total Re Analyzed in All Crucible Rinses and Condensate Solutions

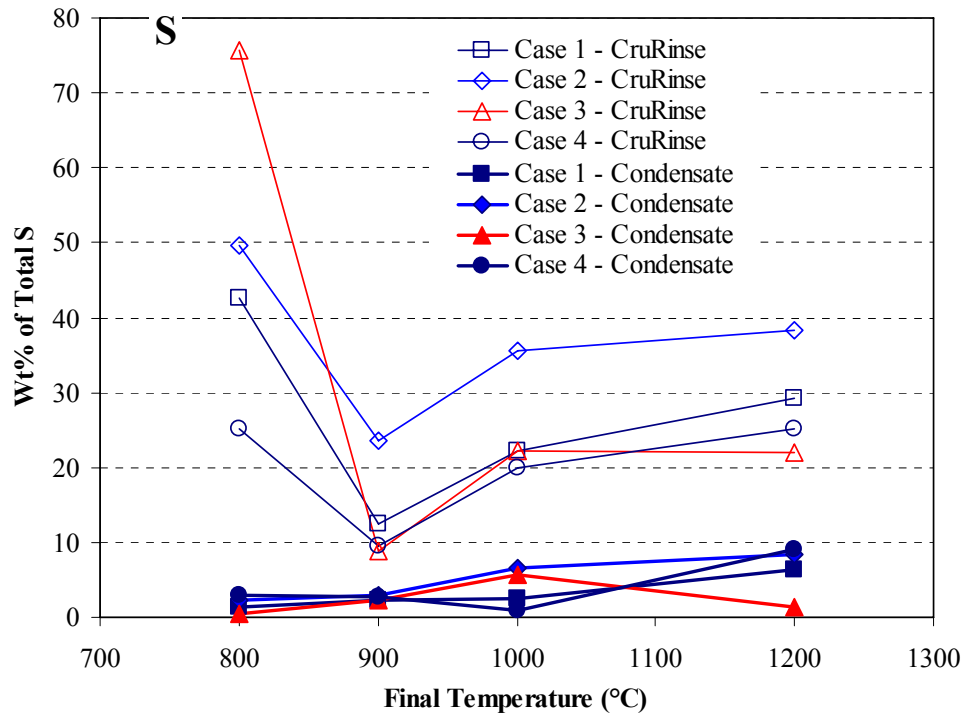


Figure 9.19. Wt% of Total S Analyzed in All Crucible Rinses and Condensate Solutions

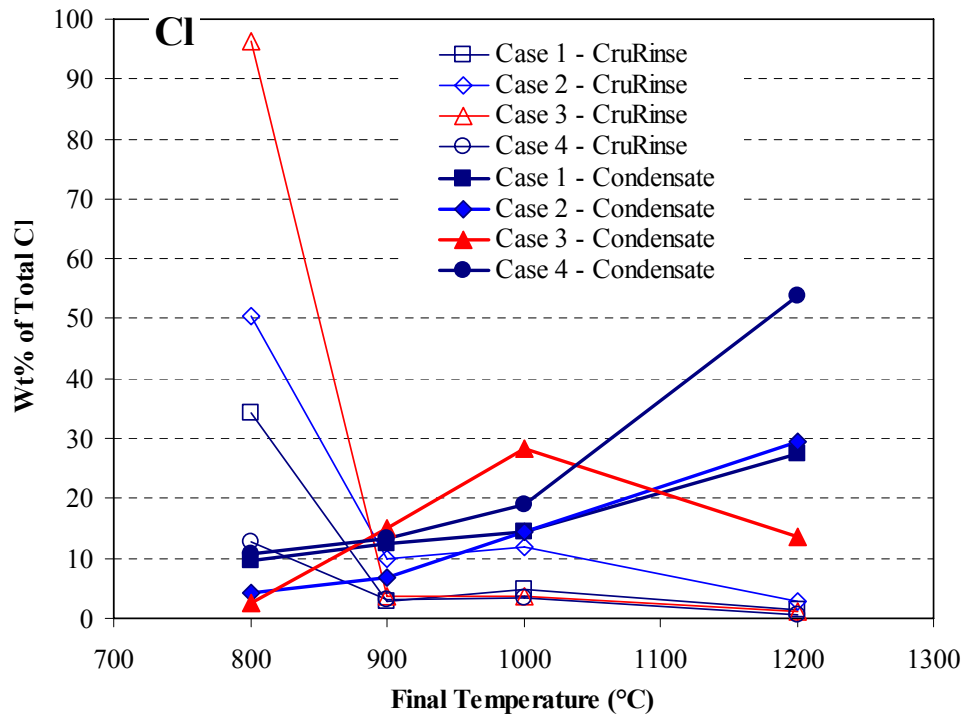


Figure 9.20. Wt% of Total Cl Analyzed in All Crucible Rinses and Condensate Solutions

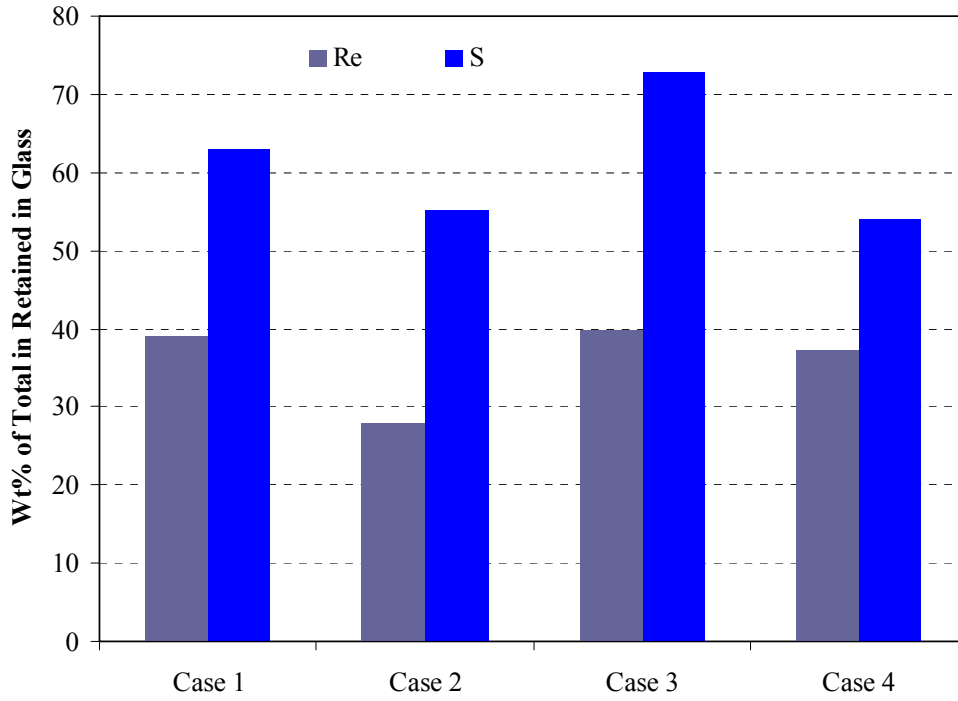


Figure 9.21. Wt% of Total Re and S Retained in Glass Tested at 1200°C

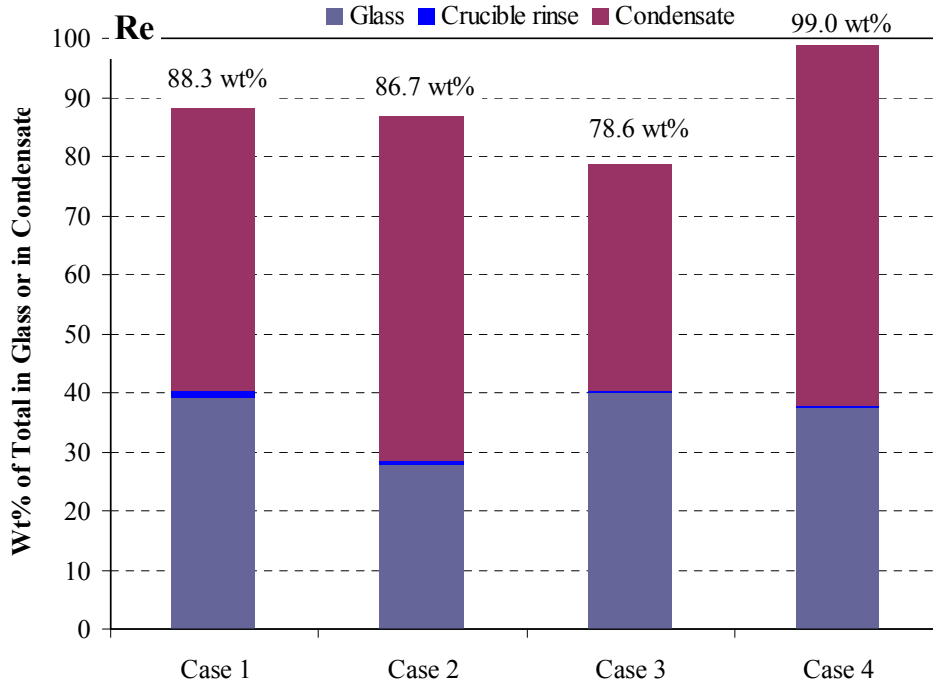


Figure 9.22. Wt% of Total Re Retained in Glass and Analyzed in Crucible Rinse and Condensate Tested at 1200°C

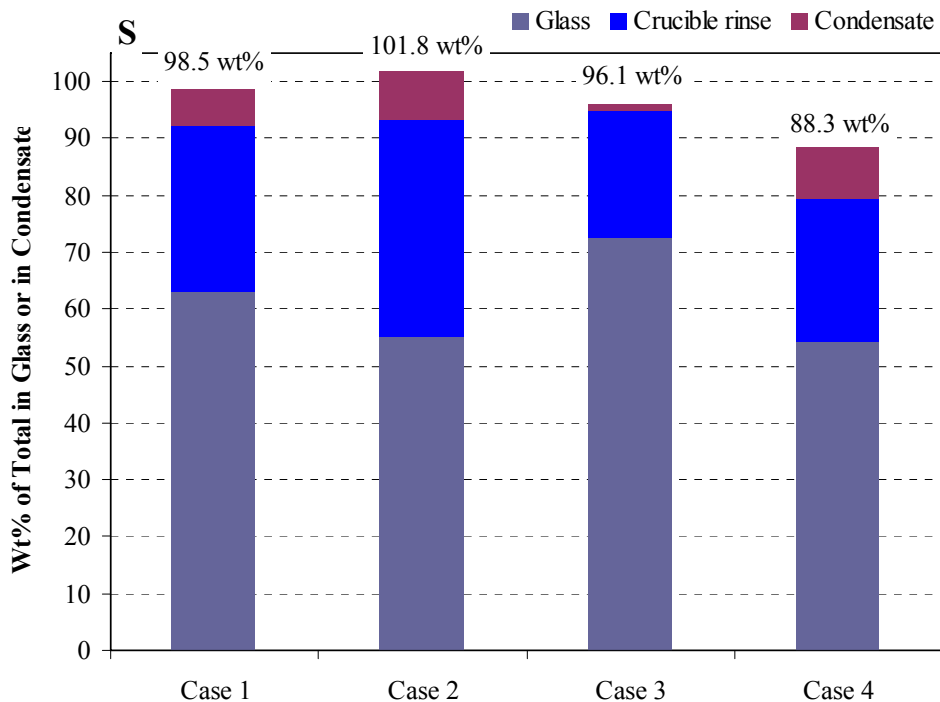


Figure 9.23. Wt% of Total S Retained in Glass and Analyzed in Crucible Rinse and Condensate Tested at 1200°C

9.4 Summary

The tests with pre-melted glass showed that Re is more volatile than S and Cl with an estimated $r = 20.4 \text{ wt\%/h}$ at 1200°C. The volatilization rate of Re showed a strong dependence on temperature with an activation energy of 258 J/mole.

The results of dried feed (Cases 2 to 4) in relation to the baseline feed (Case 1) are summarized below:

- The feed with high Cl and F (Case 2) resulted in higher volatilization of Re during melting and consequently lower Re retention in glass than the baseline feed. The high Cl and F concentrations in the feed resulted in more separated salt, which is likely responsible for higher Re volatilization.
- The feed with CaO and MgO added (Case 3) resulted in comparable Re retention in glass to the baseline feed. As expected, the CaO and MgO increased S retention in the melt, but this did not lead to the desired increase in Re retention. The results gave some indication of lower Re volatilization, but this result is questionable because of the low Re mass balance for this feed at 1200°C.
- The feed with crushed soil (Case 4) resulted in a comparable Re retention in the glass to the baseline feed. The crushed soil accelerated the formation of the glass-forming melt to a lower temperature, but that did not improve the Re retention in glass. The results gave some indication of higher Re volatilization, but this result is questionable because of the unusually high Re mass balance for this melt. Severe foaming observed in this melt is consistent with greater Re volatilization. Increased foaming leads to better convection and higher surface areas that might increase Re volatilization rates.

However, foaming is a phenomenon that is exaggerated in crucible scale melts and, therefore, may not be significant in the full-scale process.

10.0 Incorporation of Re into Glassy Phase

This section documents the results of tests to determine the temperature range at which the Re, initially concentrated in the MIS, incorporates into the glassy phase during the feed-melting process. This information is necessary for better understanding of the factors controlling MIS and Re migration into CRB.

10.1 Experimental

The dry baseline feed to make ~200 g glass was heated from room temperature at 5°C/min to predetermined final temperatures of 400, 500, 600, 700, 800, 900, and 1000°C (i.e., seven separate test runs) and air quenched. The partially reacted feed was ground into coarse particles and washed with dilute nitric acid solution following the same procedure discussed in Section 9 for preparing crucible wash samples, except that these tests used ~300 mL instead of 200 mL. The crucible rinse samples were analyzed for Re, Na, and S. The remaining partially reacted feeds (solids) were ground into fine particles for homogenization, and a sample was taken for the analyses for Re, Na, and S.

10.2 Results and Discussion

Table 10.1 summarizes the concentration of Re, Na, and S analyzed in the crucible rinse and in the solids from tests with baseline feed. The results at 25°C are for the feed before heat treatment. Table 10.2 summarizes the mass of each element found in the crucible rinse and in the solids and total batched. The mass of each element found in the crucible rinse was obtained by multiplying the concentration in Table 10.1 with the mass of DIW used for rinse. The mass of each element found in the solids was obtained by multiplying the concentration in Table 10.1 with target mass of glass calculated from the mass of feed used in each test, based on oxide mass fraction of the feed, 0.7933. The total batched mass of each element was calculated from the mass of feed used in each test and the target feed composition given in Table 9.6. Table 10.3 summarizes the wt% of total Re, Na, and S analyzed in the crucible rinse and solid. Table 10.3 also includes the total wt% recovered in the combined crucible rinse and solid.

Table 10.1. Analyzed Concentration of Re, Na, and S in Crucible Rinse and Solids

Final Temp (°C)	Crucible rinse, mg/kg			Solid, mg/kg		
	Re	Na	S	Re	Na	S
25	2.63	44600	1290	1.15	40300	579
400	1.98	32750	942	0.784	36650	283
500	1.61	26600	756	1.85	53500	815
600	1.93	30400	914	2.09	65200	715
700	1.85	25900	918	2.90	77800	906
800	0.517	7740	384	6.58	108000	1860
900	0.583	838	369	5.40	139000	2670
1000	0.219	647	349	3.65	142000	2250

Table 10.2. Mass of Re, Na, and S in Crucible Rinse and Solids and Total Batched

Final Temp (°C)	Crucible Rinse			Solid			Total Batched		
	Re, mg	Na, g	S, g	Re, mg	Na, g	S, g	Re, mg	Na, g	S, g
25	0.789	13.4	0.387	0.226	7.93	0.114	1.59	29.2	0.666
400	0.594	9.83	0.283	0.154	7.20	0.056	1.59	29.2	0.665
500	0.483	7.98	0.227	0.364	10.5	0.160	1.59	29.2	0.667
600	0.579	9.12	0.274	0.411	12.8	0.141	1.59	29.2	0.666
700	0.555	7.77	0.275	0.576	15.4	0.180	1.61	29.5	0.672
800	0.155	2.32	0.115	1.31	21.4	0.369	1.61	29.4	0.672
900	0.175	0.251	0.111	1.08	27.9	0.536	1.63	29.8	0.679
1000	0.0657	0.194	0.105	0.724	28.2	0.447	1.61	29.4	0.672

Table 10.3. Wt% of Total Analyzed in Crucible Rinse and in Solids and Total Recovered

Final Temp (°C)	Crucible rinse			Solid			Total recovered		
	Re	Na	S	Re	Na	S	Re	Na	S
25	49.51	45.83	58.09	14.20	27.16	17.10	63.71	73.00	75.19
400	37.32	33.70	42.47	9.68	24.70	8.36	47.00	58.40	50.83
500	30.29	27.32	34.03	22.84	36.06	24.07	53.13	63.38	58.10
600	36.35	31.26	41.18	25.80	43.94	21.12	62.16	75.21	62.30
700	34.51	26.38	40.97	35.80	52.44	26.76	70.32	78.81	67.72
800	9.65	7.89	17.15	81.23	72.79	54.93	90.89	80.68	72.08
900	10.76	0.84	16.29	66.67	93.68	78.85	77.43	94.53	95.14
1000	4.09	0.66	15.58	45.06	95.71	66.45	49.15	96.36	82.03

Figure 10.1 shows the wt% of total batched Re, Na, and S analyzed in the crucible rinse. Figure 10.1 also includes the results from Section 9.3 for the temperature range from 800 to 1000°C. Figure 10.2 shows the wt% of total batched Re, Na, and S analyzed in the solid. Figure 10.3 plots the wt% of total batched Re, Na, and S recovered in the crucible rinse and solid together.

Because no measurable volatilization is expected below 800°C based on the results in Section 9.3, it is expected that the total wt% of total batched elements recovered in this series of tests should be close to 100%. However, as seen in Figure 10.3, the total wt% recovered is very low, indicating significant loss of materials. One of the likely sources of loss is that the present tests used two or three DIW wash steps after the crucible rinse before analyzing solid samples. These wash steps were performed to prevent the soluble components, which remained in the residual dilute acid leach solution that did not drain from the solid particles, from being included in the solids. However, the DIW wash process could also dissolve additional soluble components that were not captured in the initial dilute nitric acid leach, especially for lower temperature tests. The low total recovery shown in Figure 10.3 suggests that the latter was the case. A better overall mass balance may have been obtained if the leached solids were dried without rinsing, or if rinse solutions were collected and analyzed. Therefore, these tests give a good indication of the extent of Re, S, and Cl incorporation into the solid phase, but they provide a poor overall mass balance. Note that similar issues were not discovered in Section 9 because solid samples were analyzed only from 1200°C tests that have distinct and fully separated soluble and durable glass phases.

Figure 10.1 shows that the as-dried feed (25°C test) dissolved only ~50% of the soluble Re during the crucible rinse. The soluble Re, Na, and S in general decreased as the temperature increased with a rather sudden change between 700 and 800°C. They all followed the same general trend up to 800°C, and Na disappeared at 900°C, suggesting that almost complete decomposition of sodium nitrate occurred as discussed in Section 9. There was a significant discrepancy between the two sets of results for the tests from 800 to 1000°C, although the only experimental difference was in the amount of dilute nitric acid used in the rinsing operation. The source of this discrepancy is not understood. Although there is a quantitative disagreement, the following two qualitative observations hold true: 1) Re is contained in the sulfate salt at temperatures between 800 and 1000°C, and 2) significant volatilization begins only at 1000°C as discussed in Section 9.

Figure 10.2 shows that the wt% of Re, Na, and S retained in the solid phase all increased in parallel up to 700°C, and then (1) Na increased to reach >90 wt% at 900°C, which agrees well with the crucible rinse results, (2) the Re and S sharply increased as more Re and S was incorporated into the glass-forming melt. However, Re was incorporated into the glass earlier between 700 and 800°C while S increased up to 900°C. The decrease of Re between 800 and 1000°C was likely a result of volatilization enhanced by convection. It is also possible that some salt inclusions embedded in the glassy phase coalesced as a separated salt phase as melting progressed. The present results are inconclusive and suggest that microscopic observations of the partially melted feed by SEM may improve the understanding of the Re volatilization mechanism.

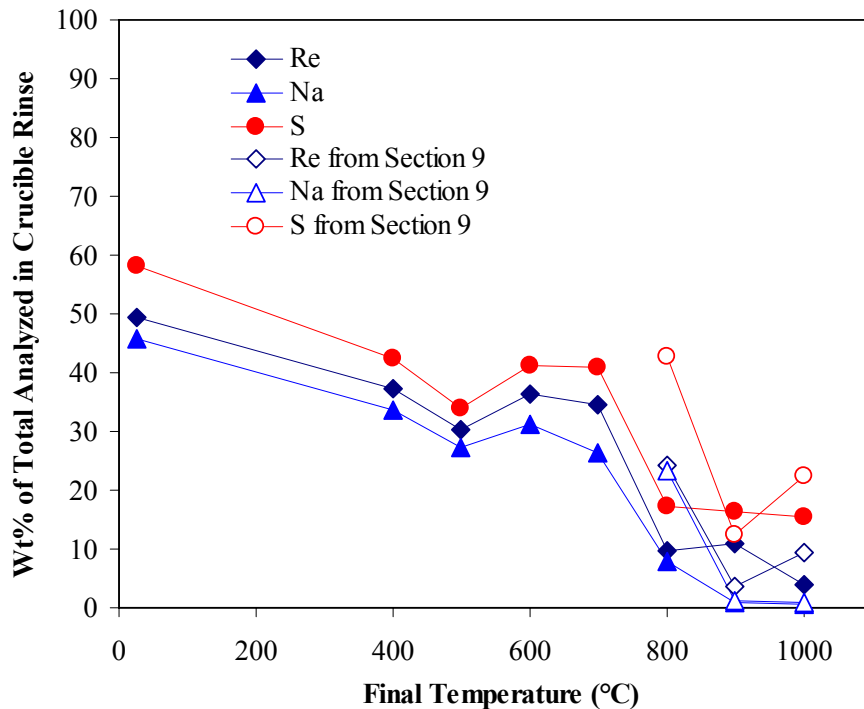


Figure 10.1. Wt% of Total Batched Re, Na, and S Analyzed in Crucible Rinse

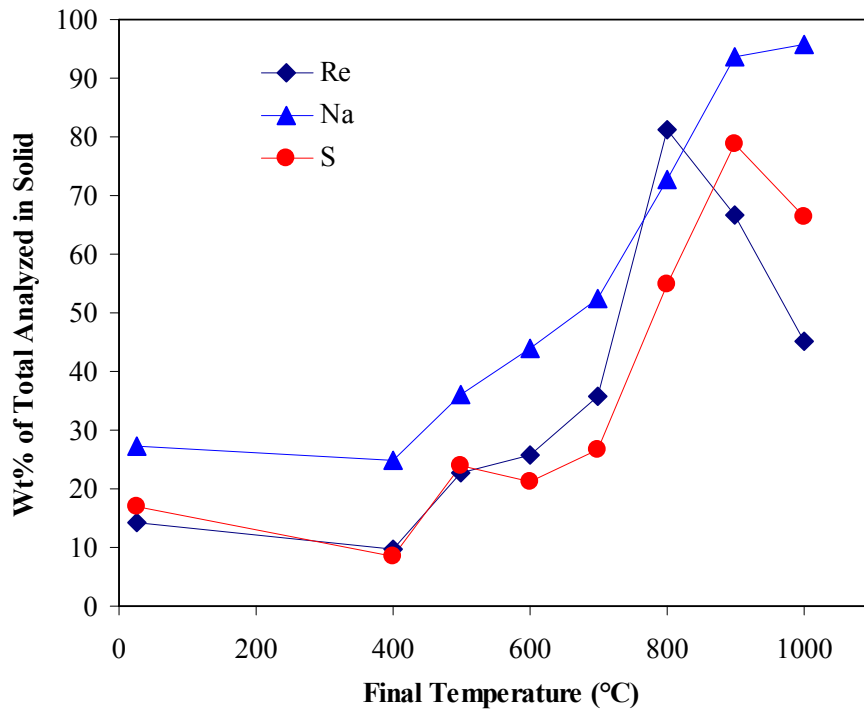


Figure 10.2. Wt% of Total Batched Re, Na, and S Analyzed in Solid

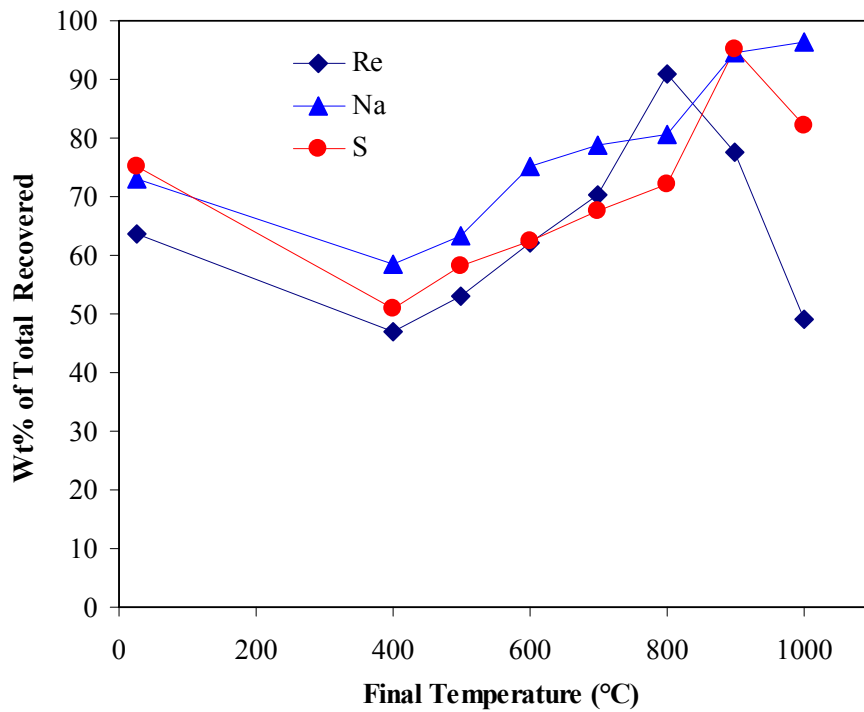


Figure 10.3. Sum of Wt% of Total Batched Re, Na, and S Recovered in Crucible Rinse and Solid

10.3 Summary

The Re was incorporated into a glass forming melt at approximately 700°C, and the incorporation of Re in the glass-forming melt reached a maximum at ~800°C and then decreased as the temperature increased up to 1000°C. The rather sharp decrease of Re present in the glass-forming melt between 800 and 1000°C may suggest that the decrease of Re was not solely from volatilization from the glass-forming melt, but may have been partly caused by partitioning to small salt inclusions that coalesced to form a separated salt phase at higher temperatures.

The poor mass balance closure at low temperatures for the present Re incorporation tests was likely caused by multiple steps of DIW washes performed after the crucible rinse, which seemed to dissolve additional soluble components that were not captured in the initial dilute nitric acid wash. A better overall mass balance can be obtained if the washed solids are dried without additional rinsing, or if rinse solutions are collected and analyzed.

11.0 Conclusions

Water and MIS capillary experiments confirmed that suction of MIS into CRB through capillary forces can be a dominant mechanism for MIS penetration. This conclusion was supported by the preliminary modeling results, which suggested that the MIS penetration process is completely dominated by capillary action, and neither the MIS layer thickness nor any other scaled parameter has a significant effect. The effective capillary radius in the castable refractory was estimated as 1.7 nm from the experiment with water.

Hot-stage microscopy was proven useful for detailed observation of the feed-melting and liquid-formation processes. Hot-stage observations show that the behavior of a dry blended feed and a feed prepared from liquid simulant are significantly different. A dry blended feed seemed to form a higher fraction of liquid than a feed prepared from liquid simulant, which could cause an increase in MIS migration into CRB. This may suggest that the information obtained in the full-scale tests conducted with dry blended feed may need to be verified with drier prepared feed in future operations.

Thin-section profile measurements with FS-38B CRB samples provided new information on how the MIS and Re penetrate as the melt progresses. For the CRB samples above the melt line and at the melt line, soluble Re is present only up to ~2 cm from the glass interface. For the CRB above the melt line, Re penetrates into CRB by a vapor disposition mechanism, i.e., Re deposits when the CRB is cold, becomes molten as temperature increases, and then penetrates further into the CRB by capillary action. The extent of penetration and the concentration of Re above the melt line are small. For the CRB at the melt line, Re penetrates into the CRB through both vapor deposition at the early stages of processing and then liquid MIS formation and penetration at later processing stages. The CRB at the melt line close to the glass interface had the highest soluble Re concentration. For the CRB below the melt line, a relatively low concentration of soluble Re was present on the surface layer whereas a higher concentration of soluble Re was observed in the outer layer close to the CRB/sand interface. Insoluble Re at a higher concentration than the blank level was observed only in the first 0- to 1-cm layer of the CRB at the melt line. The below melt line results indicate that regions of the CRB that experienced Re penetration through MIS migration early in the process that were subsequently covered by the progressing melt did not incorporate the Re in an insoluble melt phase, but instead pushed the Re salt outward through evaporation and/or melting and flow of molten salt.

The new experimental setup developed in this study to investigate Re migration during feed processing and glass melting was successful in achieving a high mass balance closure. The new setup was designed to capture all the volatiles by condensing them inside a stainless steel tube or dissolving them in a pair of scrub solutions. The tests with pre-melted glass showed that Re is more volatile than S and Cl with an estimated $r = 20.4$ wt%/h at 1200°C. The volatilization rate of Re also showed a strong dependence on temperature with an activation energy of 258 J/mole.

The results of dried feed Cases 2 to 4 in relation to the baseline feed (Case 1) are summarized below:

- The feed with high Cl and F (Case 2) resulted in higher volatilization of Re during melting and consequently lower Re retention in glass than the baseline feed. The high Cl and F concentrations in the feed resulted in more separated salt, which is likely responsible for higher Re volatilization.

- The feed with CaO and MgO added (Case 3) resulted in comparable Re retention in glass to the baseline feed. As expected, the CaO and MgO increased S retention in the melt, but this did not lead to the desired increase in Re retention. The results gave some indication of lower Re volatilization, but this result is questionable because of the low Re mass balance for this feed at 1200°C.
- The feed with crushed soil (Case 4) resulted in a comparable Re retention in the glass to the baseline feed. The crushed soil accelerated the formation of the glass-forming melt to a lower temperature, but that did not improve the Re retention in glass. The results gave some indication of higher Re volatilization, but this result is questionable because of the unusually high Re mass balance for this melt. Severe foaming observed in this melt is consistent with greater Re volatilization. Increased foaming leads to better convection and higher surface areas that might increase Re volatilization rates. However, foaming is a phenomenon that is exaggerated in crucible scale melts and, therefore, may not be significant in the full-scale process.

From the study of Re incorporation, it was found that the Re becomes incorporated into glass-forming melt at approximately 700°C, reaches a maximum at ~ 800°C, and then decreases as the temperature increases up to 1000°C. The rather sharp decrease of Re present in glass-forming melt between 800 and 1000°C may suggest that the decrease of Re is not solely from volatilization from glass-forming melt, but may be partly caused by partitioning to small salt inclusions that coalesce to form a separated salt phase at higher temperatures.

The present study has focused on two routes of Re (used as a surrogate for Tc) transport to the outside of the bulk glass: (1) to the offgas stream through volatilization and (2) to the CRB through MIS penetration by capillary action. The Re is a highly volatile component, and its volatilization will even be enhanced by the presence of other volatile components such as Cl and F. Due to its inherent nature of high volatility, it seems that there is no simple effective solution except for the application of a cold cap that condenses the volatiles and brings them back to the feed to maximize their retention in glass. The thicker cold cap and lower plenum temperature would help to incorporate more Re into glass.

Using clean glass feed would help to capture the Re volatilized from melting waste-containing feed and incorporate it into the glass at the end of the bulk vitrification process. However, once the clean glass becomes melted and mixed into the main body of the melt, the Re-containing melt will become exposed to the surface. The volatilization of Re also proceeds at a relatively high rate from a melt that has already incorporated the Re. The Re can escape relatively easily from the surface as the temperature increases at the end of the process. Therefore, it is important to find the optimal heating condition at the end of the process to fully melt the clean glass feed to a reasonably durable glassy phase (because the partially melted feed may contain the volatilized Re that is soluble), but not to overheat, which would expose the hot-glass surface to volatilization.

As discussed in Section 7.0, the main mechanism of Tc transport to the CRB is penetration of MIS. The contribution of volatilization and condensation of Re to the total Re migration into CRB seems to be very small compared to MIS penetration. Using a cold cap, although very critical to control Re volatilization, is likely to promote MIS penetration into the CRB by providing the condition to increase the MIS formation: the cold cap helps to keep the feed at the temperatures favored for MIS formation (e.g., 350 to 550°C) for a longer time. A few promising methods to reduce the MIS migration have been identified and are being tested in a crucible scale under Task 30, which will be described in a separate report. Depending on the effectiveness of the methods developed under Task 30, the balance between the

transport of Re to offgas and to the CRB can be made by controlling the formation of the cold cap during the bulk vitrification process.

12.0 References

- Cooley SK, EM Pierce, LM Bagaasen, and MJ Schweiger. 2006. *Analysis of Soluble Rhenium Concentrations in the Refractory from Bulk Vitrification Full-Scale Test 38B*. PNNL-15868, Pacific Northwest National Laboratory, Richland, WA.
- Gale WF, and TC Totemeier. 2004. *Smithells Metals Reference Book (8th Edition)*. Elsevier. Available at: <http://www.knovel.com/knovel2/Toc.jsp?BookID=717>. Accessed 11-21-2006.
- Hrma P, J Matyas, LM Bagaasen, KBC Minister, AE Beck, MJ Schweiger, TM Brouns, DM Strachan, DD Caldwell, BP Tinsley, ML Elliott, and GW Hollenberg. 2005. *Bulk Vitrification Castable Refractory Block Protection Study*. PNNL-15193, Pacific Northwest National Laboratory, Richland, WA.
- Kim D, JD Vienna, P Hrma, MJ Schweiger, J Matyas, JV Crum, DE Smith, WC Buchmiller, JS Tixier, Jr., JD Yeager, and KB Belew. 2003. *Development and Testing of ICV Glasses for Hanford LAW*. PNNL-14351, Pacific Northwest National Laboratory, Richland, WA.
- Kim D-S, CZ Soderquist, JP Icenhower, BP McGrail, RD Scheele, BK McNamara, LM Bagaasen, MJ Schweiger, JV Crum, JD Yeager, J Matyáš, LP Darnell, HT Schaef, AT Owen, AE Kozelisky, LA Snow, and MJ Steele. 2005. *Tc Reductant Chemistry and Crucible Melting Studies with Simulated Hanford Low-Activity Waste*. PNNL-15131, Pacific Northwest National Laboratory, Richland, WA.
- Mann FM, BP McGrail, DH Bacon, RJ Serne, KM Krupka, RJ Puigh, R Khaleel, and S Fincock. 2003. *Risk Assessment Supporting the Decision on the Initial Selection of Supplemental ILAW Technologies*. RPP-17675, Rev 0, CH2M HILL Hanford Group, Inc., Richland, WA.
- Pierce EM, BP McGrail, LM Bagaasen, EA Rodriguez, DM Wellman, KN Geizler, SR Baum, LR Reed, JV Crum, and HT Schaef. 2005. *Laboratory Testing of Bulk Vitrified Low-Activity Waste Forms to Support the 2005 Integrated Disposal Facility Performance Assessment*. PNNL-15126, Pacific Northwest National Laboratory, Richland, WA.
- Rassat SD, LA Mahoney, RL Russell, SA Bryan, and RL Sell. 2003. *Cold Dissolved Saltcake Waste Simulant Development, Preparation, and Analysis*. PNNL-14194 Rev.1, Pacific Northwest National Laboratory, Richland, WA.
- Raymond RE, RW Powell, DW Hamilton, WA Kitchen, BM Mauss, and TM Brouns. 2004. "Initial Selection of Supplemental Treatment Technologies for Hanford's Low-Activity Tank Waste." In: *Proceedings of WM'04 Symposia*. WM-4524/RPP-19763-FP, CH2M HILL Hanford Group, Inc. Richland, WA.
- Vienna JD, P Hrma, WC Buchmiller, and JS Ricklefs. 2004. *Preliminary Investigation of Sulfur Loading in Hanford LAW Glass*. PNNL-14649, Pacific Northwest National Laboratory, Richland, WA.
- Washburn EW. 1921. "The dynamics of capillary flow." *Physical Review* 17(3):273-283.

Whitehead, JB and EW Greenfield. 1932. "Capillary action in impregnated paper insulation." *Physics* 3:324-330.

13.0 Technical Procedure

GDL-GBM, Rev. 3. 2002. *Glass Batching and Melting*. Pacific Northwest National Laboratory, Technical Procedure.